Jahresbericht 2002

des Lehrstuhls von Prof. Dr. Winfried Petry

Physik Department E13

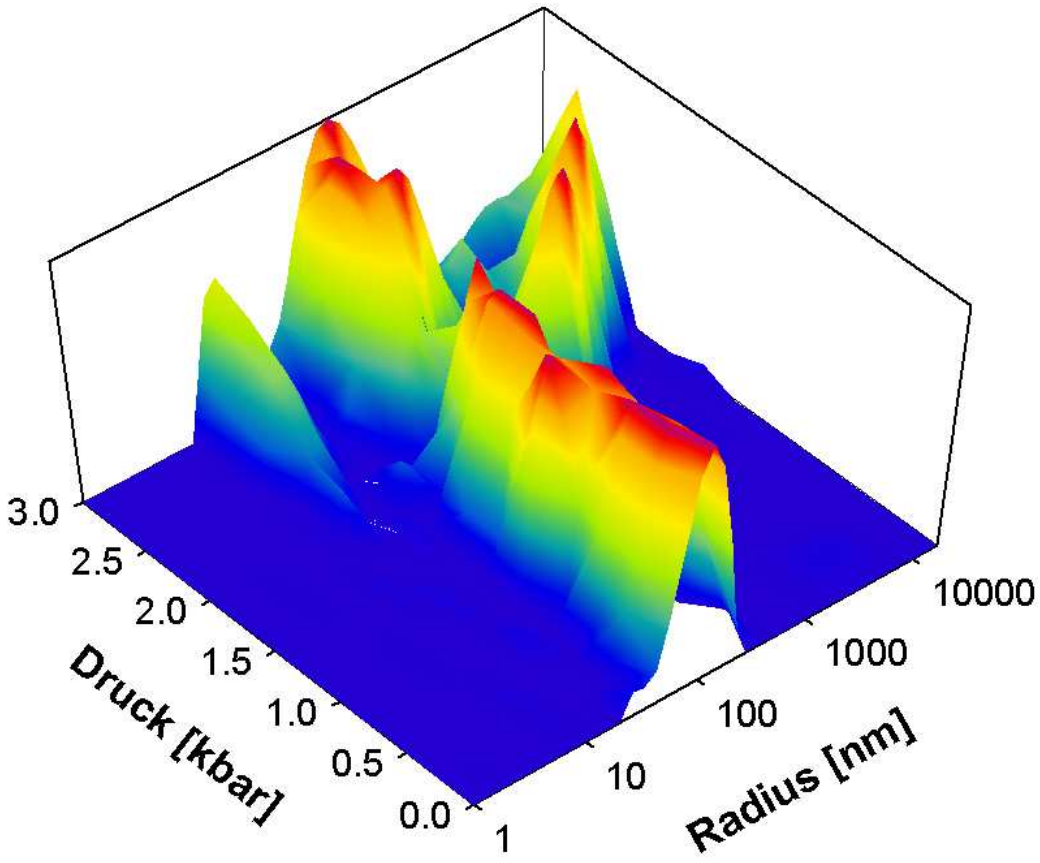

Technische Universität München

Prof. Dr. Winfried Petry
Lehrstuhl für Experimentalphysik IV
Physik Department E13

Lehrstuhlvertreter 2002/2003:
Prof. Dr. Ralf Röhlsberger

Lehrstuhlvertreter 2001/2002:
Prof. Dr. Alfons Schulte

Physik Department E13
Technische Universität München
James-Franck-Straße
D-85748 Garching

Sekreteriat: Elke Fehsenfeld

Tel.: 089 289 12452
Fax: 089 289 12473

Email: wpetry@ph.tum.de
efehsen@ph.tum.de
http://www.e13.physik.tu-muenchen.de

Titelbild:
Hochdruckforschung an biomolekularen Komplexen. Dargestellt ist die Radienverteilung der Casein-Mizelle als Funktion des Drucks untersucht mit dynamischer Lichtstreuung und einem speziellen Rückstreudetektor. Caseinmizellen sind ca. 100 nm grosse Proteinassoziate der Milch, die das in Wasser wenig lösliche Kalziumphosphat speichern. Man erkennt eine Stabilitätsgrenze bei ca. 2 kbar, bei der sich die Mizelle umorganisiert. Untersucht wird u.a., ob die Mizelle amorph strukturiert, oder aus identischen Submizellen zusammengesetzt ist. Durch Hochdruck kann die Wechselwirkung zwischen den Komponenten moduliert und deren Struktur untersucht werden.

Dezember 2002
Andreas Meyer

Vorwort

Mit diesem Jahresbericht blicken wir zurück auf ein produktives Jahr 2002 am Lehrstuhl E13 des Physikdepartments. Die hier versammelten Beiträge spiegeln die Aktivitäten der Gruppe im interdisziplinären Gebiet der Physik weicher Materie wider. Das Spektrum der untersuchten Materialien erstreckt sich von Schmelzen und ungeordneten Festkörpern über Polymere bis hin zu biomolekularen Komplexen. Den Schwerpunkt der Untersuchungsmethoden bilden Lichtstreuung sowie Neutronen- und Röntgenstreuung, wobei letztere zum größten Teil an Großforschungseinrichtungen wie dem ILL, der ESRF oder dem HASYLAB durchgeführt werden. Auch in diesem Jahr hat es dabei wieder eine Reihe von interessanten Entwicklungen gegeben.

Durch die Bewilligung von Forschungsanträgen konnten in einigen Bereichen neue Forschungsaktivitäten entfaltet werden. Der Arbeitsbereich 'biomolekulare Komplexe' unter der Leitung von Wolfgang Doster wurde mit einem Projekt zur zeitaufgelösten Kalorimetrie in den Sonderforschungbereich 588 der DFG aufgenommen.

Auch die Arbeitsgruppe 'Polymere' von Peter Müller-Buschbaum konnte sich weiter entfalten durch die Genehmigung eines Projektes zur Untersuchung von polymeren Klebstoffen, das im Rahmen eines BMBF Verbundprojektes angesiedelt ist. Durch die damit bewilligten Personal- und Investitionsmittel kann das Methodenspektrum der Gruppe weiter ausgebaut werden, z.B. durch Untersuchung des Zusammenhangs zwischen strukturellen Eigenschaften ultradünner Polymerfilme und ihrer Haftfestigkeit. Darüberhinaus ist hervorzuheben, dass Peter Müller-Buschbaum in diesem Jahr seine Habilitationsschrift mit dem Titel "Nanostrukturierte Polymerfilme" eingereicht hat und sich im Dezember dieses Jahres habilitiert hat. Zu der erwarteten Intensivierung der Polymerphysik am Lehrstuhl durch Besetzung der C3 Professur auf Zeit ist es noch nicht gekommen, da der in diesem Jahr ergangene Ruf abgelehnt wurde.

Bei der Untersuchung mehrkomponentiger Schmelzen, die unter der Leitung von Andreas Meyer durchgeführt werden, gibt es eine Reihe von interessanten Ergebnissen zum atomaren Transport in diesen Systemen. Insbesondere haben die Arbeiten der Gruppe zu den Themen Struktur und Dynamik von Silikatschmelzen Eingang gefunden in den Jahresbericht 2002 des ILL, in welchem ausgewählte Highlights der Forschung hervorgehoben werden. Andreas Meyer hat im November 2002 seine Habilitationsschrift mit dem Titel "Atomarer Transport in mehrkomponentigen Schmelzen" eingereicht.

Bereits im vergangenen Jahr hat die Methode der Kernresonanzstreuung unter Leitung von Uwe van Bürck neuen Auftrieb erhalten durch die erstmalige Anwendung der gestörten $\gamma\gamma$- Winkelkorrelation mit Synchrotronstrahlung (SRPAC) auf die Untersuchung der Dynamik weicher Materie. Diese Methode konnte in Diskussionen mit Prof. S. Dattagupta während seines mehrtägigen Aufenthalts bei E13 theoretisch weiter untermauert werden. Darüberhinaus haben diese Arbeiten durch Aufnahme in die ESRF Highlights 2002 eine besondere Würdigung erfahren.

Ich freue mich, dass die in diesem Jahr erzielten Resultate auch für das kommende Jahr spannende Entwicklungen und interessante Forschungsergebnisse erwarten lassen. Persönlich danke ich den Mitgliedern des Lehrstuhls E13 für die freundliche Aufnahme als Lehrstuhlvertreter von Prof. Petry für das akademische Jahr 2002/2003.

Ralf Röhlsberger *Dezember 2002*

Inhaltsverzeichnis

1 Instrumentelle und methodische Entwicklungen

A Super-Mirror Coated Fermi Chopper for the IN6 Time-of-Flight Spectrometer at the ILL

Markus Pöhlmann [1,2], Christian Carbogno [1,2], Marek Koza [2], Helmut Schober [2]

[1] Physik-Department E13, Technische Universit¨at M¨unchen
[2] Institut Laue-Langevin, Grenoble

In recent years much effort has been undertaken to improve existing neutron scattering facilities all over the world. In parallel numerical software has been established which allows to answer many "what were if" questions.
Here we use the program package *McStas* [1] to simulate the time-of-flight spectrometer IN6 at the ILL. The development of a Fermi chopper component for *McStas* was mandatory for this project. We provided this new *McStas* component, based on a straight-forward calculation of the neutrons' trajectory in the chopper with the option of super mirror coated chopper blades [2]. Thus, apart from the verification of the existing IN6 spectrometer (Cd chopper blades) we investigate the effects of an additional super mirror layer on top of the spacers.

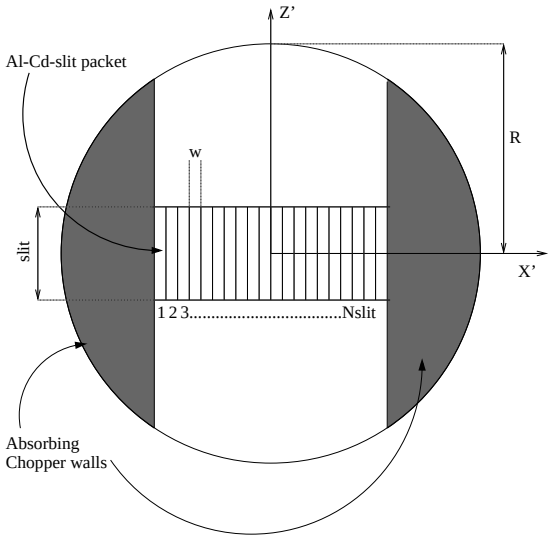

Figure 1.1: The Fermi chopper of the IN6 seen from the top. Rotation is around the y-axis [5].

The number of slits $Nslit$, their length $slit$ and width w and the features of the super mirror layer (m-value, the critical scattering vector Q_C, the slope of reflectivity α, the low-angle reflectivity R_0 and the width of super mirror cut-off W_i [3]) are the essential variables for the system. For $m = 0$ the blades are completely absorbing i.e. we are dealing with a conventional package. The goal of this investigation is then to compute the paths for a large number of neutrons. Their initial parameters are randomly generated and the trajectory is found in terms of a Metropolis algorithm [4]. If the parameters of one neutron are such that a slit of the chopper can be entered, a transformation to the rotating (chopper attached) frame turned out to be the most suitable way for further pursuit of the trajectory. This operation is a linear orthogonal transformation of the position $\mathbf{r}$ of the neutron with respect to the chopper center $\mathbf{r} \longrightarrow \mathbf{r}' : \mathbf{r}' = \mathsf{T}\mathbf{r}$ with the transformation matrix T. In this rotating frame the distances to the blades as a function of time

can easily be calculated and roots in these distances give the times for the interaction of a neutron with a blade. Unfortunately these roots cannot be found analytically and numerical methods have to be applied. A combination of a bisection and a secant method was employed since the secant method alone failed for some exotic cases and the aim is, of course to speed up the calculations as much as possible.
A similar transformation with the transformation matrix T can be applied for the velocities and therefore, in the case of a successful reflection with enabled super mirror coating, the new direction of the neutron can be obtained.
The simulations without super mirror coating compare very well to experimental data of the width of the transmitted beam after the chopper [5]. The effect of the super mirrors were investigated with particular attention to the ratio of flux gain versus resolution losses. Currently we can show that super mirror layers increase the transmission of the chopper significantly (see Fig. 1.2) while the energy resolution at the detectors remains almost unchanged (Fig. 1.3) .

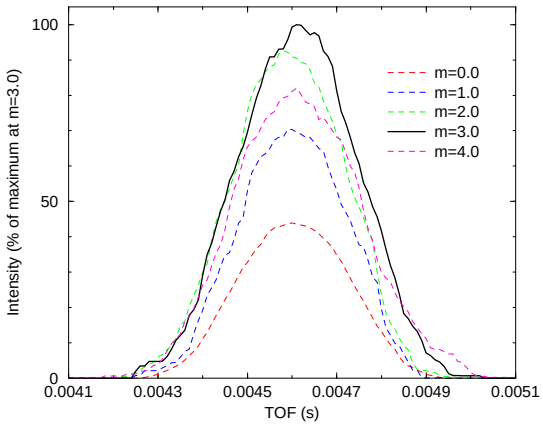

Figure 1.2: Intensity distribution as a function of super mirror quality.

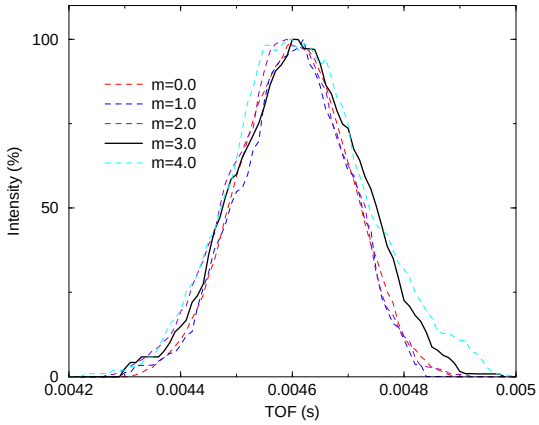

Figure 1.3: Intensity distributions (normalized on maximum) show no variation with super mirror quality.

The simulations for figures 1.2 and 1.3 have been performed for the current IN6 chopper (chopper angle 2.3^o) at a wavelength of $\lambda = 5.1\mathring{A}$. Uncertainties due to bad statistics may appear since the number of neutrons was low. Hence longer and computationally more demanding simulations are currently done to obtain reliable informations.

[1] P. K. Willendrup, K. Lefmann, E. Farhi, M. E. Hagen, McStas - A neutron ray-trace simulation package McStas Version 1.5 (2001)

[2] M. P¨ohlmann, C. Carbogno, H. Schober. Super mirror coated fermi chopper; in: *McStas - ILL Library* (2002)

[3] K. Nilsen, K. Lefmann, The McStas v1.4 Manual (July, 2000)

[4] N. Metropolis, A. W. Rosenbluth, M. N. Rosenbluth, A.H. Teller. J. Chem. Phys. 21 (1953), 1087

[5] C. Carbogno. The simulation of IN6 with $McStas$. Ill internship report, ILL (2002)

The high resolution time–of–flight spectrometer TOFTOF

T. Unruh[1], J. Ringe[1], J. Neuhaus[1], W. Petry

[1] Technische Universit¨at M¨unchen, ZWE FRM-II

The high resolution time of flight spectrometer TOFTOF is located in the neutron guide hall of the FRM–II. The instrument is being built by the Physics Department E13 of the Technische Universität München. The multichopper instrument is best suited for the investigation of e.g. local motions in polymers, proteins and biological membranes, diffusion mechanisms of atoms or molecules in condensed matter and dynamics of glass transitions.

The technological concept of the instrument described in detail elsewhere [1,2] has been developed on the basis of the results of Monte–Carlo simulations including the calculation of the elastic and inelastic resolution functions. In the following the progress of the construction of the instrument is summarized.

The primary spectrometer

Main component of the primary spectrometer is a system of seven chopper discs used to produce an intense pulsed neutron beam with widely configurable intensity / energy resolution ratios. For this spectrometer special carbon fibre discs with a diameter of 600 mm were developed in cooperation with the Lehrstuhl für Leichtbau. The discs have two and four slits respectively and are coated with elementary ^{10}B as neutron absorbing material.

Presently five of the discs are produced, tested and being mounted into the chopper vessels. Another two discs are under construction. For a first instrument version the chopper discs were tested at a rotation speed of 23000 rpm. An upgrade with discs that work on 26000 rpm or higher speeds is planned and pushed by recent successful tries with speeds up to 29000 rpm. The increase of the angular frequency of the discs leads to a significant improvement of the energy resolution of the spectrometer.

The chopper driving and control system has been completed by ASTRIUM, Friedrichshafen, including the communication software. The whole system with the mounted discs will be delivered in spring 2003. The vacuum system for the vessels and the neutron guides and the supports for the vessels and the guide tubes are already installed. Thus the chopper system should be operational in April 2003.

For neutron flux amplification at the sample position the neutron guide between the chopper vessels and the sample is constructed in an anti–trumpet–like configuration. The reflecting multilayer of the elements of the neutron guide which compresses the beam must have enlarged critical angles. Therefore neutron guides with critical angles of $m = 2$, $m = 3$ and $m = 3.6$ were ordered from the company S-DH in Heidelberg, Germany. The coating of the glass elements has recently been completed and the assembling of the guides will be finished in 2002. Most of the glass elements surpass the demanded specification significantly. The whole guide is expected to be deliverd and adjusted in the first quarter of 2003.

Figure 1.4: Flight chamber of the TOFTOF spectrometer

The secondary spectrometer

The flight chamber was built up in 2002. Fig. 1.4 gives an impression of the construction which is shielded from the outside with more than 11 t of B_4C coated polyethylene. This shield will reduce the background signal of the detectors produced by cosmic radiation and parasitic scattering of neutrons from other experiments. The inner side of the flight chamber is coated with cadmium sheets which serve as absorption material for neutrons scattered to directions where no detectors are installed. For fire protection the whole flight chamber has to be covered by a 1 mm Al-sheet. This work will be completed in January 2003.

The last part of the neutron guide, which can be replaced by a collimator to achieve higher Q–resolution, is integrated into the sample chamber. A thin aluminium sheet separates the gas volumes of the sample and the flight chamber. The installation of the sample chamber will be completed when the Al fire protection sheets are mounted.

In 2002 500 ^{3}He–detectors were delivered by Canberra Eurisys. The detectors are squashed counting tubes with an active length of 400 mm and a depth of about 15 mm. The gas pressure is 10 bar (9.7 bar ^{3}He and 0.3 bar CF_4). The geometry of all detectors was measured using a specially constructed semi automatic apparatus in order to check the agreement with the demanded specifications. Presently for all detectors the pulse height spectra are measured using a Californium–252 spontaneous fission neutron source.

Concerning the detectors and other electronic components we got excellent service and further support from the central FRM–II detector and electronics laboratory. We greately acknowledge the members of the mechanical workshop (E13), Reinhold Funer and Joachim Dörbecker, for their engaged support in the building up of the flight chamber. We also thank the central workshop of the Physics Department where several components of the spectrometer were produced.

[1] A. Zirkel, W. Schneider, J. Neuhaus, W. Petry, Physica B, **128**, 123 (2000)

[2] S.V. Roth, thesis, Technische Universit¨at M¨unchen (2001)

Time domain interferometry: Analysis of results in the quantum beat and the radiative coupling regimes

U. van Bürck, G. V. Smirnov[1], H. Franz[2], T. Asthalter[3], O. Leupold[4], E. Schreier, W. Petry

[1] Russian Research Center 'Kurchatov Institute', Moscow
[2] Hasylab, Hamburg
[3] Institut f¨ur Physikalische Chemie, Universit¨at Stuttgart
[4] Univ. Rostock; Univ. Paderborn; ESRF Grenoble

The extreme sharpness of nuclear resonant scattering is a challenge calling for applications e.g. in the field of slow atomic motions. A method not limited to nuclear resonant samples is time domain interferometry (TDI), where the quasielastic scattering of synchrotron radiation (SR) by a non-resonant sample is analyzed by means of the delayed nuclear forward scattering (NFS) from two identical resonant targets. One target is mounted upstream and the other downstream of the sample. In case of a stiff sample, and when one nuclear target is at rest and the other moved at large constant velocity, interference of the waves scattered by the two targets leads to a fast quantum beat (QB) which modulates the slow dynamical beat (DB) of the single-target response. When both nuclear targets are at rest, the wave scattered by the upstream target can be scattered again by the downstream target, and this so-called radiative coupling (RC) creates a DB corresponding to twice the optical thickness (double-target DB). If however the sample exhibits dynamics on the nuclear timescale, the phase of the radiation scattered by the upstream target becomes perturbed by the quasielastic scattering in the sample. This perturbation destroys interference and radiation coupling, leading for TDI in the QB-regime to a fading of the QB [1], whereas for TDI in the RC-regime a transition from the double-target DB to a single-target DB is expected [2].

These two regimes of TDI have been compared in an experiment [3], where the quasielastic scattering from a sample of glycerol at temperatures $T \sim$ 128, 230 and 240K was analyzed by TDI both in the QB-regime and the RC-regime, using as targets a set of two 6μm thick stainless steel foils enriched to 95% in ^{57}Fe. Measurements at different scattering angles $\sim$8, 12, 16 and 20 degrees, corresponding to scattering vectors of magnitudes $q \sim$ 1, 1.5, 2 and 2.5Å^{-1}, respectively, were performed in parallel. As an example, we show in Figs. 1.5 and 1.6 the time evolutions measured at $q \sim$1.5Å^{-1} and $q \sim$2.5Å^{-1} for the QB- and the RC-regimes at different temperatures T, with background substracted. At 128K, where the scattering sample is stiff, the time evolutions in both regimes correspond to the instrumental functions measured in forward direction. At higher temperatures the sample exhibits slow dynamics, which gradually destroys interference and radiative coupling. In the QB-regime, the well-known fading of the QB [1] is observed, which varies both with temperature and scattering angle. In the RC-regime, the predicted transformation [2] from a double-target DB (see e.g. 1.5Å^{-1} 128K: first DB minimum at $\sim$20ns) to almost a single-target DB (see 2.5Å^{-1} 240K: first DB minimum at $\sim$40ns) was observed for the first time.

This qualitative comparison has now been substantiated by a computer analysis. The solid lines in the figures are simulations based on Eqs. (32,33) of [2] in the approximation of weak scattering, where a Kohlrausch type of relaxation was assumed with parameter β =0.7 [4] fixed. At the given limited accuracy of the data, all time evolutions could be well described with a dominating self-part of the van Hove pair-correlation function. The most important point is that it was possible to find parameters by which the two sets of completely different time evolutions for the QB- and the RC-regimes were consistently fitted.

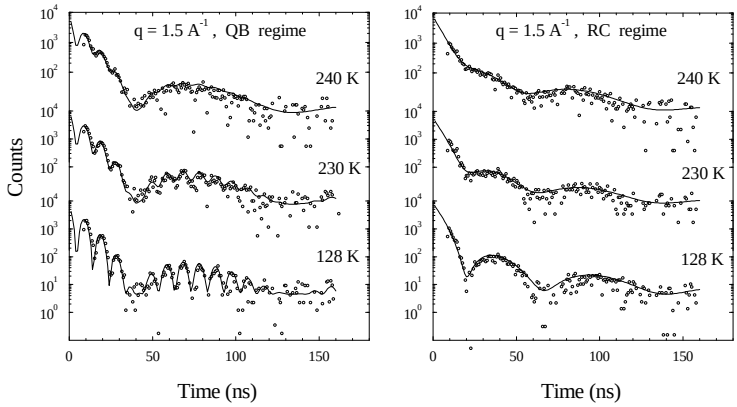

Figure 1.5:
TDI spectra of glycerol in the QB-regime (left) and the RC-regime (right) at $q \sim 1.5\text{Å}^{-1}$ at $T \sim 128$, 230 and 240K. The solid lines are fits based on the theory [2].

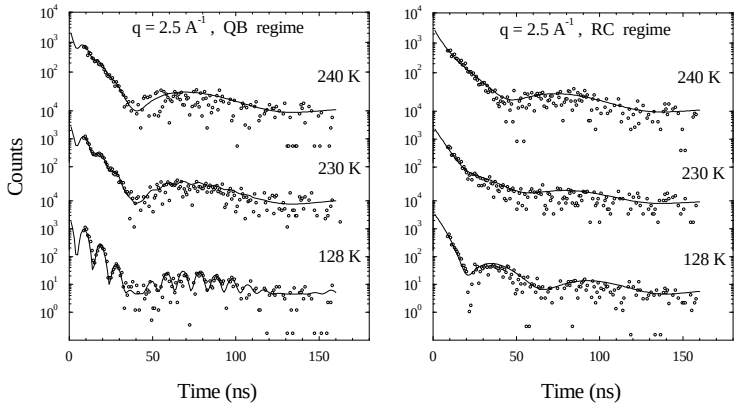

Figure 1.6:
TDI spectra of glycerol in the QB-regime (left) and the RC-regime (right) at $q \sim 2.5\text{Å}^{-1}$ at $T \sim 128$, 230 and 240K. The solid lines are fits based on the theory [2].

Since the QB is a very pronounced feature of the time evolution measured in the QB-regime, its fading due to sample dynamics is more easily recognized during the experiment than the corresponding changes of the DB in the RC-regime. The computer analysis, by contrast, is more sensitive to relaxation parameters when the time evolutions were measured in the RC-regime. Therefore, for future experiments, we suggest to use the QB-regime for a first orientation and, subsequently, the RC-regime for the major part of the measurements. We also feel that the consistent fit of such two different data sets increases the reliability of the data evaluation.

[1] A. Q. R. Baron, H. Franz, A. Meyer, R. R¨uffer, A. I. Chumakov, E. Burkel, W. Petry: Phys. Rev. Lett. **79**, 2823 (1997)

[2] G. V. Smirnov, V. G. Kohn, W. Petry: Phys. Rev. B **63**, 144303 (2001)

[3] U. van B¨urck, G. V. Smirnov, H. Franz, T. Asthalter, O. Leupold, E. Schreier, W. Petry: Ann. Report TUM Physik-Dep. E13, 42 (2001); ESRF report MI-533 (2002)

[4] J. Wuttke, W. Petry, S. Pouget: J. Chem. Phys. **105**, 5177 (1996)

SRPAC: progress in methodology

I. Sergueev[1], U. van Bürck, A. I. Chumakov[2,3], R. Rüffer[2], T. Asthalter[4], G. V. Smirnov[3], H. Franz[5], W. Petry

[1] TUM E13; ESRF Grenoble
[2] ESRF, Grenoble
[3] Russian Research Center 'Kurchatov Institute', Moscow
[4] Institut f¨ur Physikalische Chemie, Universit¨at Stuttgart
[5] Hasylab, Hamburg

Since the first application of Synchrotron Radiation based Perturbed Angular Correlation (SRPAC) to studies of dynamics in soft matter [1], the method has been improved considerably by changing several important details. In a recent beamtime at ESRF ID18, a complete set of SRPAC data has been taken under these conditions for the well-known [2,3] molecular glass former ferrocene/dibutylphthalate.

In contrast to the previous measurements [1], the incident radiation was now monochromatized to ~ 6 meV by a standard high-resolution monochromator. A larger APD detector (area $10\times10\,\mathrm{mm}^2$) was placed in a 90° out-of-plane scattering geometry at closer distance to the scattering sample mounted in the cryostat, yielding a gain in solid angle by a factor of ~ 36, accepting in the same time a slight decrease of the contrast due to angular averaging. The most important point, however, was that the measurements were now performed in single-bunch mode: First, the now sufficiently large time window enabled us to observe the slowly decaying incoherent signal (SRPAC) after the fast decaying disturbance [4] from the delayed coherent signal in forward direction (NFS) at low temperatures. Second, the large time window allowed us to follow the slow asymptotic approach of the SRPAC signal to the natural decay at high temperatures. Typical delayed countrates under these conditions were ~ 50/s (~ 1/s) with the incident energy set in resonance (off-resonance in a phonon peak), respectively.

Typical time evolutions measured in resonance are shown in Fig. 1.7, where the left panel exhibits the SRPAC signals and the right panel the NFS signals measured in parallel at various temperatures. For SRPAC, the anisotropy $A_{22}\cdot G_{22}(t)$ is displayed, which shows the deviation from the natural decay, being connected with the measured intensity $I(t)$ in the following way

$$I(t) = I_0\,\exp(-t/\tau_0)\cdot(1 - A_{22}\cdot G_{22}(t)) \tag{1.1}$$

where A_{22} is the effective anisotropy coefficient, $G_{22}(t)$ the perturbation function, and τ_0 the natural lifetime (141 ns for ^{57}Fe).

As an example for the low temperature region, the data obtained at 160 K are shown. At this temperature the Lamb-Mössbauer factor $f_{LM}\sim 0.14$, and the NFS signal is still rather intense (see right panel upper curve), exhibiting even a pronounced dynamical beat envelope. As a result, its 'shadow' by nuclear and electronic 90° scattering into the SRPAC channel dominates that channel at early times (compare left panel upper curve). The decay of the NFS signal, however, is much faster than natural. Thus after some time, say ~ 200 ns, the slowly decaying SRPAC signal can be observed without disturbances. Since there is hardly any slow dynamics yet at 160 K, the SRPAC spectrum exhibits a pronounced quantum beat (due to the electric quadrupole splitting of ferrocene) without damping until late times.

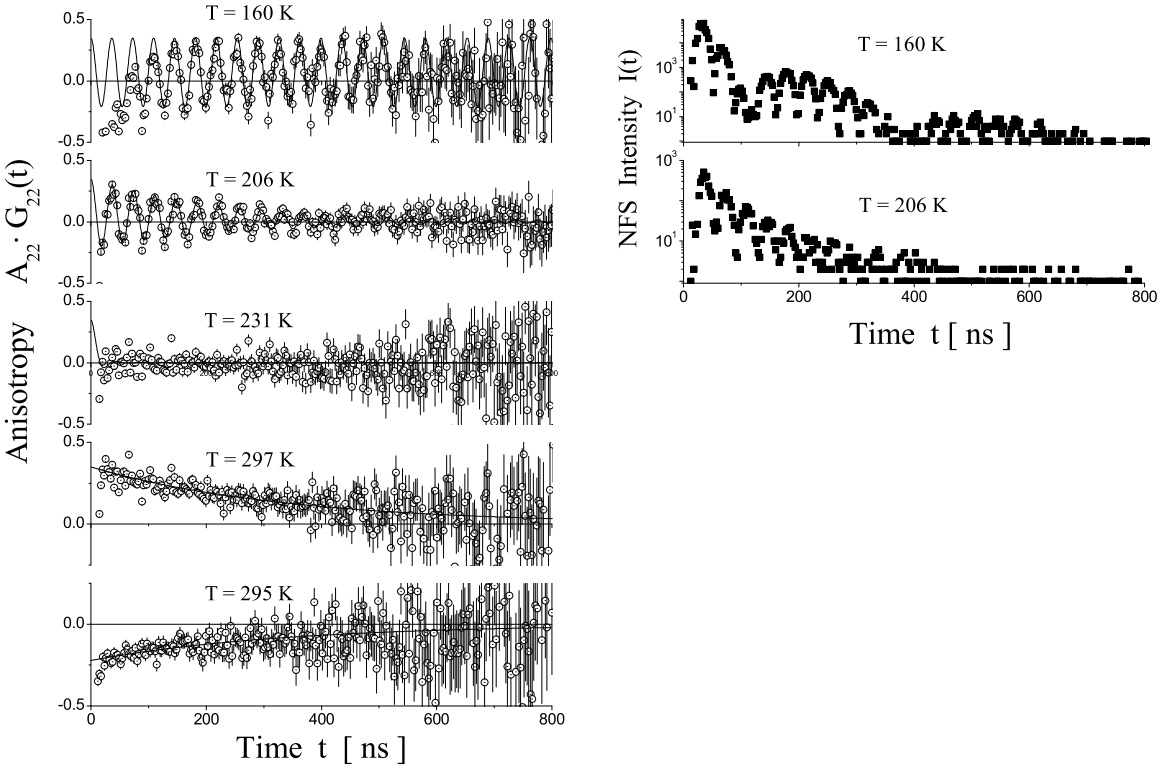

Figure 1.7:
Time evolutions of SRPAC (left) and NFS (right) at various temperatures. The solid lines are fits according to the strong-collision model [8].

Above the glass transition of ~ 178 K, very fast dynamics becomes dominating, and f_{LM} decreases rapidly. As a consequence, the NFS intensity, which is proportional to ${f_{LM}}^2$, vanishes. At 206 K, $f_{LM} < 0.01$, and the NFS is already very weak, but can still be observed (see right panel lower curve). A remarkable feature of this spectrum is its deviation from an exponential decay, giving direct evidence of Kohlrausch stretching and corroborating previous observations in the same system [5]. The NFS is so weak that it does not disturb the SRPAC evolution any more, which starts now at early times with a clear quantum beat (see left panel second curve from top). However, at this temperature structural relaxation dominates, causing a considerable damping of the quantum beat towards later times. At higher temperatures, the signal becomes overdamped, and no quantum beat can be observed any more (see left panel, third curve from top, measured at 231 K).

After passing through this intermediate region, at still higher temperatures the regime of fast relaxation (Abragam-Pound limit [6]) is reached, where a slow asymptotic approach of the natural decay is observed. In this regime the time of approach is proportional to the relaxation rate, and for this reason a large observation window is essential when high relaxation rates are to be determined. A typical spectrum measured at 295 K is shown in the left panel, fourth curve from top, which nicely exhibits this slow approach of the natural decay. In the 90° out-of-plane scattering

geometry, the SRPAC spectra start at time zero with destructive interference, and thus also the asymptotic approach occurs from the negative side. In order to corroborate this small deviation from the natural decay - which is essential for highest relaxation rates - SRPAC spectra can be measured also in 90° in-plane scattering geometry, where the initial interference is constructive, and where the asymptotic approach to the natural decay occurs from the opposite side. Such a spectrum is shown in the left panel, bottom curve. The comparison of these curves clearly demonstrates the sensitivity of the method.

Altogether data were taken in a temperature range of $\sim 100 - 330$ K, covering a range of relaxation times of ≥ 1 μs - 20 ps, respectively. The evaluation of the comprehensive set of data is under way. Of special interest is here the separation of rotational and translational dynamics, which can be achieved due to the simultaneous measurement of the SRPAC (sensitive to rotation only) and NFS channels (sensitive to translation and rotation). Of further interest is the interpretation of the SRPAC data along different extreme models for rotational diffusion [7–9].

[1] I. Sergueev, U. van B¨urck, A. I. Chumakov, T. Asthalter, G. V. Smirnov, H. Franz, R. R¨uffer, W. Petry: Ann. Report TUM Physik-Dep. E13, 39 (2001); ESRF Highlights 2002

[2] S. L. Ruby, B. J. Zabransky, P. A. Flinn: J. Physique C6 **37**, 745 (1976)

[3] A. Meyer, H. Franz, J. Wuttke, W. Petry, N. Wiele, R. R¨uffer, C. H¨ubsch: Z. Phys. B **103**, 479 (1997)

[4] G. V. Smirnov, V. G. Kohn: Phys. Rev. B **52**, 3356 (1995)

[5] I. Sergueev, H. Franz, T. Asthalter, W. Petry, U. van B¨urck, G. V. Smirnov: Phys. Rev. B **66**, 184210 (2002)

[6] A. Abragam, R. V. Pound: Phys. Rev. **92**, 943 (1953)

[7] H. Winkler: Z. Physik A **276**, 225 (1976)

[8] S. Dattagupta: *Relaxation phenomena in condensed matter physics*, Orlando: Academic Press Inc. (1987)

[9] G. Diezemann, H. Sillescu: J. Chem. Phys. **111**, 1126 (1999)

Inelastic scattering of synchrotron radiation from FeNi alloys

H. Franz[1], K. Messel[2], G.V. Smirnov[2], W. Petry

[1] Hamburger Synchrotronstrahlungslabor am DESY, Hamburg
[2] Russian Research Center "Kurchatov Institute", Moscow

In the last six years Nuclear Inelastic Absorption (NIA) has found an increasing number of applications[1]. Most experiments use the 14.4 keV resonance of ^{57}Fe, but also other isotopes like Sn or Dy have been used. By its nature NIA gives a direct access to one important thermodynamic function: phonon density-of-states (DOS). This is a primary advantage of the method. The interpretation of the NIA data is straightforward and model independent. A specific feature of NIA is that the vibrational characteristics of the local environment of the resonant atom are probed in the experiment. This may deliver a useful insight view on the relationship of various vibrational modes in complex molecular systems. However, NIA being by its nature an integrating measurement does not give a direct access to the phonon dispersion relations in contrast to inelastic neutron scattering. To overcome this drawback we have developed a code that allows, based on a Born-van-Karman model, to derive force constants from the DOS and then use these to determine dispersion relations numerically.

The code has been tested (of course) for α-iron using data supplied by A.I. Chumakov. Fig. 1.8 shows the dispersion relation calculated using only the DOS data compared to data from literature[2]. We found almost perfect agreement.

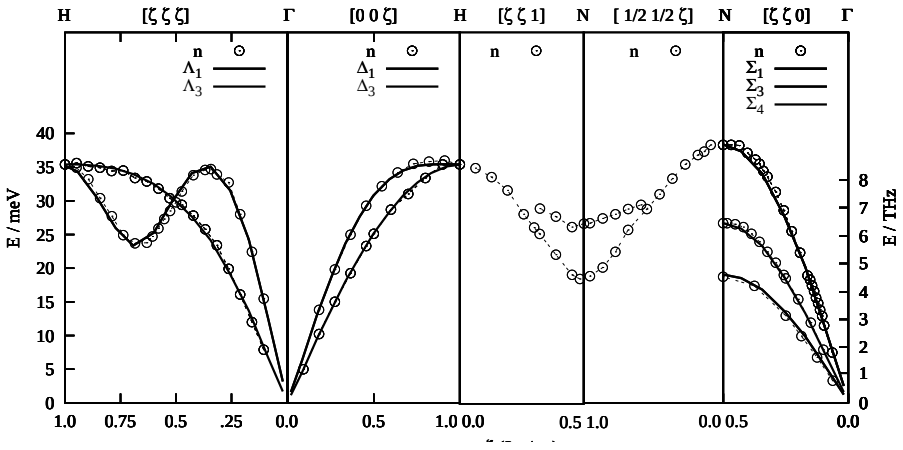

Figure 1.8:
Dispersion relation of α-iron as determined from the DOS (solide line) compared to literature data (circles and dashed line).

Encouraged by this result we analysed partial DOS data of ^{57}FeNi alloys obtained by NIA at the beamline PETRA1, HASYLAB, Hamburg. In spite of the fact that this alloy has attracted widespread interest (as soft magnetic material or INVAR) many basic properties are not yet well understood.

We have studied the temperature dependence of the iron-DOS of $Fe_{80}Ni_{20}$ and $Fe_{85}Ni_{15}$ with an energy resolution of 2.2 meV, starting from room temperature up to 720 K, well above the martensitic phase transition temperature[3]. In addition we performed in-situ diffraction measurements to

control the phase purity and the transformation behaviour at the beamline PETRA2, HASYLAB. Moreover the exact composition of the alloys was determined by X-ray fluorescence analysis at beamline L, HASYLAB.

As already reported in the previous year we

- observed a strong softening of the DOS while increasing the temperature and
- found phonon frequencies significantly below the values obtained in simulations[3].

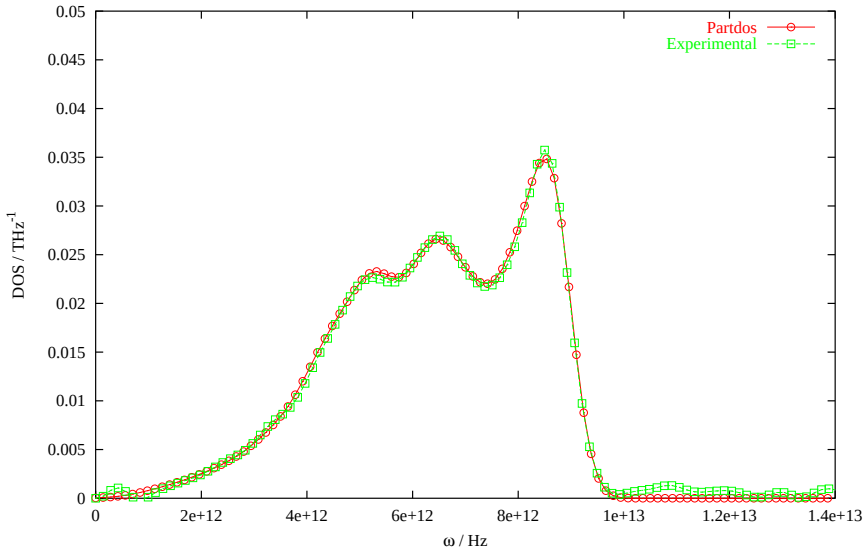

Figure 1.9:
Iron density of states of $Fe_{85}Ni_{15}$ measured at room temperature. Red circles: Born-von-Karman fit, green squares: experimental data ($1 \cdot 10^{13}$ Hz correspond to 40 meV).

Our earlier findings were now substantiated by performing Born-von-Karman fits to the inelastic data as discribed above. Fig. 1.9 shows as an example the spectrum of $Fe_{85}Ni_{15}$ taken at room temperature.

Using the force-constants from these fits dispersion relations may be determined. In Fig. 1.10 these curves are compared to results of molecular dynamics simulations[4]. Due to the lack of single crystals to our best knowledge there are no inelastic neutron scattering data for comparison. As already seen from the DOS, indicating a maximum energy of some 40 meV, the simulations yield too high phonon energies (up to some 50 meV). However, the shape of the dispersion curves fits exactly to the results of the simulations.

Thus our routines allow to extract phonon dispersion curves already from the partial density-of-states alone. There is no need for single crystals and we want to stress that data of the quality as shown in Fig. 1.9 may be obtained in few hours of beamtime and the amount of sample material is minute (few milligrams).

In spite of the very striking agreement (except for a scale factor) seen in Fig. 1.10 we want to stress that this method to determine phonon dispersion curves is certainly limited to simple (i.e.

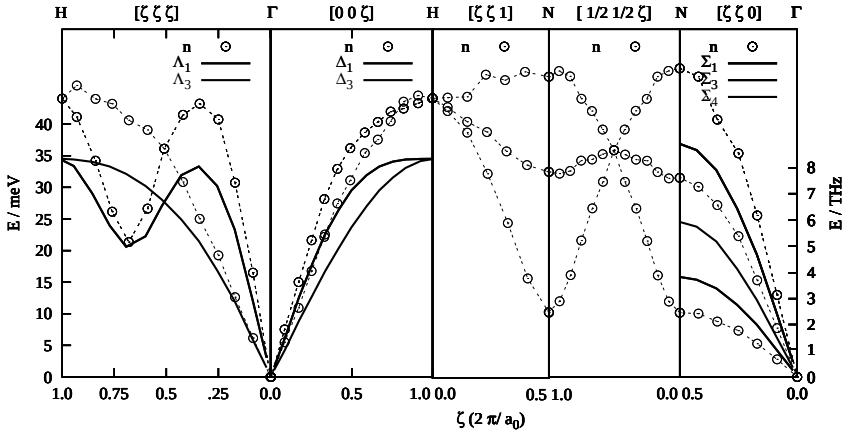

Figure 1.10:
Dispersion relations of $Fe_{80}Ni_{20}$ as determined from the DOS (solide line) compared to results of molecular dynamics simulations[4] (circles and dashed lines).

few component) systems containing a significant amount of resonant isotopes. In this sense the iron rich FeNi alloys are certainly an ideal model case. Nevertheless there is quite a number of Mössbauer isotopes suitable for this kind of investigations. Concerning the investigations of complex systems, like for example molecular crystals where the resonant isotope may couple to few modes only, the strength of NIA is certainly the ”filtering” of a limited number of interesting modes.

[1] E. Gerdau, H. de Waard (Hrsg.): *Nuclear resonant scattering of synchrotron radiation*, Bussum: Baltzer Science Publishers (1999)

[2] Landolt-B¨ornstein Vol. 13a p 54

[3] H. Franz, T. Asthalter, M. Dommach, A. Ehnes, K. Messel, I. Sergueev, Hyperfi ne Interact. **141/142**, 131 (2002)

[4] R. Meyer, P. Entel, Phys.Rev.B **57**, 5140 (1998)

2 Polymergrenzflächen

Nano-structured diblock copolymer films: A grazing incidence small-angle x-ray scattering study

P. Müller-Buschbaum, P. Panagiotou, M. Cristofolini[1], P. Volodin [2]

[1] Chemistry Department, Reading University
[2] Institut f¨ur Polymerforschung, Dresden

Nano-structured polymer surfaces are of strong interest with respect to several applications. Frequently lithographic pattern techniques are utilized. One alternative way to prepare isotropic nanostructures is based on the destabilization of extremely thin initially homogeneous films [1]. Due to mass conservation both major dewetting process, the spinodal decomposition as well as the nucleation and growth process, give rise to an increase of the most prominent in-plane length scale with increasing thickness of the initial film. In a dewetting scenario the most prominent in-plane length is given by the distance between isolated drops [2]. In addition the drop diameter and the drop distance are correlated. With decreasing drop distance the drop diameter decreases as well and frequently the denotation drop is replaced by droplet. To enter the regime of nanostructures the initial films used have to have extremely small thicknesses. In many systems these films are prepared by spin coating. Due to the film thickness which is small as compared to the radius of gyration of the unperturbed molecule, the films are confined with respect to the spatial dimension perpendicular to the substrate surface. Common destabilization techniques are the annealing above the glass transition temperature or the storage under a solvent atmosphere [3].

Surface structures right after the spin coating process are an usual phenomena in thin blend or diblock copolymer films [4]. Anyhow, most of these structures are rather large with typical lateral length scales in the order of several micrometers. In the present investigation we present the possibility to gain nanostructured polymer surfaces right after the spin coating by just following the similar rout which usually works in dewetting systems: Decreasing the film thickness by decreasing the polymer concentration in the solution used for the spin coating.

As model system we chose a symmetric poly(styrene-block-isoprene) diblock copolymer, denoted P(S-b-I), with a molecular weight of 13k. The investigation of the surface structures in real space was performed with scanning force microscopy, depicting the surface topography. To learn about possible internal structures inside the nanostructures we used an advanced scattering technique: Grazing incidence small angle x-ray scattering and grazing incidence ultra-small angle scattering. Due to extremely small scattering volume of the polymeric nanostructures these experiments were restricted to synchrotron radiation.

The grazing incidence small angle x-ray scattering (GISAXS) measurements were performed at the BW4 USAX beamline of the DORIS III storage ring at HASYLAB/DESY in Hamburg. Thus the common transmission geometry was replaced by a reflection geometry and the sample was placed horizontally on a two-circle goniometer with a z-translation table. Only one Be-window separated the storage ring from the detector side. By avoiding any additional windows the background was minimized. The selected wavelength was 0.15 nm. The scattered intensity was recorded with a two dimensional detector which consists of a 512x512 pixel array. To enlarge the accessible wave vector range two different sample-detector distances were operated. At a small distance of

1.9 m length scales between 6 and 380 nm can be resolved (GISAXS) and at a large distance of 12.8 m this interval is shifted to 39 and 2500 nm (GIUSAX) respectively. The beam divergence in and out of the plane of reflection was set by two entrance cross-slits. At one fixed angle of incident the two-dimensional intensity distribution can be cut in several vertical and horizontal slices with respect to the sample surface. Vertical slices contain mainly scattering information from structures perpendicular to the sample surface, whereas horizontal slices contain only scattering contributions with an in-plane information. Thus for the investigation of surface morphologies we restrict ourselves to horizontal slices, which are frequently called 'out-of plane-scans'.

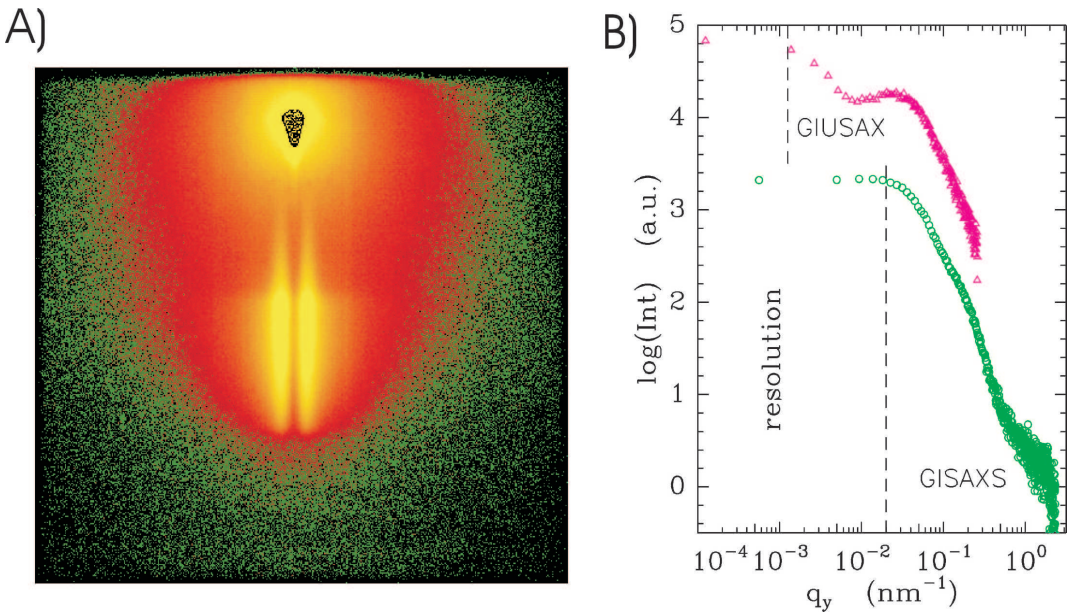

Figure 2.1:
A) Typical 2D scattering data obtained in the GIUSAX set-up. B) Out-of plane scans for surface structure determination as measured with AFM, x-ray and neutron techniques. b) Example of scattering data collected at two different sample-detector distances. From the GISAXS to the GIUSAX experiment the sample-detector distance was increased from 1.9 to 12.8 m. For clarity the curves are shifted along the y-axis. The dashed lines mark the resolution limits of both set-ups. [5]

Figure 2.1a exhibits a typical 2D scattering picture as obtained in the GIUSAX set-up. The specular and the Yoneda peak exhibit a strong scattering signal. Due to the high in-plane resolution and the presence of a nano-structured surface with a most prominent in-plane length within this resolution limit, the Yoneda peak is split up in its horizontal direction. Figure 2.1b shows an example of 'out-of plane-scans' collected at two different sample-detector distances. From the GISAXS to the GIUSAX experiment the sample-detector distance was increased from 1.9 to 12.8 m. Whereas the nano-structure is easily resolved in the GIUSAX set-up in the relaxed resolution of the GISAXS set-up it is no longer detectable from the position of a peak in the scattering data. On the other hand the GISAXS data includes the q_y-range corresponding to the intrinsic length related to the micro-phase separation L_o. In case of a symmetric diblock copolymer from the micro-phase separation a lamellar structure is expected [4], which gives rise to an internal length, since both blocks polystyrene and polyisoprene differ in their electron density. From the absence of such a peak it can be concluded that no perpendicularly arranged lamellae is present inside the

nano-strcuture [3]. Combining both information we obtain a statistical description of the surface structure: Objects are located in a mean next neighbour distance giving rise to a structure factor signal. Neither a form factor nor an internal length scale are detected. Visualised by atomic force microscopy, droplets of polymeric material are sitting on top of the silicon surface yielding a structure factor signal. The mean diameter of the droplets is varying which suppresses the form factor information.

[1] P. M¨uller-Buschbaum, J. S. Gutmann, M. Stamm; Phys. Chem. Chem. Phys. **1**, 3857 (1999)

[2] F. Brochard-Wyart, J. Daillant; Can. J. Phys. **68**, 1084 (1990)

[3] P. M¨uller-Buschbaum, M. Wolkenhauer, O. Wunnicke, M. Stamm, R. Cubitt, W. Petry; Langmuir **17**, 5567 (2001)

[4] I. W. Hamley, *The Physics of Block Copolymers*, Oxford University Press (1998)

[5] P. M¨uller-Buschbaum, N. Hermsdorf, J. S. Gutmann, M. Stamm, S. Cunis, R. Gehrke, W. Petry; to be published

Dewetting of Confined Diblock Copolymer Films

P. Müller-Buschbaum, S. Loi, E. Maurer, A. Götzendorfer, R. Cubitt [1]

[1] ILL, Grenoble

Engineered nanostructures like quantum dots, nanowires, nanotubes or nanolayers are of strong interest for basic research as well as with respect to future applications. This includes the option of new properties due to surface effects and size reduction down to a regime in which a characteristic length scale of a physical phenomenon becomes comparable with the typical length scale of the nanostructure. As a consequence the control of nano-structured surfaces marks the first basic step. Complementary to lithographic patterning techniques the creation of nanostructures due to self-organization has become increasingly important. Following the approach of soft-lithography structures down to several 10 nm are accessible and most likely these techniques are utilized for the creation on an isotropic surface pattern comparable to the common resist technique in semiconductor industry. Isotropic structures are easily created by the concept of self-assembly. While phase separated surface structures in polymer blend films are typically of micrometer size, microphase separation in diblock copolymer systems is well known to offer nanostructures in the bulk as well as in thin films [1]. Recently, it was shown, that from a destabilization of confined ultra-thin films nano-structured polymeric surfaces result as well [2]. Following the scaling laws of dewetting due to the reduced amount of polymeric material available, the size of the resulting structures decreases with decreasing film thickness. Destabilizing confined ultra-thin diblock copolymer films thus offers the opportunity to introduce two intrinsic lateral length scales, the characteristic periodicity of the micro phase separation structure L_o and the most prominent in-plane length of the dewetting structure L. For a large range of molecular weights of the diblock copolymers $L_o < L$ is fulfilled and the primary structure is given by the dewetting process. The resulting structure are pancake shaped droplets with an internally periodically arranged micro phase separation structure [3]. As usual for self-assembled structures it is isotropic which is helpful for many applications like sensors or templates (function does not depend on the orientation of the structure) [4]. In case, not only the characteristic lateral length have to be controlled but in addition the type of structure installed at the surface is of importance, final dewetting states are no longer

sufficient. Due to the minimization of the contact line area the final dewetting state is given by a drop which degenerates in case of ultra-thin films into a pancake shaped droplet. However, since there is no need to restrict only to final states, with the presented investigation we address the intermediate states which are accessible during the destabilization process.

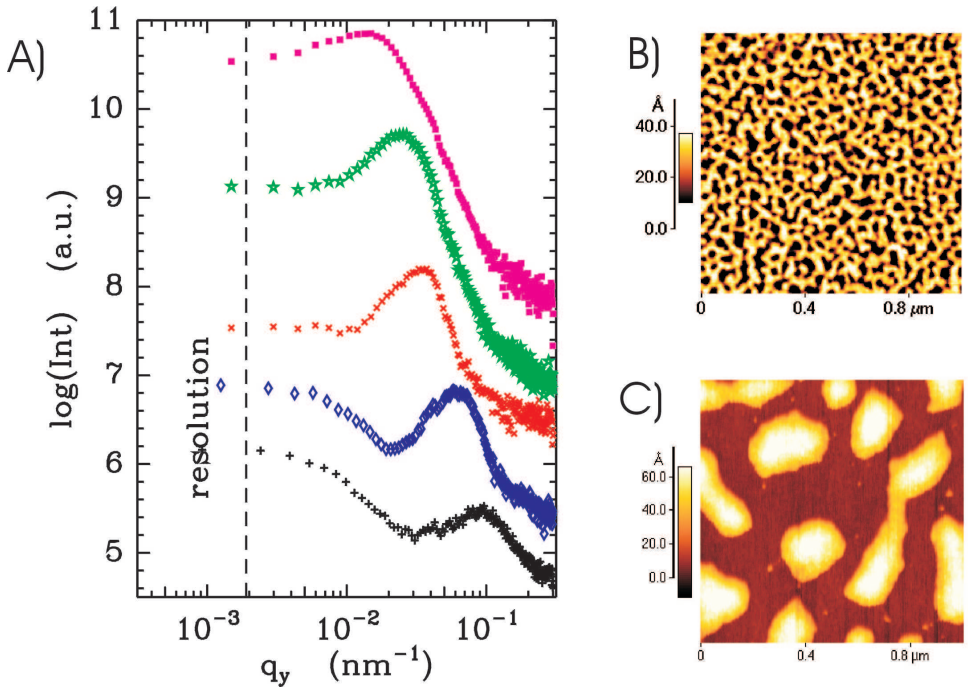

Figure 2.2:
A) Double logarithmic plot of GISAXS data from samples stored under toluene atmosphere. From the bottom to the top the storage time increases (t=1, 2, 3, 4 and 12 hours). The dashed line indicates the resolution limit. All curves are shifted along the y-axis for clarity. B) AFM picture of the surface after 1h. C) AFM picture after 4h with a markedly changed surface topography - a fixed scan range is shown [3].

The diblock copolymer poly(styrene-block-paramethylstyrene), denoted P(Sd-b-pMS) was prepared anionically (Polymer Standard Service, Mainz). The nearly symmetric P(Sd-b-pMS) has a fully deuterated polystyrene block and a protonated polyparamethylstyrene block. The degree of polymerization of the PSd block compared to the total chain is 47 %. After the spin coating homogeneous P(Sd-b-pMS) films result. Its thicknesses as measured with X-ray reflectivity were 1.5 nm, which is very small as compared to the radius of gyration in the bulk 13.6 nm. The homogeneity of the film is checked with atomic force microscopy and from the small value of the surface roughness (on the order of 0.5 nm) obtained from the X-ray data. To destabilize the initially homogeneous films, the samples are stored under toluene vapor for a fixed time interval. Storage times of 1, 2, 3, 4 and 12 hours were taken. After this exposure time, the samples were quenched to ambient air and examined.

The grazing incidence small angle x-ray scattering (GISAXS) measurements were performed at the BW4 USAX beamline of the DORIS III storage ring at HASYLAB/DESY in Hamburg. The selected wavelength was 0.138 nm. The scattered intensity was recorded with a two dimensional detector which consists of a 512x512 pixel array. A sample-detector distance of 12.7 m was chosen to resolve large in-plane structures. The beam divergence in and out of the plane of reflection

was set by two entrance cross-slits. At one fixed angle of incident the two-dimensional intensity distribution can be cut in several vertical and horizontal slices with respect to the sample surface. For the investigation of surface morphologies we restrict ourselves to horizontal slices, which are frequently called out-of plane-scans.

Figure 2.2A shows GISAXS data. Data measured at different destabilization times are compared. From the bottom to the top the storage time under toluene vapour increases. Irrespective of the annealing time all GISAXS data show a peak, which shifts towards smaller q_y values with increasing toluene atmosphere storage time. Thus with ongoing destabilization the evolving structures are increasing in their lateral size. In addition, the peak height increases which results from an increased scattering contrast. During the destabilization the height of the structures increases as well. In real space this is nicely pictured with AFM (see figure 2.2B, C). Already after 1 hour storage time (figure 2.1B) a nano-structured surface has evolved. A highly interconnected network of ribbon like structures covers the substrate surface. This nanostructure observed in the early state of structure creation is basically determined by the dimensions of the diblock copolymer molecules itself. It marks a sort of lower limit with respect to the size unless only single chains are addressed. After 4 hours of storage time (figure 2.1C) this ribbon structure is broken into isolated droplets.

[1] T. P. Russell; Science **297**, 964 (2002)

[2] P. M¨uller-Buschbaum, M. Wolkenhauer, O. Wunnicke, M. Stamm, R. Cubitt, W. Petry; Langmuir **17**, 5567 (2001)

[3] P. M¨uller-Buschbaum, R. Cubitt, W. Petry; to be published

[4] G. Bauer, F. Pittner, T. Schalkhammer; Mikochim. Acta **131**, 107 (1999)

Wetting behavior of thin polymer films on rough surfaces: A grazing incidence small-angle x-ray scattering study

P. Volodin [1], N. Hermsdorf [1], P. Panagiotou,T. Titz, P. Müller-Buschbaum, M. Stamm [1]

[1] Institut f¨ur Polymerforschung, Dresden

The stability of thin polymer films on solid substrates is an interesting phenomenon from the technological and scientific point of view. Polymeric coating, paints, lubrication of thin films, lithography, dielectric layers are often used in different modern technologies.

In principle, two kinds of instability of a thin film on a solid substrate are distinguished [1]. Spinodal dewetting is caused by amplified fluctuations of the film surface in field of repulsive interactive forces between the solid substrate and the films. In this case, the film is unstable. Nucleated dewetting is the rupture of the film due to a contamination or impurities on the substrate surface. In the past, spinodal dewetting of unstable thin films on smooth substrates was well studied. Dewetting of unstable thin films on physically and chemically heterogeneous substrates has been analysed [2,3]. If interactive forces between a film and a substrate are changed from repulsive to attractive forces along the film thickness the film becomes metastable [4]. In this case, spinodal dewetting is not observable. Break-up of the film can be caused by nucleation only. In reported study we investigate the stability of metastable polystyrene films on physically heterogeneous substrate surfaces.

As substrates we used different treated silicon wafers. The silicon wafers were washed in ammonium peroxide solution (NH_3 40 %, H_2O_2 40 %, H_2O 20 %) and rinsed several times with Milli-Q water. Then the substrate were etched in 20 % KOH-methanol solution in an ultra sonic bath at temperature 600^o C for several minutes. After etching, samples were washed several times in methanol, then in piranha (H_2SO_4 30 %, H_2O_2 70 %) and ammonium peroxide solution (NH 40 %, H_2O_2 40 %, H_2O 20 %) followed by rinsing with Milli-Q water. Control of roughness of these substrates was carried out by atomic force microscopy measurements at scan ranges of typically 25 μm x 25 μm. The root mean square (RMS) roughness parameter of the silicon surfaces etched with 20 % KOH-methanol can be varied within a range between 10 to 80 nm. In order to prepare samples with roughness smaller than 20 nm we changed the solvent for our etching conditions from methanol to ethanol. Etching in 20 % KOH-ethanol solution was applied in ultra sonic bath at temperature 60^o C for several minutes. In this case, the roughness of 20 % KOH-ethanol etched silicon surfaces ranges between 3 to 20 nm.

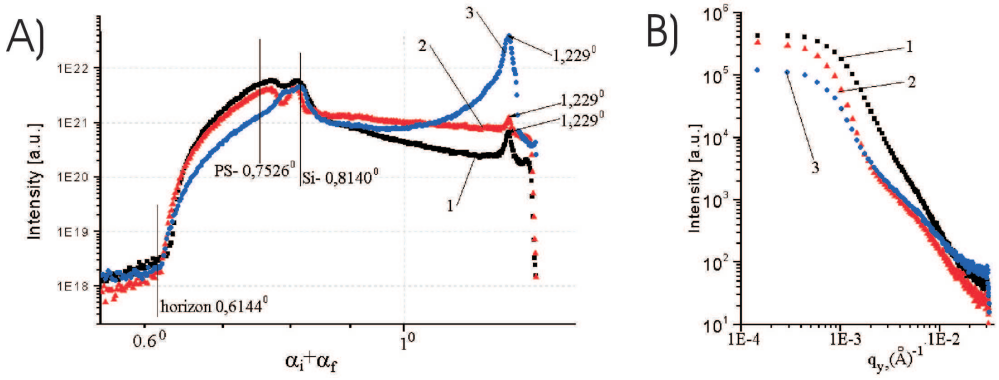

Figure 2.3:
Detector scans (A) and out-of plane scans (B) for polystyrene films of GISAX measurement of samples with roughness of virgin substrates RMS=12 nm: 1- non treated sample after spin coating, 2- annealed sample during 1 hour, 3-annealed sample during 84 hours.

The etched wafers were divided into groups of three samples with identical roughness. An additional group of three non-etched smooth clean silicon wafers was prepared as reference samples. Next the samples were cleaned in ammonium peroxide solution then in piranha . Polystyrene films (M_w=11k, M_w/M_n = 1.343) were spin coated on top of the cleaned substrates. To define the conditions of spin coating for rough substrates we have spin coated a polystyrene film of 30 nm thickness on a smooth non-etched silicon substrate. The thickness was obtained by ellipsometer measurement. Spin coating was carried out with 1 % polystyrene toluene solution with speed 2730 rpm.

After spin coating the first sample from each group was annealed for 1 hour at a temperature of 130^o C and the second sample of each group was annealed for 83 hours at 130^o C. The third sample of each group was not treated at all.

The atomic force microscopy (AFM) study of polystyrene films on rough surfaces (corresponds to 30 nm thick polystyrene film on smooth surfaces) indicated no spinodal dewetting. After spin coating of polystyrene, the power spectral density functions calculated from the AFM measurements exhibits a decrease in the power of the short wavelength part (less then 3 μm) compared with the origin etched surface without polystyrene. The surface of the polystyrene film on top of a rough silicon substrate is smoother than the surface of the original substrate. However, the polystyrene

film repeats big structural features (more than 5μm). After annealing of the polystyrene films, we observe a continuous decrease of the short wavelength part of the power spectral density. Due to the annealing of the polystyrene film the surface becomes smoother compared with an untreated polystyrene film. The grazing incidence small angle x-ray scattering (GISAXS) measurements were performed at the BW4 USAX beamline of the DORIS III storage ring at HASYLAB/DESY in Hamburg. We used a set-up of high-quality entrance slits and a completely evacuated pathway. The two-dimensional 512x512 pixels array detector was used. Distance between sample and detector was chosen to be 12690 mm. The angle of incidence was aligned to be 0.6144^o.

The specular reflected beam is observable at exit angles $\alpha_f = \alpha_i$. At $\alpha_f = \alpha_c$ the Yoneda peak is measured. Due to the dependence of the Yoneda peak position on the electron density the position is characteristic for the material illuminated with the x-ray beam. Slices with α_i=const. and α_f=const. are called out-of plane scans. These scans only include information about lateral structures. At a fixed incident angle of α_i=0.6144^o the prominent features in a detector scan, the specular as well as the Yoneda Peak are well-separated. The specular peak showed a strong decrease in its intensity with increasing surface roughness. At a rms-roughness of 12 nm it was completely vanished at the chosen angle of incidence. As a consequence, with increasing roughness the diffusely scattering intensity increases as well. Figure 2.3a shows the detector scans for a fixed medium surface roughness (1- non treated sample, 2- annealed sample during 1 hour and 3-annealed sample during 84 hours) exhibiting marked differences. In the view of our AFM study, the decrease in the intensity at the position of the Yoneda peak corresponding to PS can be explained by the decrease of the rms- surface roughness for polystyrene films during annealing above glass transition temperature. The corresponding out-of plane scans are shown in figure 2.3b. While the untreated film is characterized by a power-law decay of the intensity due to the roughened surface, in the annealed PS film already a first indication of a dominant in-plane length is present. With ongoing annealing its lateral length is not modified, but becomes more pronounced.

[1] F. Brochard-Wyart, J. Daillant; Can. J. Phys. **68**, 1084 (1990)

[2] K. Kargupa, R. Konnur, A. Sharma; Langmuir **16**, 10243 (2000)

[3] K. Kargupa, A. Sharma; Langmuir **18**, 1893 (2002)

[4] R. Seemann, S. Herminghaus, K. Jacobs; Phys. Rev. Lett. **86**, 5534 (2001)

New composite materials: magnetic nanoparticles in copolymer films investigated by specular and off-specular neutron scattering

V. Lauter-Pasyuk, H. J. Lauter [1], G. P. Gordeev [2], P. Müller-Buschbaum, B. P. Toperverg [3], W. Petry

[1] ILL, Grenoble
[2] PNPI, Gatchina
[3] IFF J¨ulich

We performed detailed studies of new composite lamellar films including a high concentration of nanoparticles. It is shown that the diblock copolymer polystyrene-block-polybutylmethacrylate P(Sd-b-BMA) multilayer orders the assembly of PS-coated Fe_3O_4 nanoparticles into a lamellar array along the PS layers of the host matrix. The application of neutron specular reflection and

off-specular scattering accompanied by a two-dimensional data analysis allows a detailed description of the nanoparticles distribution inside the copolymer matrix. As a result, the parameters of the transverse and the lateral structure without as well as with incorporated magnetite Fe_3O_4 nanoparticles (with the average diameter of 5 nm) is yielded.

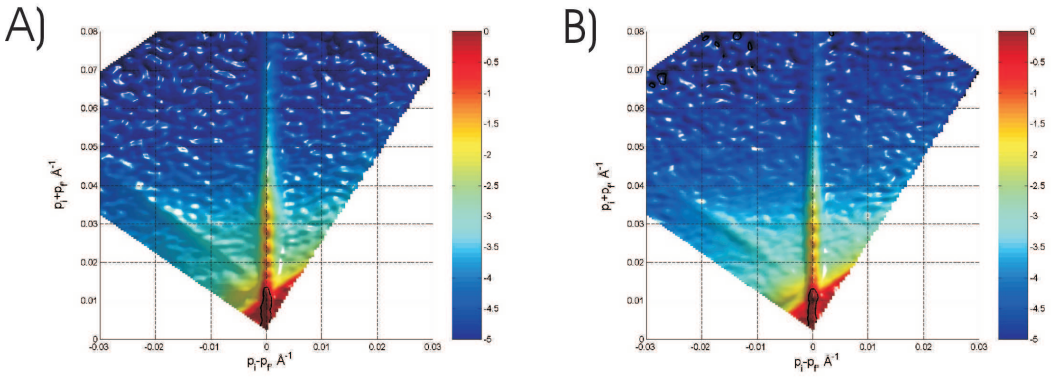

Figure 2.4:
A) Experimental 2-dimensional intensity map from not annealed samples of pure P(Sd-b-BMA) thin films and B) similar copolymer films with incorporated Fe_3O_4 nanoparticles; p_i and p_f are the components of the incoming and outgoing neutron wave vectors perpendicular to the surface, respectively. The strong intensity along the line $(p_i - p_f) = 0$ corresponds to the specular reflection, the Yoneda scattering intensity spreads to the left from the specular line.

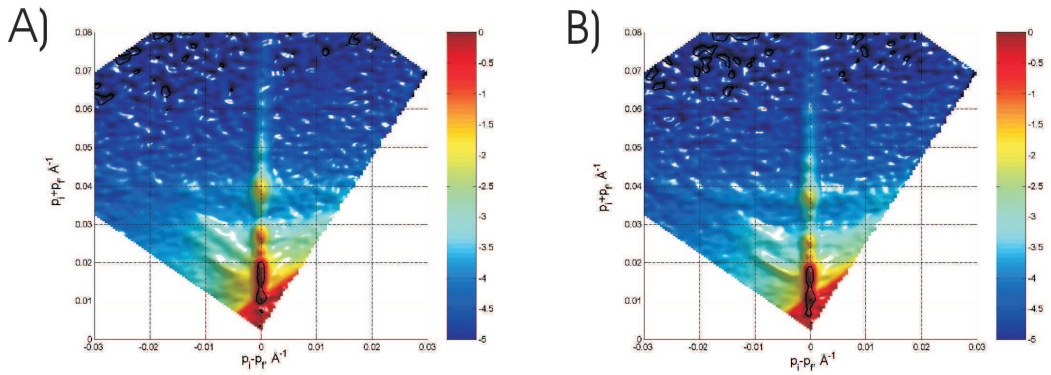

Figure 2.5:
Experimental 2-dimesional intensity maps from the samples as shown in the figure above, after annealing during 3 hours at a temperature T = 165^o C for (A) a pure diblock copolymer film and (B) a film including nanoparticles.

The diblock copolymers were dissolved in toluene and spin-coated on top of silicon substrates. The self-assembly of the copolymer matrix is determined by the non-miscibility of the two chemical components. The lamellae are oriented parallel to the substrate and the surface of the film and their thickness is given by $nL/2$ with n integer even and L the lamellar period (PBMA-PS-PS-PBMA). By coating the nanoparticles with one or another type of the polymer chains (prior to the adding to a toluene solution of the copolymer) we provide a control on the nanoparticle distribution within one or another part of the lamellar structure. We succeeded to incorporate Fe_3O_4 nanoparticles with the average diameter of 5 nm up to 7 % volume fraction. Even for a

high concentration, particles stay included in the film and the lamellar structure is not destroyed. Periodic location of the particles as well as the transverse and lateral structure of the lamellar pure copolymer and composite films was determined using neutron specular reflection and off-specular scattering. The presence of the nanoparticles induces distortion of the copolymer matrix. The neutron off-specular scattering contains valuable information about the internal structure of the film, including the nanoparticles distribution, the lateral structure of the roughness and its conformity though the lamellar multilayer as well as the surface structure of the film.

An earlier developed theoretical approach based on the Distorted Wave Born Approximation (DWBA) allows the description of a full 2-dimensional intensity map, including the dynamical range close to the total reflection region [1, 2]. The reflected and scattered intensities are depicted in figure 2.4 as a function of $(p_i + p_f) = Q_z$ and $(p_i - p_f)$ for the samples in the as prepared state. The specular reflectivity runs along the line $p_i - p_f = 0$ and shows regular oscillations, which are determined by the total thickness of the film. The off-specular intensity in a form of the Yoneda scattering spreads out left from the specular intensity line indicating the presence of the surface and the substrate roughness. After the annealing of the samples at a temperature T = 165^o C for 72 hours we repeated the measurements (see Figure 2.5). The reflected and scattered pattern has changed. The multilayer structure based on the parallel oriented lamellae causes the appearance of the Bragg peaks on the reflectivity line. The presence of the Bragg peaks for the sample with incorporated nanoparticles (Figure 2.5b) proves that the multilayer structure persists and is not destroyed by a rather high concentration of the nanoparticles. However, the positions of the Bragg peaks are shifted towards smaller values of Q_z, indicating the increase of the lamellar period due to the presence of the nanoparticles (see Figure 2.6). The pattern of the off-specular scattering has also changed after the annealing showing the Bragg sheets [4]. The off-specularly scattered intensity from the sample with nanoparticles does not change considerably, that proves a certain degree of conformity of the interfacial roughness.

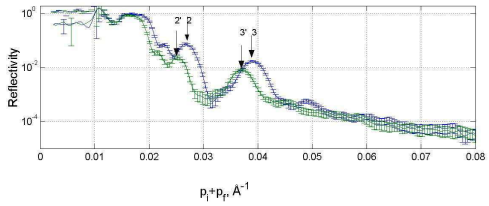

Figure 2.6:
Reflectivity profiles of the pure diblock coplymer film (right curve) and the film including nanoparticles (left curve) taken as vertical cuts along the line $(p_i - p_f) = 0$.

The two - dimensional fit to the experimental data was performed using the model described in details earlier [1-3].

This work was supported by the BMBF (grant No 03DUOTU1/4), NATO (Grant No. PST.CLG.976169).

[1] V. Lauter-Pasyuk, H. J. Lauter, B. P. Toperverg, O. Nikonov, A. Petrenko, D. Schubert, W. Petry, V. Aksenov; ILL Millennium Symposyum, 59 (2001)

[2] V. Lauter-Pasyuk, H. J. Lauter, B. P. Toperverg, O. Nikonov, A. Petrenko, D. Schubert, J. Schreiber, M. Burcin, W. Petry, V. Aksenov; Appl. Phys. A **74** (2002)

[3] B. Toperverg, V. Lauter-Pasyuk, H. J. Lauter, O. Nikonov, D. Ausserre, Y. Gallot; Physica B **283**, 60 (2000)

[4] V. Lauter-Pasyuk, H. J. Lauter, G. Gordeev, P. M¨uller-Buschbaum, B. P. Toperverg, M. Jernenkov, W. Petry; Langmuir submitted

Investigation of ultrathin polystyrene films

A. Götzendorfer, P. Müller-Buschbaum, W. Petry

The technological drive to place into service ever-thinner polymer films prepared on top of solid substrates has advanced beyond the current level of fundamental scientific understanding. In applications such as adhesion, dielectric isolation, and lubrication, successful performance can depend critically on the details of the thin film behaviour. One of the basic questions concerns the properties of homogeneous films thinner than the extension of a single polymer molecule in the melt given by the radius of gyration R_g.

Utilizing the experimental technique of spin-coating it is possible to produce such films. Recent pioneering experiments [1] suggest a lower limit for the achievable thickness of homogeneous films of about $1/3\,R_g$. We now tackle the task of exploring this frontier in a more systematic way. Our special interest aimed at the dewetting patterns obtained when the "films" fell below the critical thickness for dewetting. In contrast to other experimentalists who study the dewetting process upon annealing [2,3] we are interested in the surface structure directly after spin-coating the polymer.

We studied monodisperse polystyrene films on silicon (100) surfaces covered with a native oxide layer. Before coating the substrates were etched at $85^{\circ}\mathrm{C}$ for 15 minutes in a bath of sulfuric acid, hydrogenperoxide and deionized water to remove residual hydrocarbons, then rinsed under deionized water and dried with compressed nitrogen. We prepared two series of films differing in the molecular weight of the polystyrene molecules ($M_w = 207\,\mathrm{kg/mol}$, $M_n/M_w = 1.02$, $R_g = 120\,\text{Å}$ and $M_w = 1350\,\mathrm{kg/mol}$, $M_n/M_w = 1.12$, $R_g = 330\,\text{Å}$). Polystyrene was spin-coated (2000 rpm) onto the substrates from toluene solution. Different film thickness were achieved by a variation of the polymer concentration in the solution used.

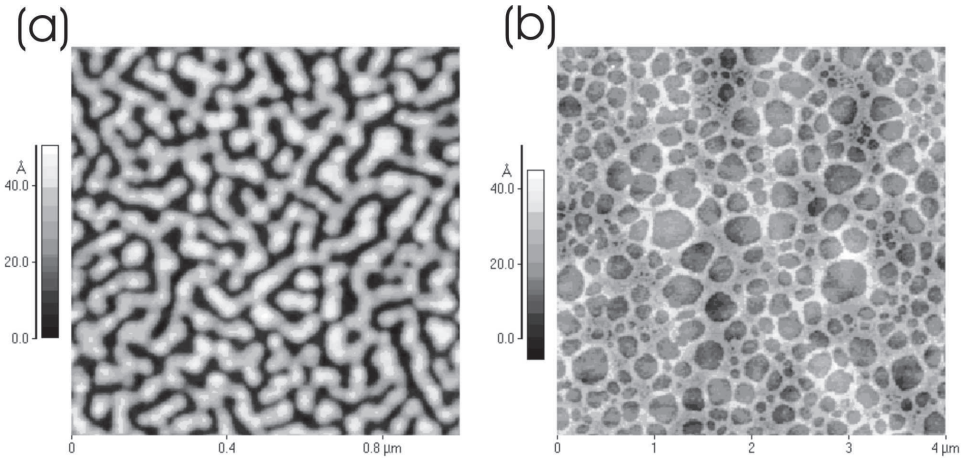

Figure 2.7:
AFM images of films spin-coated from solutions with PS concentration of 1.1 mg/3ml (a) and 0.44 mg/3ml (b)

For thick films far above the radius of gyration an empirical formula was reported by Schubert [4]. Thus the resulting film thickness h depends on polymer concentration in the solution c, on rotational frequency f of the spin-coater, and on the molar mass M_w of the polystyrene molecule.

$$h[nm] = A\Big(\frac{1950\,\mathrm{min}^{-1}}{f}\Big)^{1/2}\frac{c}{20\,\mathrm{mg/ml}}\Big(\frac{M_w}{100\,\mathrm{kg/mol}}\Big)^{1/4}$$

The empirical factor $A = 93.5\,\mathrm{nm}$ is device dependent and therefore different for other experimental setups.

In this investigation the validity of this relation between the polymer concentration and the resulting film thickness is checked in the range below the radius of gyration of the undisturbed molecule. Films were spin-coated out of solutions of polystyrene with $M_w = 207\,\mathrm{kg/mol}$ and concentrations between $0.10\,\mathrm{mg/3ml}$ and $36.97\,\mathrm{mg/3ml}$, which would result in films of thickness between $1.8\,\text{Å}$ and $682.5\,\text{Å}$ if all films were homogeneous and Schubert's formula as presented above would remain valid.

To determine the film thickness x-ray reflectivity measurements were carried out. Films spin-coated out of solutions with less than 1.1 mg/3ml polystyrene concentration do not show the typical features of a homogeneous film any more. This can be caused by the presence of marked surface structures. Films prepared out of solutions with higher concentrations are homogeneous and a parameter $A = 83.6\,\mathrm{nm}$ was determined. The thinnest film assumed to be homogeneous ($c = 1.1\,\mathrm{mg/3ml}$) had a thickness of $25\,\text{Å} \approx 1/5\,\mathrm{R_g}$.

To explore the transition region between homogeneous and dewetted state in more detail we took AFM images of the surfaces. They reveal that already the film spin-coated from the 1.1 mg/3ml solution shows strong surface undulations (figure 2.7a) resulting in the creation of small holes. Decrease of the polymeric material leads to larger holes until they form a sort of honeycomb pattern (figure 2.7b). Further material reduction forces a decay of the rims between adjacent holes and next the decay into droplets on the substrate at the lowest concentrations.

Characteristic length scales of the surface patterns can be determined by GISAXS measurements described in [1]. For the films showing the undulating pattern in the AFM images we obtain very well defined characteristic lengths which lie around 50 nm. The surface with the honeycomb pattern results in less pronounced characteristic lengths because the hole sizes are not uniform. At surfaces with less polymeric material almost no characteristic length can be seen.

[1] P. M¨uller-Buschbaum, J. S. Gutmann, M. Stamm: Phys. Chem. Chem. Phys. **1**, 3857 (1999)

[2] G. Reiter: Phys. Rev. Lett. **78**, 186101 (2001)

[3] R. Seemann, S. Herminghaus, K. Jakobs: J. Phys.:Condens. Matter **13**, 4925 (2001)

[4] D. W. Schubert: Polym. Bull. **38**, 177 (1997)

Gradient samples: heterogeneous polymer films

T. Titz, P. Müller-Buschbaum, W. Petry

Thin polymer films become more and more interesting for many high tech applications like functional coatings. For such application the controlled and customised design of films of polymer blends is getting higly important. Thus thin polymer blend films which show structures with a great range of length scales within the sample are one major aim.

A new way to prepare these structures is the use of gradients. Gradient samples are based on polymer blends and thus have three independent free variables within the system. In a blend of two homopolymers the external gradient is the third free variable. Gradients are introduced by temperature, film thickness and polymer blend ratio. Along the gradient local equilibrium structures will change steadily and therefore the gradient will introduce an artificial length on the structure of the observed system.

To produce a temperature gradient a temper-cell (figure 2.8) has been planned which is now under construction. The temper-cell is designed to work under inert gas or vacuum and the samples can be observed in situ with synchrotron radiation and optical microscopy by using a portable video microscope. The video microscope will be installed on top of the temper cell on a micro positioning system and will picture the sample surface through a glass window with a maximum magnification of 11.8.

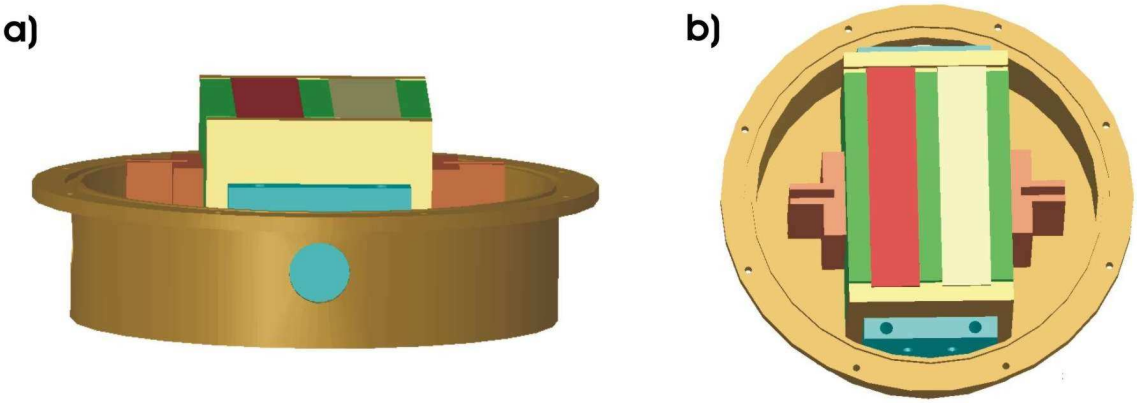

Figure 2.8: a) side view of the open temper-cell and b) top view, respectively

To produce the temperature gradient the sample is placed on two copper plates thermally separated by a teflon block. One copper plate is heated by a heating foil and the other copper plate is cooled by peltier elements to get a temperature difference through the sample. With regard to the temperature-time superposition the temperature gradient is equivalent to a time gradient and we will get different local phase separation or microphase separation structures.

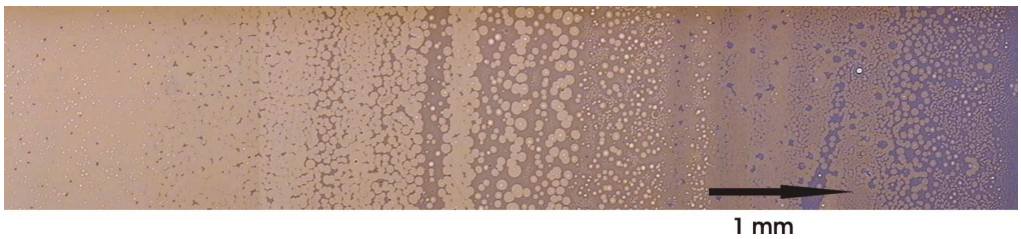

Figure 2.9:
Sample with film thickness gradient introduced by solution casting, film thickness is increasing from left to right

A second possibility for producing an external gradient is to change the film thickness, by using gravitational force. The easiest way is by tilting the substrate and than casting the polymer solution on the inclined substrate. Figure 2.8 shows a microscope picture of a sample casted under

gravitational force. The film thickness is increasing from left to right and the size of the structures is changing.

Investigation of thin films of diblock-copolymer/metal composites

J. S. Gutmann [1], P. Panagiotou, P. Müller-Buschbaum

[1] MPI f¨ur Polymerforschung, Mainz

Diblock-copolymers are a class of polymers in which two chemically different polymers are liked together via a covalent bond. Since polymeric systems are typically imiscible due to their very small entropy of mixing, both block of the block copolymer typically phase separate from each other. The size scale of the phase separation is however limited due to the additional topological constraint introduced by the covalent linkage between the two blocks. The structures resulting are extremely rich and span a phase range from cubic to hexagonal to lamellar structures. This phase behavior has found extensive use in the past in the creation of organic-inorganic composites via sol-gel chemistry [1] with a very high control over the morphology of the composites. Current work is now progressing toward the incorporation of metal into these composite materials, while retaining the established high degree of shape and size control.

In this study we addressed the possibility of metal incorporation into thin films of a poly-isoprene-block-poly-dimethylaminoethylmethacrylate (PI-b-PDMAEMA) copolymer. The block-copolymer had a molecular weight of 33113 g/mol and a polydispersity index of 1.03 as measured by GPC. The mole fraction of the PDMAEMA block was 0.18 resulting in a cubic arrangement of PDMAEMA spheres inside a PI matrix.

The thin films were prepared by spin-coating from toluene solutions onto silicon (100) wafers and had a typical film thickness of around 100 nm. Since the PDMAEMA block provides ternary amine groups as potential metal complexing ligands we used copper(II)chloride as a metal source. In order to incorporate the metal into the thin films we immersed the as spin-coated films in a 9.69 mmol metal salt solution.

Since the total amount of sample within the thin film is of the order of a few **?**g, it is not feasible to investigate these thin films in a transmission geometry SAXS experiment. We therefore used a set-up at the BW4 beam-line for ultra-low angle X-ray scattering under grazing incidence (GIUSAXS) [2]. The experimental set-up at the BW4 beam-line consisted of a 2D wire detector positioned at a distance of 12.7 m from the sample. In order to reduce the background the sample chamber and the sample-detector flight-tube were completely evacuated. The angle of incidence was kept constant during each measurement and was set to about 0.6^o. For more details about the beam-line see [3].

Figure 2.10a shows a typical 2D scattering image as obtained from the GIUSAXS experiments. On the top, the specular reflected peak is clearly visible. In the lower half an additional peak, the so called Yoneda peak is present, indicating that the thin films exhibits lateral structures. Furthermore the Yoneda peak is broadened along the horizontal from the presence of laterals structures within the resolution limit of the experiment.

In order to further analyze the scattering image, horizontal cuts through the Yoneda peak are taken. These so called out-of-plane scans probe only the q_y component of the scattering vector

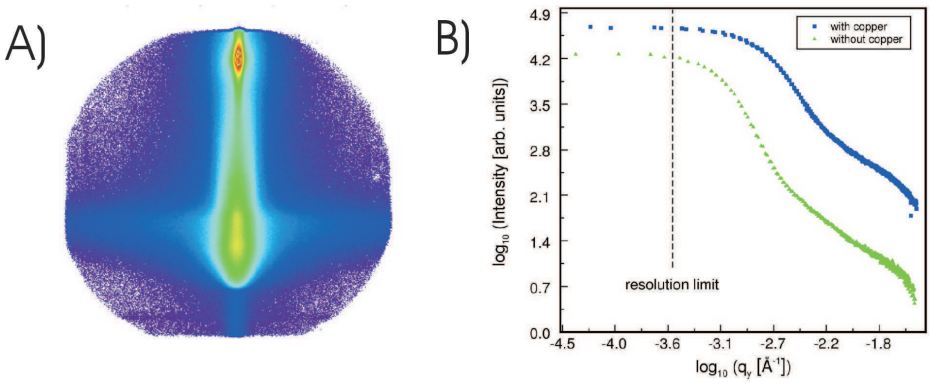

Figure 2.10:
A) Typical 2D detector image of a GIUSAXS experiment on a PI-b-PDMAEMA copolymer film containing copper(II) ions. The image is analyzed in terms of horizontal cuts (so called out-of-plane scans) with an in-plane resolution of 2.842*10^{-4} $Å^{-1}$. B) Comparison of the out-of-plane scans for a thin film before (lower curve) and after metal incorporation (top curve).

and are therefore only sensitive to lateral structures within the thin film. Figure 2.10b shows the comparison of two such out-of-plane scans from a thin film before and after metal incorporation. The curve for the metal containing film (top) is clearly shifted towards larger q-values, indicating the formation of lateral structures within the thin film. The absence of a clear cut-maxima suggests that the structures are polydisperse, however their average structure can be estimated to be of the order of 400 nm.

[1] P. F. W. Simon, R. Ulrich, H. W. Spiess, U. Wiesner; Chem. Mater. **13**, 3464 (2001)
[2] P. M¨uller-Buschbaum, J. S. Gutmann, M. Stamm; Phys. Chem. Chem. Phys. **1**, 3857 (1999)
[3] R. Gehrke; Rev. Sci. Instrum. **63**, 455 (1992)

Surface morphology of thin immiscible ternary polymer blend films investigated with GISAXS

P. Panagiotou, N. Hermsdorf [1], I. Tokarev [1], S. Mavila-Chathoth, S. S. Funari [2], A. Meyer [2], M. Dommach [2], P. Müller-Buschbaum,

[1] IPF, Dresden e.V.
[2] HASYLAB, Hamburg

For some decades the use of polymers increased rapidly due to their broad field of applications and competitive production. Meanwhile instead of synthesising new types of elaborated polymers, blends of commercial polymers are used. Since it is known that thin polymer films have different physical properties as compared to their bulk, they became increasingly interesting for research as well as technological usage.

In the presented investigation three different polymers (polystyrene PS, poly(α-methylstyrene) PαMS and 1,4-trans-polyisoprene PI) with different glass transition temperatures and different molecular weights were blended with toluene. Each polymer was solved separately at a mass

concentration of 1 mg/ml in toluene. Afterwards the solutions were mixed in a weight fraction of PS:PαMS:PI = 5:1:4. The native oxide covered silicon substrates were cut into pieces of (24x50) mm. The organic impurities on top of the surface were removed by a piranha bath for 15 min at 80^o C. Then the substrates were rinsed several times with deionised water and dried with compressed nitrogen. Subsequently the substrates were spin-coated at 2000 rpm for 33 sec using the ternary blend solution. Afterwards the samples were annealed at 85^o C at different times (0, 1, 3, 5, 7, 10, 20, 30, 40, 50, 75, 100, 300 and 500 min) to investigate the mechanism of phase separation of thin films [1, 2]. This procedure leads to a relaxation of the individual substance towards equilibrium of the morphology [3, 4]. Consequently due to the chosen temperature, which is above the glass transition temperature of PS and sufficiently above the one of PI but below the one of PαMS varying domain structures with different in-plane length scale ξ results. Basic origin is an immobility of PαMS, while PI and PS stay mobile.

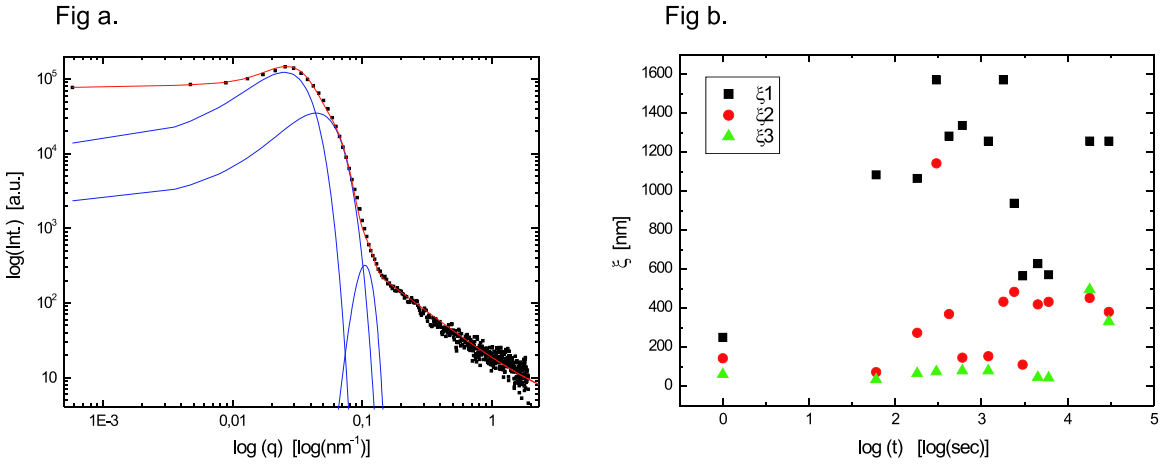

Figure 2.11:
a) Typical GISAXS cut with a fit of the data with a model explained in the text and b) resulting lateral length scales as a factor of the annealing time.

The technique of grazing incidence of small-angle x-ray scattering (GISAXS) was performed to get information about the surface structure and the inner film morphology [5]. With GISAXS a statistical statement about the observed length scales is resulting. The GISAXS measurements were realised at the A2 beamline of the Doris III storage ring at the synchrotron radiation facility HASYLAB/DESY at Hamburg, Germany. The selected wavelength was λ = 0.15 nm and the sample-detector distance was 2023 mm. Within the utilised reflection geometry, the sample was placed horizontally on a two circle-goniometer attached on a z-translation table with a fixed angle of α_i = 1.2^o to the incident beam. The complete pathway of the beam was evacuated and a beam stop was installed. An image plate with an array of 1024x1024 pixel was used to record the specular as well as the non-specular intensity (like the Yoneda-peak). From this 2-dim intensity distribution typical vertical (so-called detector) and horizontal (so-called out-of-plane) cuts were performed. For the position of the out-of plane cuts the critical angle of the mobile polymers PS (0.150^o) and for PI at (0.142^o) was chosen. From this data the dominant in-plane length scale ξ as function of the annealing time was calculated.

This calculation is based on a fitting procedure including the structure factor, the microscopic structure and the resolution limit. Due to the ternary blend multiple length scales evolves, which gives rise to more than one structure information. Figure 2.11a shows the typical example of

GISAXS cut. The solid lines are the resulting fit and the extracted structure factor information. In this particular case three different length scales were detected. Figure 2.11b exhibits the obtained structure factor information as function of the annealing time. Clearly three different length scales can be separated.

On a first view the value of these length scales seems to be independent of the annealing time. It should be noted anyhow with AFM and optical microscopy its change in the surface structures was observed. In addition the GISAXS signal changes drastically during annealing time. Therefore the obtained structure information at different times corresponds to different real space structures. In a detailed assignment the values obtained from AFM have to be linked to the data obtained from the GISAXS experiment. Only with the help of the real space information an understanding of the kinetic phase separation process is possible. This behaviour is quit typically for complex blend systems like ternary blends.

[1] K. Binder: Journal of Chemical Physics **79** (12), 6387 (1983)

[2] G. Krausch: Material Science and Engineering **R14** (1), 1 (1995)

[3] P. M¨uller-Buschbaum, J. S. Gutmann, M. Stamm: Macromolecules **33**, 4886 (2000)

[4] S. Walheim, M. Ramstein, U. Steiner: Langmuir **15**, 4828 (1999)

[5] P. M¨uller-Buschbaum, J. S. Gutmann, R. Cubitt, M. Stamm: Colloid and Polymer Science **277**, 1193 (1999)

In-situ USAX and GISAXS investigation of adhesive polymers film properties

S. Loi, E. Maurer, A. Götzendorfer, P. Müller-Buschbaum

The adhesion between different polymers as well as between polymer and nonpolymer surfaces is important for a wide range of applications. In many cases a high adhesion is required, like in the glue industries or coating and paint techniques. On the other hand, some adhesives combine the high tackiness with the ability to be removable. The pressure sensitive adhesives (PSA) belong to this class of adhesives and allow the bond formation by simple contact with the surface [1]. Examples from the everyday life are stick-on-notes or adhesives stickers. The peculiarity of the PSA is that the tackiness depends strongly on the bond history, which means on parameters like contact pressure, contact time, temperature and debonding rate [2, 3]. It has been observed that the surface roughness and topology greatly affect the tack energy, too [4]. This is attributed to the restriction of the true area of contact between probe and polymer film. In practise, the tackiness is tested by the following procedure (figure 2.12a): The adhesive film is deposited on a glass substrate and a flat ended cylindrical punch is brought into contact with the adhesive, under certain values of pressure and contact time. Then the probe is withdrawn from the surface with a constant velocity. The measured force presents a strong peak and does not fall to zero but rather stays essentially constant, till the probe finally separates from the film at a relatively high probe-sample distance. Corresponding to the region of constant force, the adhesive film splits into separate filaments or fibrils that are elongated giving rise to a plateau in the force. The measured force versus distance curves allow a mechanical characterisation of the adhesive. Anyway the debonding phase and fibrils formation are not quantitatively explained. In order to achieve information on a microscopic scale, we perform experiments with x-ray scattering during the debonding phase.

The PSA films consist of blend of 10% polystyrene (PS) and 90% poly(n-butylacrylat) (PnBA). They are prepared by solution casting. In the utilised thin film, a phase separation occured inducing

the creation of surface morphology. The dimension of the structures is on the order of 50 μm, as estimated from optical micrographs. The probe (a glass cylinder of 2 mm diameter) was pressed with a force of 6 N onto the PSA film surface and after 10 sec it was withdrawn for 100 μm from the film surface. The scattering measurements were performed at several probe-film distances. This yields information of possible substructures of fibrils as a function of the probe-film distance.

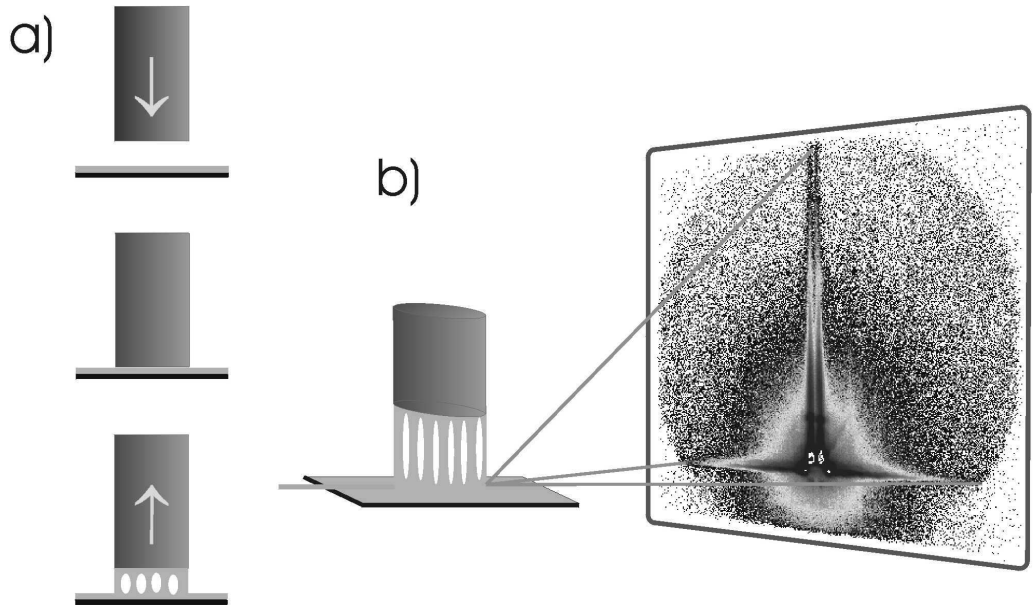

Figure 2.12:
a) The tack test consist of three steps: at first, the probe is brought into contact with the PSA film; then, it is pressed onto the film with a certain force and for a certain contact time; finally, it is retracted from the film at a constant velocity. b) Schematic of the experimental set-up and a typical scattering image. The fibrils forming during the debonding process are perpendicular to the film surface. The transmission signal is detected in the horizontal direction and parallel to the film surface.

For the first time a combined in-situ ultra small angle x-ray scattering (USAX) [5] and grazing incidence small angle scattering (GISAXS) [6] experiment was performed. The measurements were taken at the BW4 beamline of the DORIS III storage ring at HASYLAB/DESY in Hamburg. A sample-detector distance of 13.2 m allows to detect scattering with an angular range up to 0.5°. The selected energy was 8.979 keV. The scattered intensity was recorded with a two dimensional detector which consists of a 512x512 pixel array. A centred beam stop avoids that the primary beam used for the transmission geometry damages the detector. The beam was splits in that way that part of it transmitted the sample in the common USAX way and the rest of the beam probed the surface properties in GISAXS. Due to the angle of incidence of zero degree in the GISAXS geometry only the diffuse scattering signal results. As a consequence simultaneously surface information and bulk film information were collected on one detector picture. This allows a correlation between properties parallel to the surface and perpendicular to it.

Figure 2.12b represents a schematic of the experimental set-up and a typical scattering image. The fibrils formed perpendicular to the polymer surface. Located at the bottom of the detector and in the horizontal direction (parallel to the film surface), the scattering from the fibrils is observable. In the middle of the horizontal signal the primary beam is covered by the beam stop. The horizontal

cut through the position of the primary beam displays information from the fibrils structure as in common USAX experiments. Along the vertical direction the GISAXS signal is located. At the critical angle of the sample the Yoneda peak is observed. Its horizontal intensity decay shows marked modulation carrying information about the structure parallel to the surface. A detailed data analysis is in progress.

[1] H. Lakrout: Adhesion **69**, 307 (1999)

[2] C. Creton, L. Leibler: J. Polym. Sci. **34**, 545 (1996)

[3] A. Zosel: J. Adhesion Sci. Technol. **11**, 1447 (1997)

[4] K. N. G. Fuller, D. Tabor: Proc. R. Soc. Lond. **A.345**, 3275 (1975)

[5] U. Lode, T. Pomper, A. Karl, G. von Krosigk, S. Cunis, W. Wile, R. Gerke: Macromol. Rapid Commun **19**, 35 (1998)

[6] P. M¨uller-Buschbaum, M. Casagrande, J. Gutmann, T. Kuhlmann, M. Stamm, G. von Krosigk, U. Lode, S. Cunis, R. Gehrke: Europhys. Lett. **42(5)**, 517 (1998)

Microscopic properties of adhesive polymer films

E. Maurer, S. Loi, A. Götzendorfer, P. Müller-Buschbaum

Most glues typically are based on polymers. One way to distinguish them is based on the durability of the connection created by the glue. Either a permanent connection between two interfaces is formed by a chemical bonding or a controlled bonding and debonding is allowed. Pressure sensitive adhesives (PSA) are of the second type [1,2]. Examples in daily life are adhesive stickers, Scotch tape or stick-on notes. Beside these industrial applications PSA are of interest in basic research, too. Characteristic of PSA is a sensitivity of the adhesion on the bonding history. Beside the material characteristics of the applied polymer there is a number of parameters determining the quality of the adhesion. Examples are the force applied to press the interfaces together, the contact time during which the force is present or the temperature. In order to debond the interfaces, a characteristic force has to be applied as well. The value of this force is a function of all the bonding parameters and in addition of the parameters characterizing debonding like the retracting velocity. Frequently, fibrils are created between the former connected interfaces during the debonding [3,4,5]. Up to now, no fundamental understanding of the fibrils role in the debonding process is established.

Especially, the microscopic properties of the creation and failure of fibrils is of great interest. A macroscopic understanding is usually performed by mechanical testing experiments [4,6,5]. In the so-called tack test the debonding process is quantified in terms of force versus distance (in-between interfaces) curves. The tack test can be subdivided into three steps (see figure 2.13A). First a probe punch, like a flat-ended glass cylinder is pressed onto a polymer film with a defined force. Second, the force is maintained for a defined time. Finally, in order to study the debonding the prope is retracted from the film with a constant velocity. During the process the force versus distance curve is recorded. Normally, the curve shows characteristic features as a maximum force and a force plateau. This plateau is caused by the stretching of fibrils. In order to find a possible microscopic substructure of the fibrils we investigate the debonding with x-ray scattering. PSA films of 0.20 polymethylmethacrylat (PMMA) and 0.80 polyethylhexylacrylat (PEHA) were prepared by solution casting. A glass cylinder of 2 mm diameter was pressed with a force of 6 N onto the PSA film surface. After 10 sec the debonding process was started. At several probe-film distances the

scattering measurement was performed. This yields to information of possible substructures of fibrils as a function of the probe-film distance. In scattering experiment a transmission geometry was used. In order to detect length scales of several nanometers we utilized ultra small angle x-ray scattering (USAX).

The measurements were performed at the BW4 beamline of the DORIS III storage ring at HASYLAB/DESY in Hamburg. A sample-detector distance of 13.2 meter allows to detect scattering with an angular range below 0.5 . The selected energy was 8.979 keV. Two entrance cross-slits set the beam divergence. The scattered intensity was recorded with a two dimensional detector which consists of a 512x512 pixel array. A centered beam stop avoids that the primary beam is detected. A calibration resulted from a lupolen test measurement. The tack geometry forces the fibrils to be perpendicular to the film surface. The film is placed horizontally and thus we are only interested in the horizontal signal on the detector (see figure 2.13B). As a consequence horizontal cuts through the position defined by the primary beam display the information.

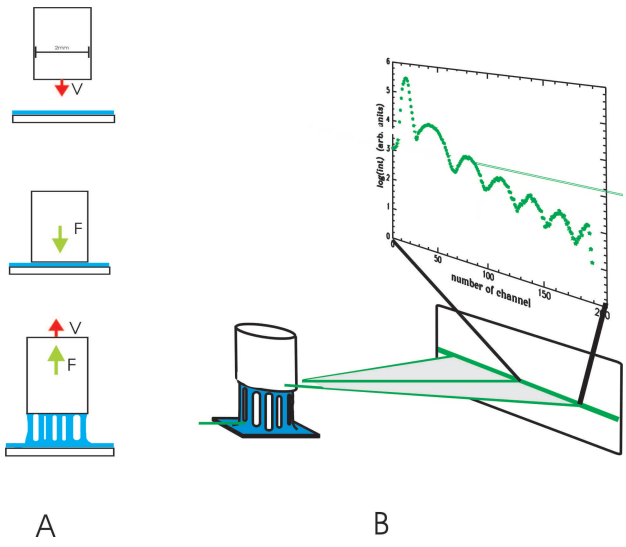

Figure 2.13:
A) The tack test is proceeded in three steps: 1. A glass cylinder (probe) is pressed onto a PSA film. 2. The applied force is maintained. 3. The probe is retracted from the film. B) Scattering geometry: The fibrils created in the debonding process are oriented perpendicular to the scattering plane (gray plan). The transmission signal is detected. Horizontal cuts including the primary beam position yield information about the substructure of the fibrils.

During the debonding for small film-probe distances a modulation of the USAXS signal is detected [7,8,9]. It is originated by a substructure of the fibrils giving rise to a modulation due to its form factor. It was verified that the scattering before tacking did not show any sign of a modulation. During the debonding we could not detect any structure factor peak, which possibly means that there are no regular distances between the nanofibrils or that their length scale is out of the resolution limit [8]. For larger probe-film distances the modulation of the horizontal signal becomes weaker. This either means an increase of nanofibrils failures or that the nanofibrils sizes become less well defined

[1] C. Gay, L. Leiber; Phys. Rev. Lett. **82**, 936 (1999)

[2] J. S. Higgins, H. C. Benoit; Polymers and Neutron Scattering, pp.192-244. New York: Oxford University Press (1996)

[3] C. Hui, Y. Lin, J. Baney; J. Polym. Sci. **38**, 1485 (2000)

[4] H. Lakrout; Adhesion **69**, 307-359

[5] U. Lode, T. Pomper, A. Karl, G. von Krosigk, S. Cunis, W. Wilke, R. Gehrke; Macromol. Rapid Commun **19**, 35 (1998)

[6] A. Paiva, N. Sheller, M. Foster, A. Crosby, K. Shull; **34** 2269-2276 (2001)

[7] S. Roth, M. Burghammer, C. Ferrero, A. Diethert, P. M¨uller-Buschbaum; J. Appl. Cryst. **36**, in press (2003)

[8] A. Zosel; J. Adhesion Sci. Technol. **11**, 1447 (1997)

Scanning-USAX and Scanning-microfocus SAXS as tools to investigate defects at polymer-polymer interfaces: A comparison

C. Lorenz-Haas[1], P. Müller-Buschbaum, M. Stamm[2]

[1] Max-Planck-Institut f¨ur Polymerforschung, Mainz
[2] Institut f¨ur Polymerforschung Dresden e.V., Dresden

In the previous two years we reported about Scanning-USAX (Jahresbericht 2000) and Scanning-microfocus SAXS (Jahresbericht 2001) as techniques for the investigation of failure at polymer-polymer interfaces. This year we will compare both complementary methods and draw conclusions from our analysis.

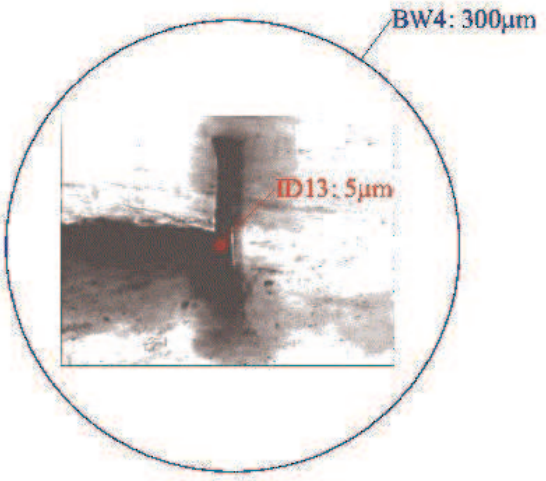

Figure 2.14:
Comparison of beam diameters: 300 μm S-USAX at BW4 (Hasylab/DESY Hamburg, big circle), 5 μm SM-SAXS at ID13 (ESRF Grenoble, tiny circle in the middle). The micrograph in the background shows the zone around a crack.

The sample consisted of two welded PMMA-plates with a crack along the interface between them. Defects in the zone around the crack tip were investigated by scanning X-ray scattering in two different ways:

1. Scanning-USAX. The experiments were carried out at the BW4 beam-line at HASYLAB/DESY in Hamburg with a beam diameter of 300 μm and an observable q-range of 0.018 $nm^{-1} \leq q \leq$ 0.29 nm^{-1}.

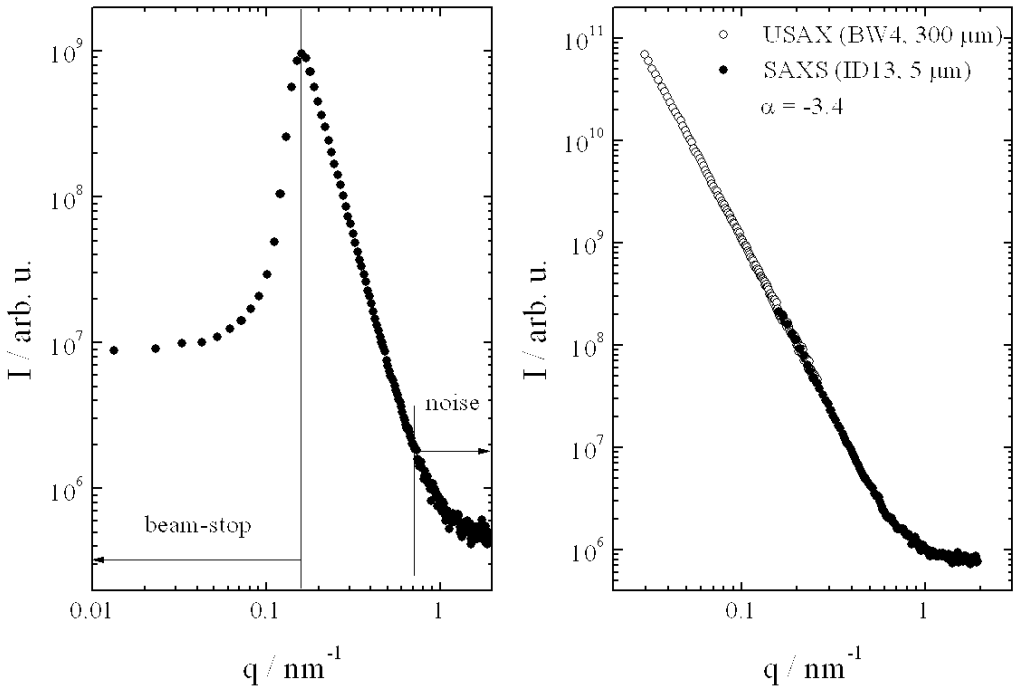

Figure 2.15:
Left: typical example of a complete scattering curve with the low q-region shadowed by the beam-stop and the high q-region dominated by noise (here SAXS). Right: SAXS-data as a continuation of the USAX-data for a selected slope of -3.4.

2. Scanning Microfocus-SAXS. These experiments were done at the ID 13 beam-line at ESRF in Grenoble. The resolvable q-range had been 0.15 $nm^{-1} \leq q \leq$ 9.18 nm^{-1} in this set-up.

Figure 2.14 shows the comparison of beam diameters. In the background a micrograph of a crack tip is given in the correct scale with respect to the two beam diameters. With the microfocus beam at ID13 a detailed analysis of the structure features with a high spatial resolution is possible (scan field size: 160 $\times$ 250 μm^2). The beam diameter at BW4 allows only a more averaging scanning over a macroscopic sample region (scan field size: 1200 $\times$ 1250 μm^2) but due to the access to lower q-values a detection of bigger defect sizes can be probed. Therefore both beam-lines give complementary results.

On the left side of Figure 2.15 a typical scattering curve is shown. In the region of low q the scattering from the sample is shielded by the beam-stop whereas at high q the noise dominates the signal. The q-region suitable for analysis is in between. All scattering curves looked similar no matter whether these had been results from S-USAX or SM-SAXS. The difference had only been the absolute q-range and the decline of the curve. In the whole observed q-range no Bragg-peaks occurred. This means that no highly ordered structures are present. Both the USAX and the SAXS datasets followed scaling laws. As the right side of Figure 2.15 suggests the results for a selected exponent α (here -3.4) both q-ranges can be put together to cover the whole q-range. Therefore

techniques can be treated with the same analysis. The observed exponents reach from -5.0 up to -3.0 depending on the measurement position on the sample. An interpretation of the whole interval of exponents is given with a variation of Porod's Law for scattering from craze fibrils with diffuse boundaries by Salomons et al. [1]:

$$I_{obs} \propto q^{-5+2\beta} \quad with \quad \alpha = -5 + 2\beta. \tag{2.1}$$

Thus α can vary between -3 ($\beta \to 1$) for perfectly sharp boundaries and -5 ($\beta \to 0$) for a completely smeared out density profile of the defect structures. The defect boundaries were found to be diffuse close to the crack and getting sharper with increasing distance from it. The area with the highest amount of dissipated energy is close to the crack. Therefore most of the energy is placed in the creation of diffuse boundaries. This can be also interpreted as the generation of a bigger interface on nanometer scale although it is not fractal.

[1] G. J. Salomons, M. A. Singh, T. Bardouille, W. A. Foran, M. S. Capel; J. Appl. Cryst. **32**, 71 (1999)

3 Struktur und Dynamik von Schmelzen

Schnelle Relaxation in Natriumboratschmelzen

A. Meyer, F. Kargl, H. Schober[1], Z. Chowduri[2]

[1] Institut Laue-Langevin, Grenoble, Frankreich
[2] NIST Center for Neutron Research, Gaithersburg, USA

Natriumboratschmelzen sind mehrkomponentige Systeme, in denen eine Komponente, die Natriumatome, in einer relativ starren Matrix der anderen Komponenten diffundiert. In Natriumdiborat ist zum Beispiel der Diffusionskoeffizient von Natrium bei 750 K etwa $1.4 \times 10^{-12} \mathrm{m^2 s^{-1}}$ [1], während bei dieser Temperatur die Beweglichkeit der Matrixatome etwa 8 Größenordnungen kleiner ist. Im hier untersuchten Temperaturbereich beträgt der Unterschied in der Beweglichkeit der verschiedenen Komponenten etwa 2 Größenordnungen. Natriumdiboratschmelzen waren Gegenstand von Neutronenstreuexperimenten am Flugzeitspektrometer IN 6 des ILL und am Neutronenrückstreuspektrometer HFBS des NIST [2].

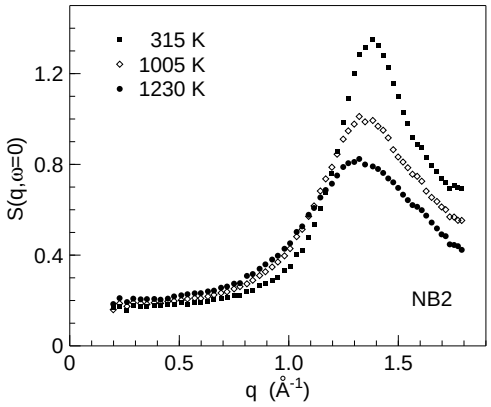

Abbildung 3.1:
Elastischer Strukturfaktor von zähflüssigem Natriumdiborat (NB2). Zu kleinen q dominiert die inkohärente Streuung des Natriums das Signal, während im Strukturfaktormaximum q_0 die kohärenten Streubeiträge von Sauerstoff und ^{11}Bor dominieren.

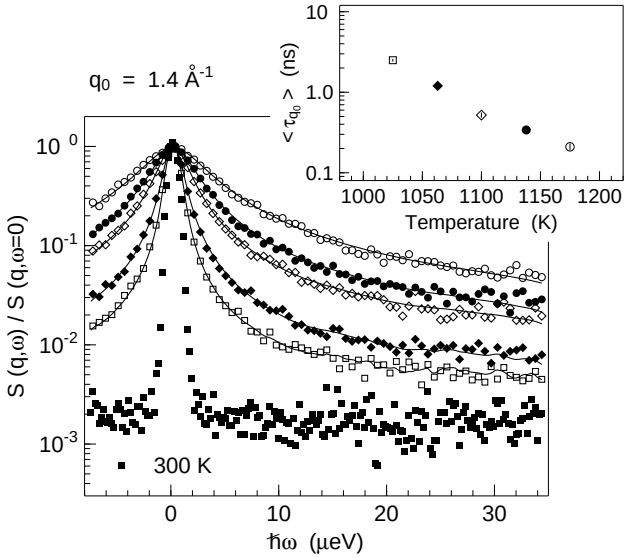

Abbildung 3.2:
Strukturelle Relaxation der B-O Matrix einer Natriumdiboratschmelze: Die Linien sind Anpassungen mit der Fouriertransformierten einer gestreckten Exponentialfunktion mit Entfaltung der instrumentellen Auflösung (Spektrum bei 300 K) und einem Streckungsexponenten $\beta_{q_0} = 0.76$.

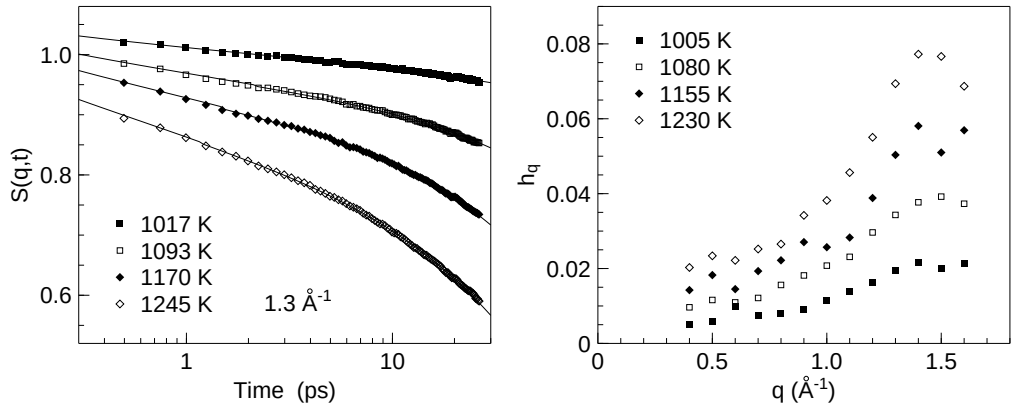

Abbildung 3.3:
Schnelle β Relaxation in Natriumdiboratschmelzen: Die Linien sind Anpassungen mit dem β Skalengesetz der Modenkopplungstheorie. Alle Komponenten führen eine schnelle Rüttelbewegung im Käfig der sie umgebenden Atome aus.

Abbildung 3.1 zeigt den elastischen Strukturfaktor $S(q, \omega = 0)$ von zähflüssigem Natriumdiborat und Natriumtrigermanat. Im Strukturfaktormaximum q_0 dominieren die kohärenten Streubeiträge von Bor (Germanium) und Sauerstoff das Signal. In einem Experiment am Rückstreuspektrometer HFBS wurde so im Strukturfaktormaximum von Natriumdiborat die Relaxation der B-O Matrix vermessen (Abbildung 3.2). Relaxationszeiten liegen im Temperaturbereich der Messung in der Größenordnung einer Nanosekunde und somit zeitlich getrennt von einer schnellen Relaxation und der 10 ps Zeitskala der Natriumdiffusion.

Abbildung 3.3 zeigt die Dichtekorrelationsfunktion – nicht normiert mit dem statischen Strukturfaktor $S(q, t = 0)$ – von zähflüssigem Natriumdiborat im Strukturfaktormaximum. Über den vermessenen Temperatur- und q-Bereich lassen sich die Spektren konsistent mit dem β Skalengesetz der Modenkopplungstheorie [3] mit einem temperatur- und q-unabhängigen Linienformparameter $\lambda \simeq 0.76$ beschreiben. Die Übergangszeit τ_σ ist dabei q-unabhängig. Die Amplitude der Relaxation h_q weist eine starke Temperaturabhängigkeit auf und ist eng korreliert mit dem statischen Strukturfaktor $(S(q, t = 0))$.

Daraus lässt sich schließen, dass sowohl Natrium, als auch die Matrixelemente Bor und Sauerstoff an der β Relaxation beteiligt sind. Es führen also alle Atome eine schnelle lokalisierte Rüttelbewegung in dem Käfig der sie umgebenden Atome aus, auch wenn die Zeitskalen für das Verlassen dieses Käfigs für die verschiedenen Komponenten sehr unterschiedlich sein können. Weitere Experimente zur detaillierten Untersuchung der Natriumdiffusion in diesen Schmelzen sind in Vorbereitung.

[1] U. Schoo, H. Mehrer, Solid State Ionics **130**, 243 (2000).

[2] A. Meyer, R. M. Dimeo, P. M. Gehring, D. A. Neuman, (Rev. Sci. Instr., im Druck).

[3] W. G¨otze, T. Voigtmann, Physikalische Bl¨atter, **57/4**, 41 (2001).

Struktur und Dynamik von Natriumtrigermanat-Schmelzen

A. Widmann, A. Meyer, F. Kargl, H. Schober[1]

[1] Institut Laue-Langevin, Grenoble, Frankreich

Mikroskopische Dynamik von Natriumtrigermanatschmelzen wurde am Flugzeitspektrometer IN6, am Institut Laue-Langevin in Grenoble, Frankreich, untersucht. Die Messungen an Natriumtrigermanat-Schmelzen wurden durchgeführt, um den Einfluß des Netzwerkbildners auf die Struktur und auf die Dynamik des Natriums im Netzwerk zu untersuchen. Natriumsilikatschmelzen weisen eine Kanalstruktur innerhalb des Si-O Netzwerkes auf, über die das Natrium schnell diffundieren kann [1,2].

Natriumtrigermanat-Glas wurde aus hoch reinem und getrocknetem Germaniumdioxid und Natriumkarbonatpulver synthetisiert. Die Pulvermengen wurden gemäß der Stöchiometrie von Natriumtrigermanat abgewogen, gut durchgemischt, und dann bei ca. 1400K bis 1600K im Platin-Tiegel aufgeschmolzen. Eine differentielle kalorimetrische Analyse (DSC) mit einer Heizrate von 40 K/min ergab einen Glasübergangspunkt T_g von 772 K, der gut mit dem Wert aus der Literatur übereinstimmt [3]. Für das Streuexperiment am IN6 wurde ein Hohlzylinder aus Platin mit 23 mm Durchmesser gewählt. Eine Wellenlänge von 5.9 Å der einfallenden Neutronen ergibt einen zugänglichen q-Bereich für elastische Streuung von 0.3 $Å^{-1}$ bis 1.7 $Å^{-1}$, bei einer Energieauflösung von 50μeV (FWHM). Natriumtrigermanat streut aufgrund der hohen kohärenten Streubeiträge von Germanium und Sauerstoff überwiegend kohärent. Einzig das Natrium hat einen nicht zu vernachlässigenden inkohärenten Streuquerschnitt. Bei kleinen Impulsüberträgen dominiert dann die inkohärente Streuung vom Natrium.

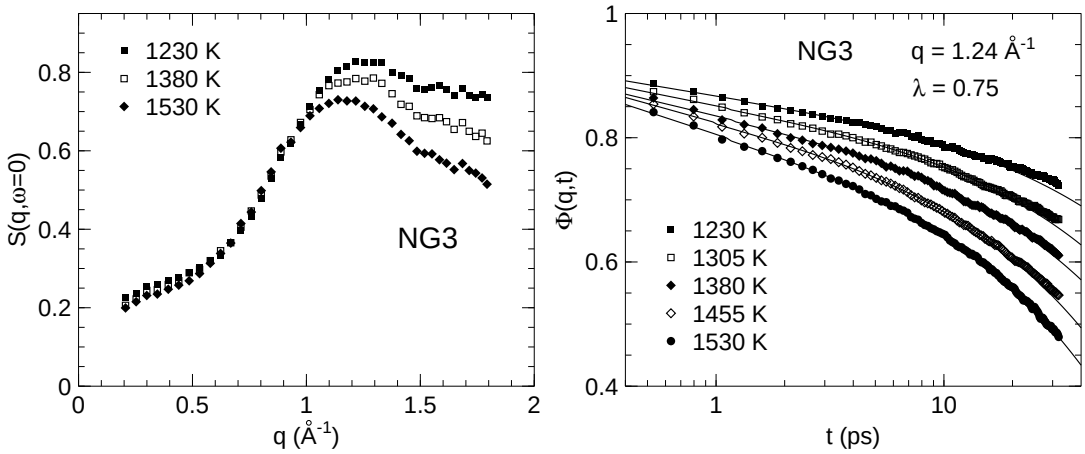

Abbildung 3.4:
linke Abbildung: Dichtekorrelationsfunktion $\Phi(q,t)$ mit Anpassungen des β-Skalengesetzes der Modenkopplungstheorie; rechte Abbildung: elastischer Strukturfaktor

Abbildung 3.4 links zeigt den elastischen Strukturfaktor von NG3. Ein Prepeak vor dem ersten Maximum, wie ihn Natriumsilikatschmelzen aufweisen, lässt sich nicht beobachten. Dies vergleicht sich gut mit den Ergebnissen an Natriumdiborat (siehe Beitrag von A. Meyer). Die Bildung von natriumreichen Kanälen scheint charakteristisch für die Si-O Bindung zu sein.

Die rechte Abbildung zeigt die Dichtekorrelationsfunktion $\Phi(q,t)$ der Natriumtrigermanatschelzen. Wie in Natriumdiborat lässt sich die mikroskopische Dynamik mit dem β-Skalengesetz der Modenkopplungstheorie beschreiben [4]. Auch in Natriumtrigermanat gibt es einen ausgeprägten β-Relaxationsprozeß.

[1] A. Meyer, H. Schober, D. B. Dingwell, Europhys. Lett. **59** 708-713 (2002)

[2] F. Kargl: *Struktur und Dynamik von Natrium-Silikat-Schmelzen untersucht mit inelastischer Neutronenstreuung*, Diplomarbeit, Technische Universit¨at M¨unchen (2002)

[3] T. J. Kiczenski, Chris Ma, E. Hammarsten, J. Non-Cryst.Solids **272**, 57-66 (2000)

[4] W. G¨otze, T. Voigtmann, Physikalische Bl¨atter, **57/4**, 41 (2001)

Nahordnung in Natriumsilikatschmelzen

F. Kargl, A. Meyer, H. Schober[1], W. Kob[2], J. Horbach[3]

[1] Institut Laue-Langevin, Grenoble, Frankreich

[2] Laboratoire des Verres, Université Montpellier II, Frankreich

[3] Johannes Gutenberg Universit¨at Mainz

In Alkalisilikaten, die als einfache binäre Analoga zur Magma und als Prototypen für glasbildende Ionenleiter betrachtet werden können, ist das Verhalten grundlegender physikalischer Eigenschaften noch weitgehend unverstanden. Eine erste Modellbildung der Struktur wurde schon von Zachariasen vorgenommen, welche von einer statistischen Verteilung der Alkaliatome in der SiO-Matrix ausging [1]. Mit diesem Modell kann jedoch weder die Abhängigkeit der Viskosität von der Natriumkonzentration, noch die schnelle Dynamik der Na-Atome erklärt werden. Von Greaves et al. wurden zahlreiche Untersuchungen zur Struktur der Silikate unter anderem mit EXAFS durchgeführt. Ausgehend von diesen Messungen zur lokalen Umgebung der Si und Na Atome postuliert er eine modifizierte Netzwerkstruktur, in der die Na-Atome Cluster bilden [2]. Im Fall der Erdalkalisilikate wurde von Gaskell mittels Neutronendiffraktion die Struktur im Glas untersucht. Die Messungen gaben einen ersten Hinweis, dass eine Korrelation der Ca-Atome auf mittlerer Längenskala besteht [3]. In geschmolzenem Natriumdisilikat konnten wir im elastischen Strukturfaktor einen Prepeak vor dem ersten Strukturfaktormaximum nachweisen [4]. Molekulardynamik(MD)-Simulationen identifizieren die Position des Prepeaks mit dem typischen Abstand von Na-reichen Kanälen im Silikatnetzwerk [5]. Die Bildung von Na Clustern wird nicht beobachtet.

Mit inelastischer Neutronenstreuung haben wir die strukturelle Nahordnung in Alkalisilikaten in Abhängigkeit von der Alkalikonzentration untersucht. Für die Messungen wurden $Na_4Si_3O_8$ (NS1.5), $Na_2Si_3O_7$ (NS3) und $Na_2Si_4O_9$ (NS4) reinsten SiO_2- und Na_2CO_3-Pulvern synthetisiert. Die Experimente wurden am Flugzeitspektrometer IN6 des ILL in Grenoble bei einer Wellenlänge von $\lambda = 5.9$ Å der einfallenden Neutronen durchgeführt. Gemessen wurde bei Raumtemperatur und in der Schmelze bei Temperaturen bis zu 1600 K.

In Abb. 3.5 a) sind die elastischen Strukturfaktoren für NS2, NS3 und NS4 bei 1600 K aufgetragen. Man erkennt deutlich den Prepeak bei $q \approx 0.9$ Å^{-1}. Der Prepeak ist mit steigender Na-Konzentration stärker ausgebildet. Die Position des Prepeaks ändert sich jedoch in diesem

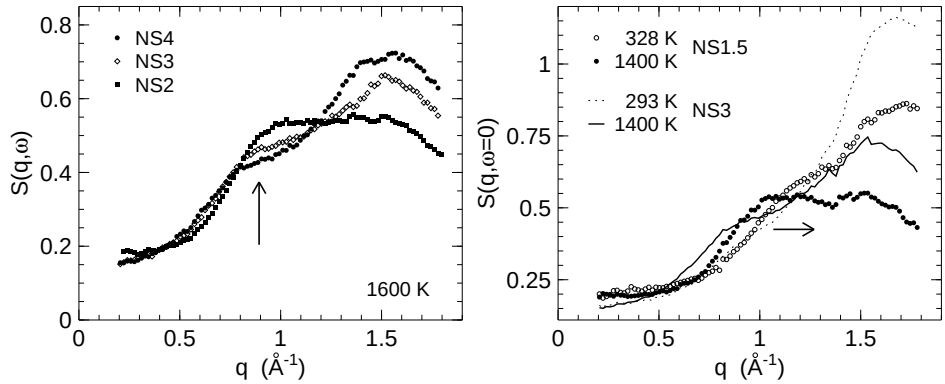

Abbildung 3.5:
Elastischer Strukturfaktor $S(q, \omega = 0)$: a) f¨ur NS2, NS3 und NS4 bei 1600 K und b) f¨ur NS1.5 (Punkte) und NS3 (Linien) bei Raumtemperatur und 1400 K.

Konzentrationsbereich nicht mit Zu- oder Abnahme der Na-Konzentration. Das erste Strukturfaktormaximum bei $q \approx 1.6$ Å^{-1}, welches mit SiO-Tetraeder Abständen korreliert ist, nimmt mit zunehmender Na-Konzentration ab.

Betrachtet man nun NS1.5, d. h. eine Alkalisilikatschmelze, in der die Zahl der Na-Atome (N_{Na}) größer als die der Si-Atome (N_{Si}) ist, so stellt man folgende Änderungen fest: Bereits bei Raumtemperatur ist im Gegensatz zu NS2, NS3 und NS4 ein Prepeak vor dem ersten Strukturfaktormaximum erkennbar. Die Position des Prepeaks ist zu größeren Wellenzahlen $q \approx 1.2$ Å^{-1} verschoben (vgl. Abb. 3.5 b)). Der Prepeak wächst ebenfalls mit zunehmender Temperatur an. Das Strukturfaktormaximum nimmt analog zu NS2, NS3 und NS4 mit steigender Temperatur gemäß dem Debye-Waller-Faktor ab. Für NS1.5 bedeutet dies, dass die, in den anderen Silikaten vorhandene und relativ starre SiO-Tetraeder Matrix, durch den Netzwerkmodifizierer Na stärker aufgebrochen ist.

Neueste Ergebnisse der Simulation an NS2, die nahe der experimentellen Dichte durchgeführt wurden, liefern folgendes Ergebnis für den elastischen Strukturfaktor.

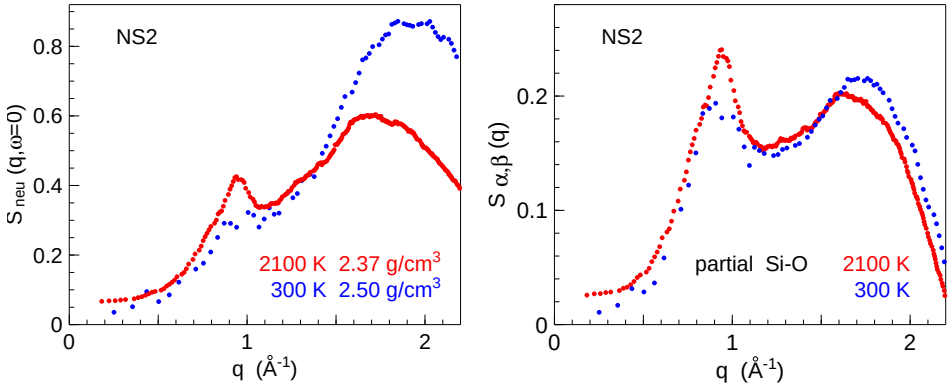

Abbildung 3.6:
Ergebnisse der MD-Simulation an NS2: a) Elastischer Strukturfaktor bei 300 K und 2100 K. b) Partielle Strukturfaktoren ebenfalls bei 300 K und 2100 K.

In Abb. 3.6 a) ist der elastische Strukturfaktor bei 300 K und 2100 K aufgetragen. Er zeigt bei 2100 K ebenfalls einen Prepeak bei $q \approx 0.9$ Å^{-1}, der im Rahmen der Simulation mit dem typi-

schen Abstand von Na-Kanälen ($\simeq 7$ Å) identifiziert wird. Im Gegensatz zu früheren Simulationen [4], die bei deutlich größeren Dichten durchgeführt wurden, ist der Prepeak ähnlich wie im Experiment bei Raumtemperatur nahezu nicht vorhanden. Mit zunehmender Temperatur wächst er vor dem, mit dem DWF abnehmenden, Strukturfaktormaximum.

Die Simulation ermöglicht auch eine Bestimmung der partiellen Strukturfaktoren (Abb. 3.6 b). Aus den partiellen Strukturfaktoren erkennt man, dass die Korrelation der Atome die durch den Prepeak wiedergegeben wird, auch im Glaszustand vorhanden ist. Gewichtet man jedoch die partiellen Strukturfaktoren mit den Streuquerschnitten der Atome für die Neutronenstreuung und summiert sie anschließend auf, so fällt der Prepeak nahezu weg. Die Dichteänderung, die in den Alkalisilikaten zwischen 300 K und 2100 K fast 20 % beträgt, sorgt für eine Verschiebung der partiellen Strukturfaktoren, die bei Summation jener den Prepeak sichtbar macht. Demzufolge wäre die Struktur der Schmelze mit einer perkolierenden Kanalstruktur, über welche die schnelle Diffusion der Na-Ionen stattfindet, auch im Glas vorhanden.

Die Messungen zur Struktur der Natriumsilikatschmelzen für verschiedene Na-Konzentrationen haben gezeigt, dass sich im Bereich $N_{Na} \leq N_{Si}$ die Position des Prepeaks im Strukturfaktor nicht ändert. Im Fall von NS1.5 verschiebt sich die Position des Prepeaks, und folglich die zugrundeliegende Korrelationslänge der Atome im Ortsraum, deutlich. Für NS2 konnte durch einen Vergleich mit der MD-Simulation gezeigt werden, dass das Anwachsen dieses Peaks mit der Temperatur auf eine Dichteänderung des Systems zurückgeführt werden kann.

Eine weitere offene Frage ist, wie sich die Struktur der Schmelze bei Austausch oder Zugabe einer anderen netzwerkbildenden Komponente verhält. Neueste Messungen an Natriumsilikatschmelzen mit Al_2O_3-Anteil (November 2002) gaben im Rahmen einer ersten Auswertung einen weiteren Hinweis darauf, dass die Kanalstruktur und die schnelle Diffusion des Na eng verknüpft sind. Untersuchungen an Natriumborat zeigen dagegen keinen Prepeak im Strukturfaktor und im Gegensatz zu den Natriumsilikaten einen ausgeprägten schnellen β-Relaxationsprozess.

[1] W. H. Zachariasen: J. Am. chem. Soc. **54**, 3841 (1932)

[2] G. N. Greaves et al.: Nature **293** 611-616 (1981)

[3] P. H. Gaskell et al.: Nature **350** 675-677 (1991)

[4] A. Meyer, H. Schober, D. B. Dingwell: Europhys. Lett. **59** 708-713 (2002)

[5] J. Horbach, W. Kob, K. Binder: Chem. Geo. **174** 87-101 (2001)

Car-Parinello Computer Simulations on Hydrous Silica(te) Systems

Markus Pöhlmann [1,2,3], Andreas Meyer [1], Magali Benoit [2], Walter Kob [2]

[1] Physik-Department E13, Technische Universit¨at M¨unchen

[2] Laboratoire des Verres, Université Montpellier II

[3] Institut Laue-Langevin, Grenoble

In recent years the influence of water on the structure and viscosity of silica (SiO_2) and silicate melts has attracted the interest of many experimental groups due to its importance in geology (e.g., magmatic flow in the earth crust) as well as technology (e.g., glassy optical fibers). These, mostly

spectroscopic, measurements suggest that the mechanism of dissolution of water in silica(te) melts varies strongly with the composition of the bulk. In particular aluminosilicate compositions seem to have different dissolution mechanisms than Al-free silicates. In addition to dissolved water, molecular water may be present. The ratio of dissolved and molecular water depends on temperature and governs the viscosity of the melts above the glass transition temperature T_g.

We use computer simulations in order to obtain a quantum-chemical verification of the existing experimental data and hence to obtain a deeper understanding of the dissolution mechanisms of water, in particular in systems containing Al. In a first step we simulate pure (Al and Na free) SiO_2 systems with a variable water content. Water free SiO_2 has already been investigated by our collaborators [1,2,3]. These systems will be equilibrated in the liquid state and then quenched to a glassy state. Structure and dynamics of the resulting glass are investigated with particular attention to dissociation and recombination of the water as a function of temperature.

Classical molecular dynamics are currently not able to give a realistic description of this reaction since reliable potentials for water and the dissolution products OH^- and H_3O^+ are missing. Therefore a quantum-mechanical treatment using the method of Car-Parrinello can be expected to be more successful. Since this type of ab initio calculations is computationally extremely demanding (CPU time as well as memory) the use of a parallel supercomputer is mandatory. The calculations are performed using the CPMDcode, developed by Parrinello's group (Manno, Switzerland).

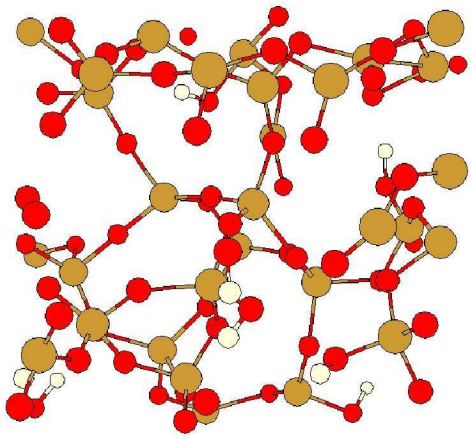

Figure 3.7: CPMD calculations on a system of 30 SiO_2 and 4 H_2O groups at a temperature of 3000K; all hydrogen atoms (white spheres) are well attached to the silica network (silicon: yellow spheres, oxygen: red spheres), molecular water is not present

A system of 30 SiO_2 and 4 water molecules (3.84% of mass H_2O) in a cubic simulation box has so far been equilibrated. Figure 3.7 shows, that all hydrogen atoms well linked to the SiO_2 network. Molecular water is not observed at this concentration and temperature. Experiments [4] predict a relative abundance of 6% of molecular water in the final glass (at room temperature) for our initial water concentration. Since at 3000K all the water has been dissolved (figure 3.7), we are interested in the structural changes during the quench of the glass.

In figure 3.8 the radial pair distribution function $g(r)$ of the system is presented. The typical features of the structure appear clearly: a sharp peak at 1.6 Å labeling the typical $Si-O$ distance in

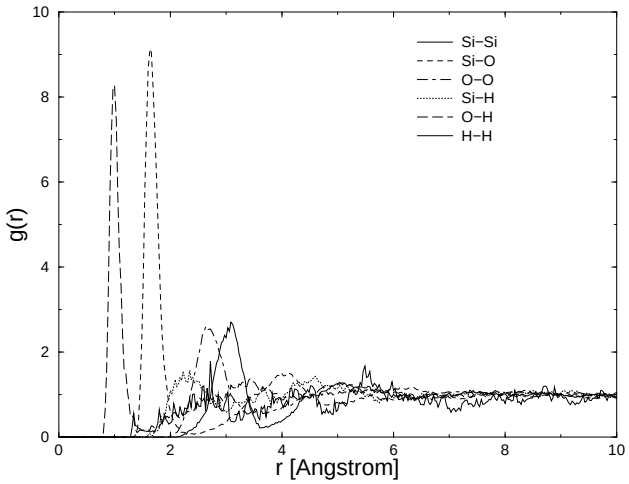

Figure 3.8: CPMD calculations on a system of 30 SiO_2 and 4 H_2O groups at a temperature of 3000K; radial pair distribution function.

SiO_4 tetrahedras and the O-H bond length of about 0.99 Å.
The calculations are in strong relation to investigations on similar systems with neutron scattering at the Institut Laue-Langevin. Elastic and inelastic neutron spectroscopy is able to measure the time and space correlation function of silica melts. In particular the presented radial pair distribution is the Fourier transform of the neutron scattering cross section:

$$S(\mathbf{q}) = 1 + \int d^3r \, (g(\mathbf{r}) - \rho) \; e^{i\mathbf{qr}} \tag{3.1}$$

Since equivalent data to the observables of our calculations can be extracted from neutron scattering, these experiments serve as cross check for the reliability of our simulations and vice versa.

[1] J. Horbach, W. Kob. Phys. Rev. B 60, 3169 (1999)
[2] K. Vollmayr, W. Kob , K. Binder Phys. Rev B, 54, 15808 (1996)
[3] M. Benoit, S. Ispas, R. Jullien Eur. Phys. J., B 13 , 631 (2000)
[4] B. O. Mysen, D. Virgo. Chem. Geology 57, 303-331 (1986)

Quasielastic Neutron Scattering on PdNiP Melts

S. Mavila Chathoth , A. Meyer, W. Petry and F. Juranyi [1]

[1] Paul Scherrer Institute, Villigen, Switzerland

The dynamic of glass formation and its puzzling features have been the subject of many experimental and theoretical studies. Multicomponent metallic alloys, that exhibit a high degree of glass forming ability, show a structural relaxation known for nonmetallic glass forming liquids. Even at well above melting point, the structrual relaxation in these metallic liquids is nonexpontional and the diffusivity is two orders of magnitude smaller than that in simple metallic liquids. In the present study we investigated the slow dynamics of $Pd_{40}Ni_{40}P_{20}$ using a cold neutron time of flight spectrometer FOCUS, at Paul scherrer institute, Villigen Switzerland with a measuring wavelength of 5.4 Å. As compared to bulk glass forming $Pd_{43}Ni_{10}Cu_{27}P_{20}$ [1], $Pd_{40}Ni_{40}P_{20}$ reveals a higher liquidus temperature and a reduced glass forming ability. Both alloys are in good

approximation hard-sphere like dense liquids and are characterized by packing fraction of about 0.52 at their melting points.

$Pd_{40}Ni_{40}P_{20}$ was prepared from a mixture of pure elements by arc melting Pd and Ni and follwed by induction melting PdNi with Phosphorus. The melt was subjected to a B_2O_3 flux treatment in order to remove oxide impurities. Differential scanning calorimetery with a heating rate of 40 K/s resulted in a $T_{sol} = 884$ K and a $T_{liq} = 986$ K in accordance with literature values [2]. For the neutron time of flight experiment a thin walled Al_2O_3 contanier has been used giving a hollow cylinder sample geometry of 22mm in diameter. A wavelength of λ = 5.4 Å of the incident neutrons result in an accessible wavenumber range $q = 0.4$ to 1.8Å^{-1} at zero energy transfer. In this q range scattering is dominated by the incoherent contributions from Nickel.

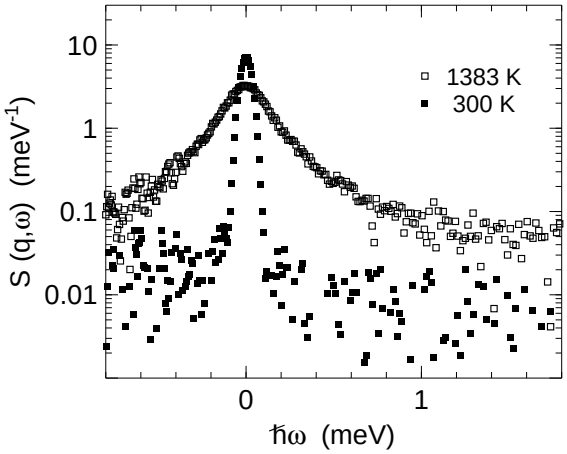

Figure 3.9:
Scattering law $S(q,\omega)$ (logarithmic scale) of liquid $Pd_{40}Ni_{40}P_{20}$. The signal is dominated by the incoherent scattering from Ni. The data at 300 K represent the instrumental energy resolution. Spectra in the liquid show a broad quasielastic signal.

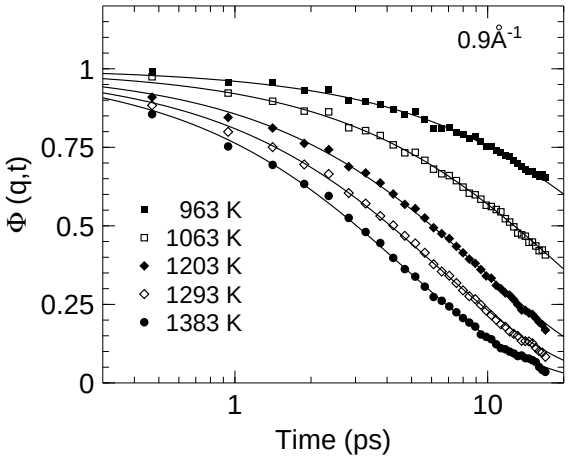

Figure 3.10:
Normalized density correlation function $\Phi(q,t)$ of liquid $Pd_{40}Ni_{40}P_{20}$ at 0.9Å^{-1} as obtained by Fourier deconvolution of measured $S(q,\omega)$. The lines are fits with a stretched exponential function.

Figure 3.9 shows the scattering law $S(q,\omega)$ of liquid $Pd_{40}Ni_{40}P_{20}$ at q = 0.9Å^{-1}. The spectra exhibit a broad quasielastic line with wings extending upto several meV. The quasielastic signal is best analysed in time with a removal of the instrumental resolution function. The density correlation function Φ(q,t) has been obtained by Fourier transformation of measured $S(q,\omega)$, deconvolution of the instrumental resolution function, and normalization with the value at $t = 0$. Figure 3.10 shows the log-time decay of $\Phi(q,t)$ at $q = 0.9$ Å^{-1}. In contrast to simple metallic liquids, liquid $Pd_{40}Ni_{40}P_{20}$ exhibit a structural relaxation that exhibits stretching in time. The lines fits with a stretched exponential function: $F(q,t) = f_q \exp[-(t/\tau_q)^{\beta_q}]$. In a first fitting process the stretching exponent $\beta_q(T)$ was treated as a parameter. $\beta_q(T)$ shows a scattering arround a mean β

= 0.85. For the further data analysis a β = 0.85 was used. As compared to $Pd_{43}Ni_{10}Cu_{27}P_{20}$ ($\beta = 0.75$) stretching is less pronounced in $Pd_{40}Ni_{40}P_{20}$.

In the hydrodynamic limit for $q \rightarrow 0$ the mean relaxation time $\langle \tau_q \rangle$ is indirectly proportional to the momentum transfer q square. In liquid PdNiP the $1/q^2$ dependence holds even up to 1.8 Å^{-1} (Figure 3.11). This allows to read off the Ni self diffusivity $D = 1/\langle \tau_q \rangle q^2$. Figure 3.12 displays the Nickel diffusivities in liquid $Pd_{40}Ni_{40}P_{20}$ as a function of temperature. Values range from $0.25 \times 10^{-9}\text{m}^2/\text{s}$ to $2.3 \times 10^{-9}\text{m}^2/\text{s}$. For a comparison the mean Cu/Ni diffusivities of $Pd_{40}Ni_{10}Cu_{30}P_{20}$ [3] and $Pd_{43}Ni_{10}Cu_{27}P_{20}$ are shown. Absolute values of the Ni diffusion in $Pd_{40}Ni_{40}P_{20}$ and $Pd_{40}Ni_{10}Cu_{30}P_{20}$ are equal within the statistical error. The presence of Cu does not influence the Ni mobility in these alloys.

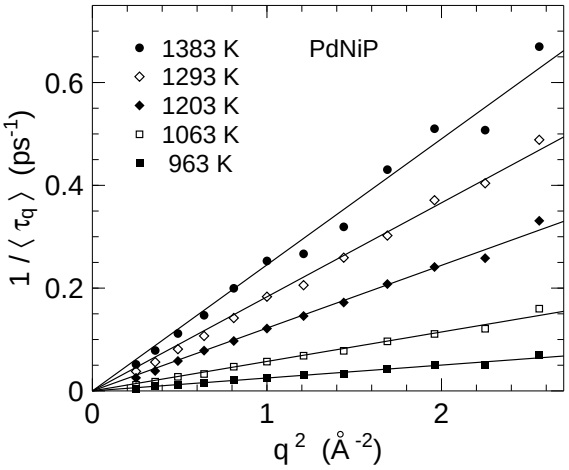

Figure 3.11:
Mean relaxation time $\langle \tau_q \rangle$ of self motion in liquid $Pd_{40}Ni_{40}P_{20}$. $1/\langle \tau_q \rangle$ shows a q^2 dependence as expected for long range atomic transport for $q \rightarrow 0$. The slope correspondance to the diffusion coefficient D

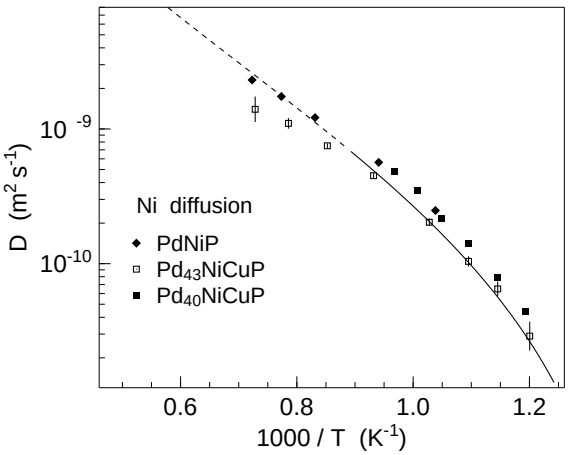

Figure 3.12:
Self diffusion coefficient of Ni in liquid $Pd_{40}Ni_{40}P_{20}$ and PdNiCuP alloys

In conclusion, the stretching of the structural relaxation in $Pd_{40}Ni_{40}P_{20}$ is with $\beta \simeq 0.85$ less pronounced than in $Pd_{43}Ni_{10}Cu_{27}P_{20}$ with $\beta = 0.75$. It appears that glass formation and stretching depend on the alloy composition. The diffusity in contrast only depends on the packing fraction.

[1] A. Meyer, Phys. Rev. **B 66**, 134205 (2002)

[2] H. W. Kui and D. Turnbull, J. Non-Cry.Solids. **94**, 62 (1987)

[3] A. Meyer, R. Busch, H. Schober, Phys. Rev. Lett. **83**, 5027 (1999)

4 Moleküldynamik

Experimente an Benzol in der Zeit– und Frequenzdomäne

S. Wiebel, P. Bartolini[1], A. Taschin[1], M. Ricci[1], R. Righini[1], W. Petry, R. Torre[1]

[1] LENS (European Laboratory for Non Linear Spectroscopy), Firenze

Depolarisierte Lichtstreumessungen an flüssigem und unterkühltem Benzol haben demonstriert, dass diese denkbar einfache molekulare Flüssigkeit auch mit Modellen beschrieben werden kann, die ursprünglich für glasbildende Systeme entwickelt wurden [1]. Dies wurde bereits im Jahresbericht 2001 diskutiert.

Die Untersuchungen wurden um Experimente in der Zeitdomäne erweitert. Dabei wurde mit einem Anregungspuls eine Doppelbrechung in der Probe induziert (optischer Kerr-Effekt, OKE), die dann mit einem schwächeren Sondenpuls abgetastet wurde. Diese Experimente wurden am LENS (European Laboratory for Non Linear Spectroscopy) in Firenze (Italien) durchgeführt. Bei dieser Methode entspricht das Messsignal der zeitlichen Ableitung der Korrelationsfunktion $\Phi(t)$, in der Lichtstreuung arbeiten wir mit der dynamischen Suszeptibilität $\chi''(\nu)$. Beide Messsignale beruhen auf Fluktuationen des dielektrischen Tensors und gehen durch Fouriertransformation ineinander über. In Abb. 4.1 sind die beiden Datensätze gegenübergestellt.

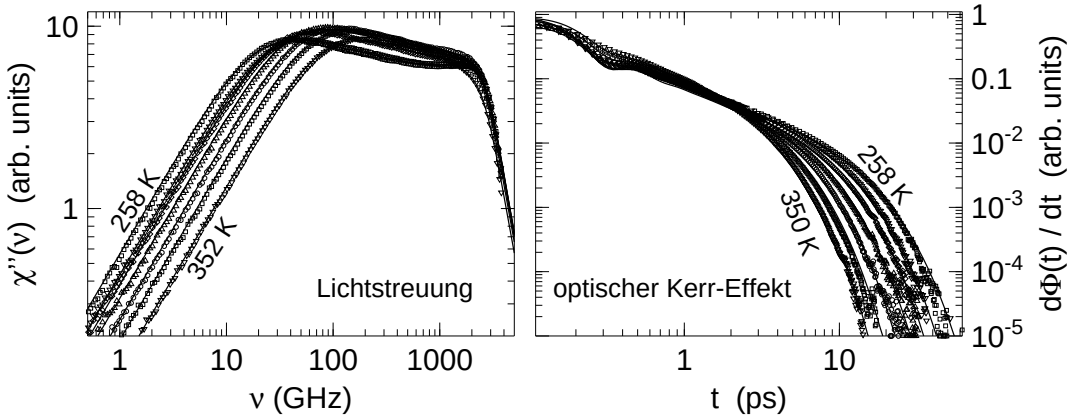

Abbildung 4.1:
Messdaten von Benzol im Temperaturbereich zwischen 258 und 350 K. Links sind die dynamischen Suszeptibilitäten aus der Lichtstreuung gezeigt; rechts der Zerfall des optischen Kerr-Effekts.

Die komplementären Messungen erlauben uns einen sehr genauen Blick auf die strukturelle Relaxation und bieten zusätzlich die Möglichkeit, die beiden experimentellen Methoden intensiv zu vergleichen. Ein erster qualitativer Vergleich [2] legt nahe, die beiden Datensätze als gleichwertig zu betrachten. Wir belegen dies durch die Fouriertransformation unserer Daten. Zusätzlich verwenden wir das schematische F_{12}-Modenkopplungsmodell, das wir mit identischen Parametern an beide Datensätze angepasst haben. Die Parametrisierung durch das Modell umgeht das Problem, dass die gemessenen Datensätze nur in einem endlichen Zeit– bzw. Frequenzfenster verfügbar sind und deshalb nur näherungsweise transformiert werden können.

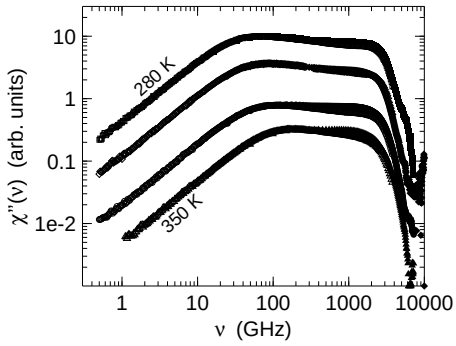

Abbildung 4.2:
Dynamische Suszeptibilitäten von Benzol aus quasielastischer Lichtstreuung (offene Symbole) und das fouriertransformierte Signal des optischen Kerr-Effekts (ausgefüllte Symbole).

Bei der Fouriertransformation der optischen Kerr-Daten zeigt sich, dass das Verhältnis von Hoch– und Niederfrequenzintensität stark von der Form der Auflösungsfunktion abhängt, die nicht genau analytisch beschrieben werden kann. Die Entfaltung gelingt nicht bei allen Messungen gleich gut, insgesamt ist die Übereinstimmung mit den Lichtstreuergebnissen jedoch, wie in (Abb. 4.2) gezeigt, zufriedenstellend.

Das schematische F_{12}-Modell der Modenkopplungstheorie [3], ist in der Lage, beide experimentellen Datensätze konsistent mit einem einzigen Parametersatz zu beschreiben. Die Fitkurven sind in Abb. 4.1 mit eingezeichnet. Sie gehen durch Fouriertransformation ineinander über.

Es wurde bereits in mehreren Flüssigkeiten beobachtet, das die strukturelle Relaxation in der Zeitdomäne weniger gestreckt erscheint als in der Frequenzdomäne. Dies ist in erster Linie auf die Darstellungsform zurückzuführen. Im Fall von Benzol, wo die in der Lichtstreuung beobachtete Streckung der Relaxation ein überraschendes Resultat war, schien es deshalb lohnend, die Analyse in diesem Bereich an den neuen Daten zu wiederholen. Abb. 4.3 zeigt die in diesem Bereich ska-

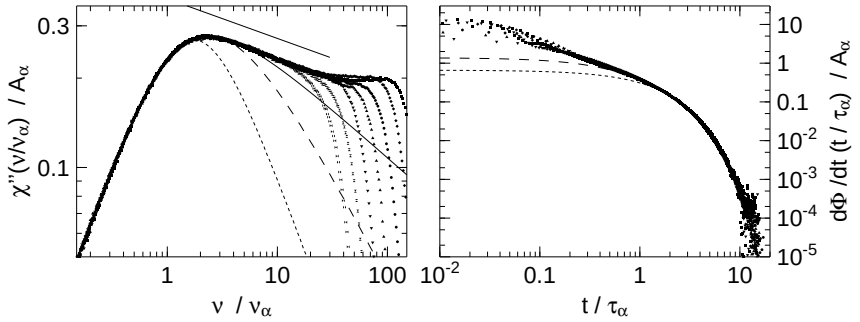

Abbildung 4.3:
Das Skalengesetz und die Streckung der α–Relaxation lässt sich in der Zeitdomäne (aus Lichtstreuung, links) und in der Frequenzdomäne (aus OKE, rechts) bestätigen.

lierten Datensätze. Bei den Lichtstreudaten sind eine Cole-Davidson-Funktion mit $\beta_{\mathrm{CD}} = 0.33$ (durchgezogen), eine gestreckte Exponentialfunktion nach Kohlrausch mit $\beta_{\mathrm{K}} = 0.73$ (gestrichelt) und eine einfache Exponentialfunktion (gepunktet) eingezeichnet. Auch die in der Zeitdomäne gemessenen Daten werden durch eine Kohlrauschfunktion deutlich besser beschrieben als durch eine einfache Exponentialfunktion. Dabei finden wir $\beta_{\mathrm{K}} = 0.86$.

[1] S. Wiebel, J. Wuttke: N. J. Phys. **4**, 56 (2002)
[2] S. Kinoshita, Y. Kai,M. Yamaguchi und T. Yagi: Phys. Rev. Lett. **75**, 148 (1995)
[3] W. G¨otze: Z. Phys.B **56**, 139 (1984)

Der Modenkopplungsansatz in Methanol und Ethanol

S. Wiebel, M. Goldammer und J. Wuttke

Im Rahmen von systematischen Untersuchungen an molekularen Flüssigkeiten haben wir depolarisierte Lichtstreumessungen an Methanol und Ethanol durchgeführt. Diese beiden Substanzen wurden als zwei strukturell verwandte, relativ einfache Systeme ausgewählt, die mit ihren Wasserstoffbrückenbindungen zwischen van-der-Waals-Flüssigkeiten wie n-Butyl-Benzol oder Toluol und chemisch gebundenen Systemen wie etwas Quarzglas liegen. Wir finden in beiden Alkoholen

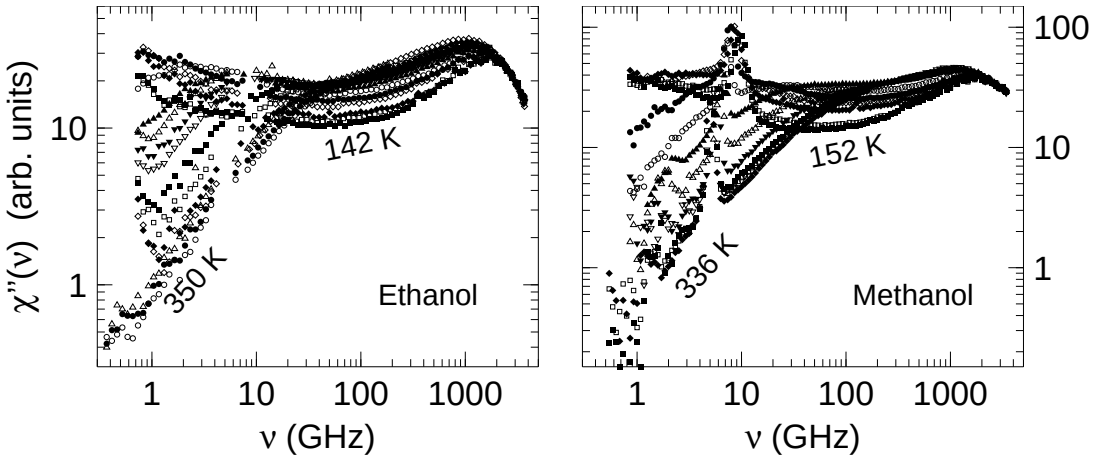

Abbildung 4.4:
Dynamische Suszeptibilitäten von Ethanol (links) bei $T = 142$, 147, 152, 164, 180, 200, 220, 230, 240, 250, 270, 290, 310, 320, 330, 340 und 350 K und Methanol (rechts) bei $T = 152$, 160, 168, 178, 195, 220, 245, 270, 293, 320, 328 und 336 K.

eine strukturelle Relaxation, die dem Zeit-Temperatur-Verschiebungssatz gehorcht. In beiden Substanzen lässt sich diese α-Relaxation durch eine gestreckte Exponentialfunktion von Kohlrausch mit dem einheitlichen Streckungsexponenten $\beta = 0.54$ beschreiben. Die aus diesen Fits extrahierten mittleren Relaxationszeiten $\langle\tau\rangle$ sind nicht proportional zur Viskosität η der beiden Substanzen, sondern verhalten sich annähernd proportional zu η/T, was der Stokes-Einstein-Beziehung entspricht.

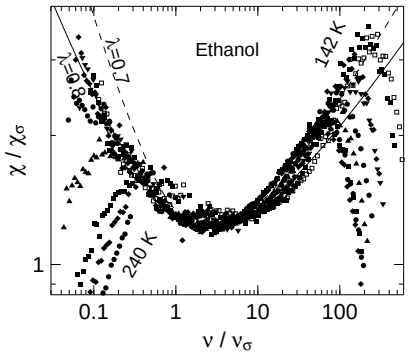

Abbildung 4.5:
Skalenplot der schnellen β-Relaxation in Ethanol, eingezeichnet sind die Skalenfunktionen mit $\lambda = 0.8$ und $\lambda = 0.7$

Da beide Substanzen ein Minimum der schnellen β-Relaxation zeigen, haben wir die Gültigkeit der asymptotischen Skalenfunktion $\chi_\sigma g_\lambda(\nu/\nu_\sigma)$ der Modenkopplungstheorie ausgelotet. Die

Suszeptibilitäten von Ethanol lassen sich für 7 Temperaturen auf eine Meisterkurve reskalieren. (Abb. 4.5) Eine iterative Skalenanalyse liefert einen Exponentenparameter $\lambda \approx 0.8$; die zugehörige Skalenfunktion passt im Niederfrequenzflügel hervorragend an die Daten, weicht bei Frequenzen oberhalb des Minimums jedoch ab. Aus den charakteristischen Frequenzen und Amplituden kann man auf eine Übergangstemperatur von $T_c \approx 103$ K extrapolieren. Die Methanol-Spektren skalieren im Bereich der Minimums nicht, es sind deshalb auch keine asymptotischen Modenkopplungsfits mit einem konsistenten Exponentenparameter möglich.

Für beide Substanzen liegen Datensätze in einem großen Temperaturintervall vor, die einen sehr eingeschränkten asymptotischen Bereich haben. Deshalb bietet sich die Analyse durch ein schematisches Modenkopplungsmodell [1] an. Die Daten weisen keinen starken Bosonpeak auf und können durch das F_{12}-Modell beschrieben werden. Dieses Modell wurde im Jahresbericht 2001 bereits für Benzol eingesetzt. Über weite Bereiche erreichen wir eine gute Fitqualität (Abb. 4.6), lediglich bei niedrigen Temperaturen kann der Bereich der schnellen β-Relaxation nicht optimal angepasst werden.

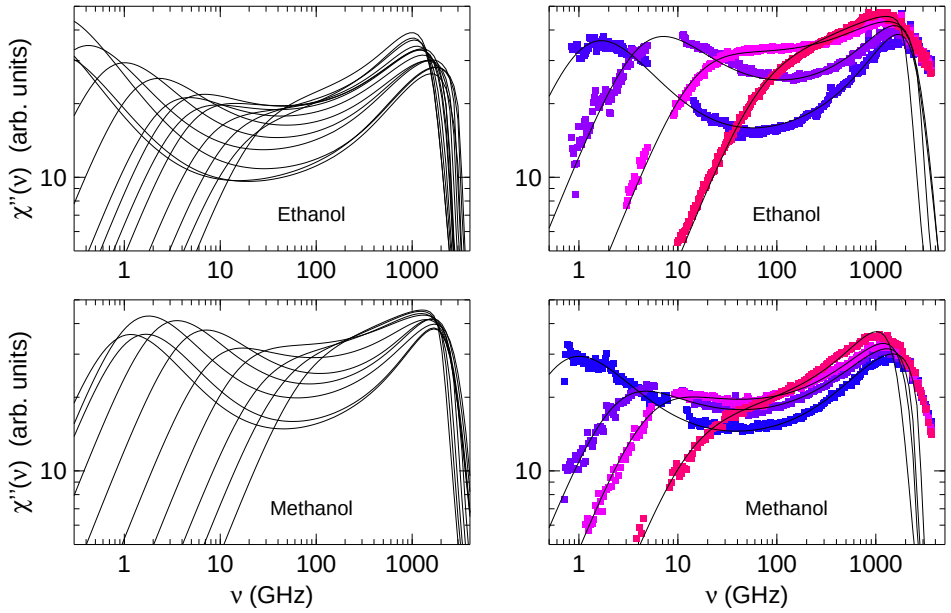

Abbildung 4.6:
Auf der rechten Seite sind die Fits an Ethanol und Methanol für alle gemessenen Temperaturen mit dem schematischen F_{12} Modell der Modenkopplungstheorie gezeigt; auf der linken Seite die Fitkurven mit den zugehörigen Messdaten bei ausgewählten Temperaturen.

Die Werte der Fitparameter Ω_s, γ und γ_s können dabei konstant gehalten werden. Die Kopplungskonstanten v_1, v_2 und v_s fallen in Übereinstimmung mit der Theorie mit steigender Temperatur kontinuierlich ab.

Das Phasendiagramm der $v_1 - v_2$-Ebene verdeutlicht, wie sich die Flüssigkeiten der idealen Glasübergangstemperatur nähern, ohne sie im gegebenen Temperaturintervall ganz zu erreichen. Der Verlauf der Kopplungskonstanten im diesem Phasendiagramm erlaubt Rückschlüsse auf den Exponentenparameter λ. Damit haben wir bei den Ethanol und Methanol die Möglichkeit, die asymptotischen Modenkopplungsfits auf Konsistenz mit den Fits durch das schematische F_{12}-Modell zu prüfen. Eine Extrapolation auf die Phasengrenze führt auf die Exponentenparameter $\lambda = 0.70$ bei Ethanol und $\lambda = 0.68$ bei Methanol.

Bei Ethanol wurde die Asymptote mit $\lambda = 0.70$ als gestrichelte Linie mit in Abb. 4.5 eingezeichnet. Man sieht, dass diese Asymptote im Niederfrequenzflügel weniger gut an die skalierten Suszeptibilitäten passt, im Hochfrequenzflügel jedoch die Daten sehr viel besser beschreibt. Dies bestätigt, wie empfindlich ein aus dem asymptotischen Verhalten bestimmter Exponentenparameter vom gewählten Fitbereich abhängt und demonstriert, dass die aus den schematischen Fits gewonnene Funktion ebenfalls für die Messdaten gültig ist.

Im Fall von Methanol liegt die Asymptote mit $\lambda = 0.68$ zwischen den verschiedenen möglichen asymptotischen Fitfunktionen, die für die verschiedenen Temperaturen an die Messdaten angepasst werden könnten. Die Spektren liegen also durchaus im relevanten Temperaturbereich, der Gültigkeitsbereich der asymptotischen Gesetze ist jedoch hier zu stark eingeschränkt für eine iterative Skalenanalyse.

[1] W. G¨otze: Z. Phys.B **56**, 139 (1984)

The order-disorder phase transition in octamethyl-ethinyl-ferrocene (I): an organometallic rotator phase

T. Asthalter[1], H. Franz[2], U. van Bürck, K. Messel [2], E. Schreier, R. Dinnebier[3]

[1] IPC, Universit¨at Stuttgart
[2] Hasylab/DESY, Hamburg
[3] MPI f¨ur Festk¨orperforschung, Stuttgart

Substituted ferrocenes exhibit a variety of interesting properties, in view of possible applications (UV photocathodes, photochemical quenching agents, anionic photoinitiators), but also under more fundamental aspects of the properties of soft condensed matter. In particular, several ferrocene derivatives were reported to exhibit a mesophase with translational symmetry but rotational disorder between the ordered crystalline and the liquid phase [1–3]. Octamethyl-ethinyl-ferrocene (OMFA) exhibits a sharp decrease of the Lamb-Mössbauer factor at a temperature $T_{pc} \approx 248\,\mathrm{K}$, well below the melting point [4–7]. It has been suggested that this phenomenon is of intramolecular origin, e.g. due to the coupling of librations of the whole molecule to the rotation of the substituted cyclopentadienyl rings [4,5]. No single crystal X-ray diffraction data could be obtained at room temperature due to lack of suitable samples [7].

We have used a combination of quasielastic nuclear forward scattering (QNFS), high-resolution X-ray powder diffraction (XRD) and differential scanning calorimetry (DSC), in order to elucidate some aspects of the associated phase transition on a microscopic basis, dealing with the dynamic processes as well as with the structural changes in the vicinity of T_{pc} [8].

Quasielastic nuclear forward scattering (QNFS) provides information about slow dynamics on the ns-μs scale as well as about the fast dynamics as described by the Lamb-Mössbauer factor. Using this technique at the beamlines PETRA1, Hasylab [9], and ID18, ESRF [10], we were able to demonstrate that below 246 K the dynamics of the Fe atom associated with the phase transition is much slower than the QNFS timescale (141 ns); at 246 and 247 K, the relaxation times are (2.4$\pm$1.7) μs and (1.3$\pm$1.0) μs, respectively; and at 248 K, the relaxation immediately becomes so fast that it can not be monitored any longer by QNFS, but leads to a sharp (however finite) decrease

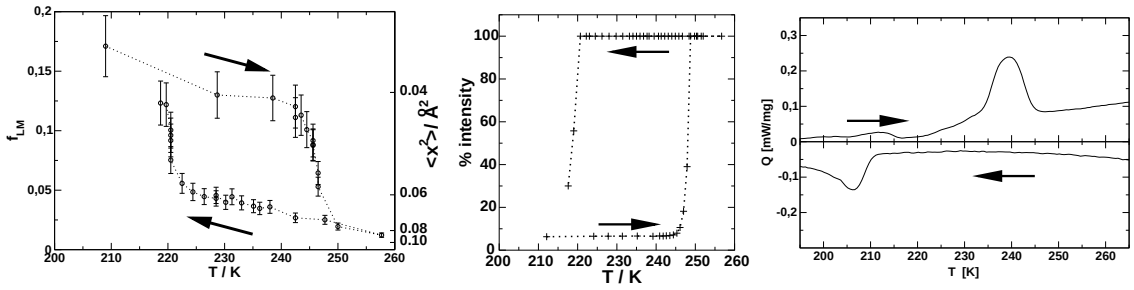

Figure 4.7:
Hysteresis of the order-disorder transition in OMFA. Arrows indicate the direction of heating/cooling. Left: Lamb-Mössbauer factor as determined form QNFS; centre: intensity of XRD peak at 2θ = 6.93°; right: DSC trace at a heating/cooling rate of 10 K/min.

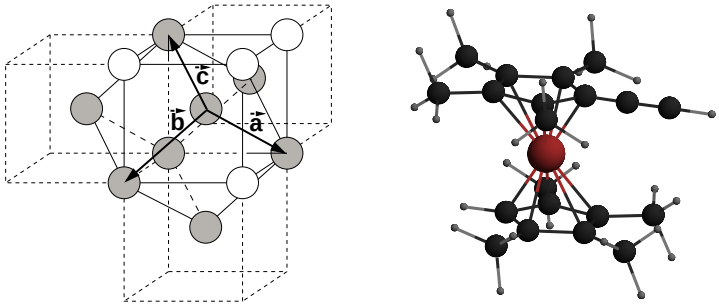

Figure 4.8:
Left: relation between rhombohedral and pseudo-cubic unit cell of the HT phase of OMFA; right: sketch of the OMFA molecule

in the LMF. Furthermore, a strong thermal hysteresis of the LMF was found and confirmed both by XRD and DSC investigations, see Fig. 4.7.

The extremely low number of Bragg reflections and the high diffuse background as obtained by standard laboratory XRD suggested that a rotator phase, where the molecules are positionally ordered but rotationally disordered, is present above the transition temperature. XRD data obtained at the X3B1 beamline (NSLS) allowed us to determine the space group at room temperature (RT). Indexing with ITO led to a hexagonal unit cell (Z = 1) with lattice parameters $a = b$ = 12.9475(1) Å, c = 9.5578(1) Å, which in the rhombohedral setting correspond to a = 8.1258(1) Å, α = 105.63°. Since the rhombohedral angle is close to the tetrahedral angle of 109.47°, it is possible to deduce a related body-centered cubic packing with a "pseudo-cubic" unit cell parameter of 9.383 Å. The geometrical relations between the cubic and the rhombohedral unit cell and the locations of the OMFA molecules are depicted in Fig. 4.8 (left), a sketch of the molecule is shown in Fig. 4.8 (right). No extinctions were found in the powder pattern, indicating $R\bar{3}m$ as the most probable space group. This space group has a higher symmetry than would be compatible with a fixed arrangement of OMFA molecules, whose point symmetry is much lower in all possible conformations, which confirms the assumption of orientational disorder of OMFA in its HT phase.

Using differential scanning calorimetry, an order-disorder transition enthalpy of (9.85±1.05) J g^{-1} or (3186±340) J mol^{-1} was determined, corresponding to a transition entropy of (13.3±1.4)J mol^{-1}K^{-1}. In a very simple model, where all molecular orientations are energetically equal and have well-defined rotation angles for each minimum of the potential well, these

values are compatible with – but no proof for – the assumption that the transition involves the onset of rotation of a substituted cyclopentadienyl ring.

In summary, we conclude that the solid-solid phase transition in OMFA, first found by Mössbauer spectroscopy, is a first-order transition from a low-symmetry low-temperature phase to a high-symmetry high-temperature phase having nearly body-centered cubic symmetry, where the central iron atom moves with a large but finite amplitude around its equilibrium position. Several questions, however, remain to be answered:

What are the driving forces of the observed order-disorder transition? Is it exclusively due to intramolecular degrees of freedom, or does intermolecular steric hindrance come into play? Are the involved degrees of freedom pure rotations of the cyclopentadienyl rings? Is it possible to freeze orientational disorder on a short-range scale and thus to obtain an orientational glass, or does the LT phase simply undergo domain formation?

To this end, XRD investigations of the low-temperature phase, as well as SRPAC (synchrotron radiation-based perturbed angular correlation) experiments, which will allow us to determine rotational relaxation times in the high-temperature phase, are planned or under way.

[1] M. F. Daniel, A. J. Leadbetter, R. M. Richardson, J. Chem. Soc.: Faraday Trans. 2 **77**, 1851 (1981)

[2] K. Sato, M. Iwai, H. Sano, M. Konno, Bull. Chem. Soc. Jpn. **57**, 634 (1984)

[3] K. Sato, M. Katada, H. Sano, M. Konno, Bull. Chem. Soc. Jpn. **57**, 2361 (1984)

[4] I. Nowik and R. H. Herber, Inorg. Chim. Acta **310**, 191 (2000)

[5] R. H. Herber and I. Nowik, Hyperfi ne Int. **126**, 127 (2000)

[6] R. H. Herber, Inorg. Chim. Acta **291**, 74 (1999)

[7] H. Schottenberger, K. Wurst, and R. H. Herber, J. Organomet. Chem. **625**, 200 (2001)

[8] T. Asthalter, H. Franz, U. van B¨urck, K. Messel, E. Schreier, R. Dinnebier, J. Phys. Chem. Solids, in press

[9] H. Franz, B. Hukelmann, J. R. Schneider, Hyperfi ne Int. **126**, 397 (2000)

[10] R. R¨uffer, A. I. Chumakov, Hyperfi ne Int. **97/98**, 589 (1996)

The order-disorder phase transition in octamethyl-ethinyl-ferrocene (II): a nuclear inelastic absorption study

T. Asthalter[1], U. van Bürck, H. Franz[2], E. Schreier, I. Sergueev[3], A. I. Chumakov[4,5]

[1] IPC, Universit¨at Stuttgart
[2] Hasylab/DESY, Hamburg
[3] TUM E13/ESRF, Grenoble
[4] ESRF, Grenoble
[5] Russian Research Centre 'Kurchatov Institute', Moscow

The low-frequency vibrational properties of glasses and other disordered systems are a topic of long-term interest in condensed matter physics [1]. Especially the microscopic origin of the Boson peak is a recent matter of debate. We have applied nuclear inelastic absorption (NIA) to an organometallic compound, octamethyl-ethinyl-ferrocene (OMFA), which was recently found to

undergo a first-order solid-solid phase transition to a rotator phase above T_{pc} = 248 K [2,3]. NIA is a powerful tool for element-selective studies of the vibrational dynamics of crystalline solids and glasses [4]. It yields the vibrational density of states (VDOS) selectively for the resonant Mössbauer nuclei in a material at a resolution that is now comparable to standard infra-red and Raman measurements, and it provides background-free measurements because only the resonant nuclei contribute to the delayed signal.

The issue of the present experiment was twofold:

[1] First, to find out whether the orientationally disordered state might be undercooled, yielding an orientational glass. Thus, in one and the same compound the acoustic modes and in particular the Boson peak might be investigated both for the orientationally ordered and the orientationally disordered state.

[2] Second, to obtain precise phonon densities of states above and below the order-disorder phase transition and to identify the phonons whose DOS undergoes significant changes at T_{pc} and thus possible the driving forces for the phase transition on a microscopic basis.

After first tentative NIA experiments at PETRA1, Hasylab [5] with an energy resolution of 2 meV, the necessity of very high energy resolution, which allows to separate elastic and inelastic contributions also for soft acoustic modes, became obvious. A subsequent experiment was carried out at ID18, ESRF [6], using a three-bounce high-resolution monochromator (HRM) with two highly asymmetrically cut Si (9 7 5) reflections and a Ge(3 3 1) symmetrically cut crystal that ensures an approximately horizontally outgoing beam. A new set of crystals providing an energy resolution of about 0.5 meV was used. Within this bandwidth, a high flux of $3{\cdot}10^8$ s^{-1} was achieved by collimating the beam in front of the HRM by a compound refractive lens. The sample, a pellet of about 0.35 mm thickness, was mounted between thin Be sheets into a copper holder sealed with Kapton windows in a closed-cycle cryostat.

The extraction of the one-phonon contribution and the evaluation of the phonon DOS was carried out using DOS V2.1 [7]. Five spectra were measured, four for OMFA cooled down slowly from room temperature and one for OMFA quenched by immersion into liquid nitrogen. The percentage of subtraction of the elastic line was optimized as described in [8].

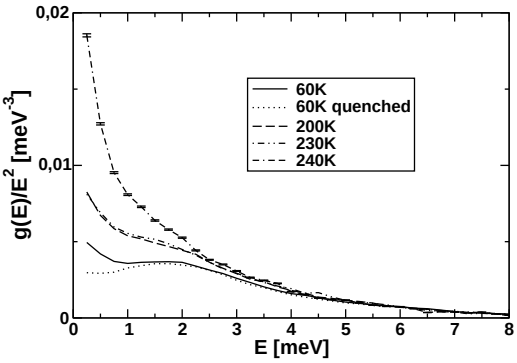

Figure 4.9: Reduced partial Fe VDOS of OMFA

Fig. 1 shows the reduced DOS $g(E)/E^2$ for the slowly cooled (annealed) and the quenched substance for the same temperature (60 K), as well as three temperatures below and slightly above the

order-disorder transition. The deviation from Debye behaviour is small in the annealed phase, but becomes more pronounced on quenching. Frozen orientational disorder is expected to enhance the Boson peak intensity. Instead, a cut-off of the reduced VDOS for lowest energies is observed, much like in our study of glassy ferrocene/dibutylphthalate in nanopores [8]. Whether we have true frozen-in orientational disorder or whether this can be attributed to phonon confinement owing to the formation of nanostructured domains in the undercooled crystal remains to be clarified. The phase transition itself yields an abrupt further increase of the number of very-low-energy modes. From the VDOS, the contribution of the Fe atom vibrations to the phase transition entropy can be estimated using the 230 K and the 240 K data according to

$$S = 3R \int_0^\infty g(E) \left[\frac{\beta E}{2} \frac{\mathrm{e}^{\beta E} + 1}{\mathrm{e}^{\beta E} - 1} - \ln(\mathrm{e}^{\beta E/2} - \mathrm{e}^{-\beta E/2}) \right] \mathrm{d}E \ ,$$

where $\beta = 1/(k_B\,T)$. We obtain a value of $S_{\mathrm{HT,240\,K}} - S_{\mathrm{LT,230\,K}}$ = 0.88 J mol^{-1}K^{-1}, which accounts (not surprisingly) for only 7 % of the total entropy change as determined by DSC [3].

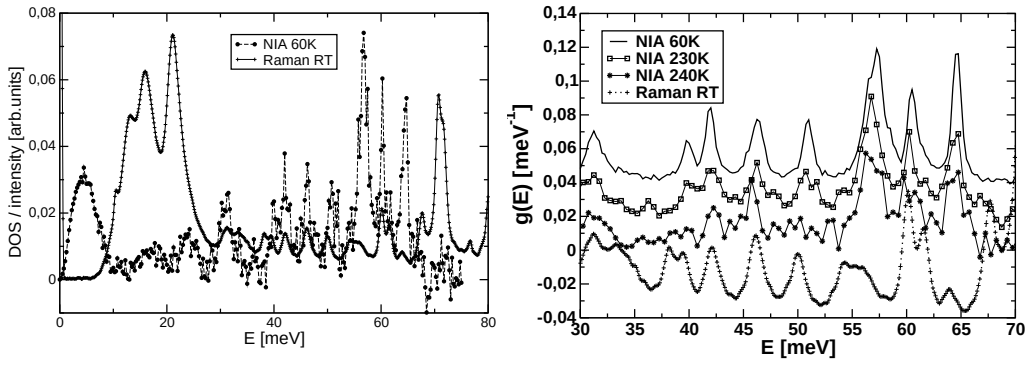

Figure 4.10: Partial Fe VDOS of OMFA vs. Raman intensity

Fig. 2 (left) shows the partial Fe VDOS of OMFA at 60 K together with a room-temperature Raman spectrum. Owing to different selection rules, the acoustical phonons are not visible to Raman but to NIA. Moreover, the relative intensities of the optical phonons, which appear rather well separated from the acoustical phonons, differ strongly in both methods. In particular, the modes between 10 and 30 meV belong mainly to vibrations of the carbon framework of the substituted cyclopentadienyl units with only a low vibrational amplitude of the central iron atom, hence they only appear with significant intensity in the Raman spectrum.

Fig. 2 (right) shows a part of the optical phonon spectrum for 60, 230, and 240 K (set temperature of cryostat), in comparison to the RT Raman spectrum. Error bars for the NIA spectra are about 3–4 times the symbol size. For the sake of clarity, the upper two NIA spectra and the Raman spectrum are offset, and the Raman spectrum has in addition been rescaled.

Some changes in the optical phonons can be observed clearly in the 240 K spectrum but also appear to start already 10 K below: the 51 meV band disappears, and the band at 60.5 meV splits. The latter phenomenon is also observed in the Raman spectrum. An assignment of the phonon bands to different molecular modes should allow us to explain this possible interplay of intra- and intermolecular vibrational modes.

In order to interpret some of the phenomena observed in this study more in detail, X-ray diffraction and Raman studies on both the quenched and the annealed phase of OMFA are planned.

[1] W. A. Phillips (Ed.): *Amorphous solids : low-temperature properties*, Springer, Berlin; Heidelberg 1981

[2] R. H. Herber and I. Nowik, Hyperf. Int. **126,** 127 (2000)

[3] T. Asthalter, H. Franz, U. van B¨urck, K. Messel, E. Schreier, R. Dinnebier, J. Phys. Chem. Solids, in press

[4] A. I. Chumakov, W. Sturhahn, Hyperf. Int. **123/124,** 781 (1999)

[5] H. Franz, B. Hukelmann, J. R. Schneider, Hyperfi ne Int. **126**, 397 (2000)

[6] R. R¨uffer, A. I. Chumakov, Hyperfi ne Int. **97/98**, 589 (1996)

[7] V. G. Kohn, A. I. Chumakov, Hyperf. Int. **125,** 205 (2000)

[8] T. Asthalter, M. Bauer, U. van B¨urck, I. Sergueev, H. Franz, A. I. Chumakov, submitted to Hyperf. Int.

Lichtstreuung an molekularen Fl¨ussigkeiten unter hohem Druck

A. Schulte, W. Doster, R. Gebhard, S. Wiebel

Der Glasübergang in unterkühlten Flüssigkeiten kann durch Temperaturerniedrigung oder isotherme Erhöhung der Dichte erfolgen. Im Übergangsbereich findet eine dramatische Verlangsamung der strukturellen Relaxation statt, und umfangreiche Untersuchungen der Temperaturabhängigkeit der Dynamik mit Streuexperimenten haben die von der Modenkopplungstheorie vorhergesagten Skalengesetze bestätigt. Bisher gibt es aber nur wenige Messungen der Dynamik mit Licht- oder Neutronenstreuung als Funktion des Drucks, obwohl die Einbeziehung dieser thermodynamischen Variable erlaubt, Volumen- von thermischen Effekten zu separieren. Durch eine verbesserte Geometrie zur Detektion des Streulichts und Optimierung des Strahlengangs wurde die Empfindlichkeit des E13-Ramanspektrometers und des Tandem-Fabry-Perot-Interferometers wesentlich erhöht und die Voraussetzung für Druckexperimente geschaffen. Erste Lichtstreuesm-

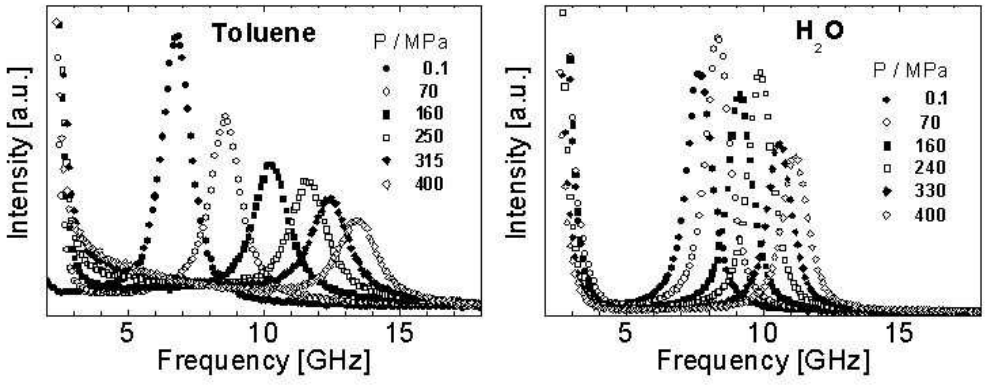

Abbildung 4.11:
Brillouinspektren von Toluol (links) und Wasser bei verschiedenen Drucken (0.1 - 400 MPa) gemessen in 180° Rückstreugeometrie. Aufgetragen ist Streuintenstät als Funktion der Frequenz. Steigender Druck verschiebt die Brillouinlinie zu höheren Frequenzen.

sungen wurden über einen Druckbereich von 0.1 bis 400 MPa in einer hydrostatischen Zelle bei Raumtemperatur durchgeführt.

Die Änderung des Brillouinspektrums mit dem Druck zeigt die Wechselwirkung longitudinaler Schallwellen mit strukturellen Relaxationsprozessen. Die Brillouinlinie verschiebt sich zu höheren Frequenzen und gleichzeitig ändert sich die Linienbreite. Eine quantitative Analyse der Linienform und Vergleich mit Relaxationsmodellen ist im Gange. Für druckabhängige Messungen der depolarisierten Streuung soll das Fenstermaterial der Hockdruckzelle weiter im Hinblick auf Polarisationseigenschaften optimiert werden.

5 Festkörpertheorie

Modenkopplungstheorie f¨ur die Beschreibung anomaler Schwingungseigenschaften von Gläsern

Edith Maurer, Walter Schirmacher und Markus Pöhlmann

Wir gehen von folgendem vereinfachten Modell für die Schwingungsanregungen in einem ungeordneten Festkörper („Glas“) aus: Wir nehmen an, daß die strukturelle Unordnung im Glas zu statistischen Schwankungen der Schallgeschwindigkeit c (beziehungweise ihres Quadrats $c^2 = \tilde{K}$, „elastische Konstante“) an verschiedenen Orten führt. Der „Unordnungsparameter“, der diese „gefrorene Unordnung“ charakterisiert, ist die Varianz $\gamma \propto \langle \Delta \tilde{K}^2 \rangle$. Weiterhin nehmen wir an, dass die Schallanregungen durch die anharmonische Wechselwirkung an momentane Dichteschwankungen gekoppelt sind. Kopplungsparameter ist der Grüneisenparameter g. Aus der hierfür maßgeblichen Lagrangedichte einer verallgemeinerten Elastizitätstheorie läßt sich mit Hilfe der Feynmanschen Pfadintegralquantisierung eine Quantenfeldtheorie für die thermischen Schallanregungen **u(r,t)** formulieren. Die Konfigurationsmittelung über die gefrorene Unordnung läßt sich mit Hilfe des „Replika-Tricks“ durchführen. Das führt auf eine nichttriviale effektive Feldtheorie für die **u(r,τ)**-Felder (τ sind imaginäre Zeiten). Mit Hilfe der sogenannten Fadeev-Popov-Transformation wird nun eine neue Feldtheorie für zusammengesetzte Matrix-Felder $Q_{\alpha\alpha'}(\mathbf{r}, \tau, \tau') = \nabla \cdot \mathbf{u}(\mathbf{r}, \tau) \nabla \cdot \mathbf{u}(\mathbf{r}, \tau')$ formuliert, die es ermöglicht, die ursprünglichen Felder **u(r,τ)** auszuintegrieren. Die resultierende effektive Feldtheorie ist Ausgangspunkt für ein nichtlineares Sigma-Modell zur Untersuchung der Lokalisierungseigenschaften der Schallmoden.

Der erste Schritt bei der Ausarbeitung des nichtlinearen Sigma-Modells ist die Durchführung einer Sattelpunktsnäherung (Molekularfeldtheorie). Es stellt sich nun heraus, daß diese Sattelpunktsnäherung äquivalent zu einer schematischen Modenkopplungstheorie (MCT) für die dynamische Suszeptibilität, bzw. für die Dichte-Dichte-Korrelationsfunktion, die die Einteilchen-Schwingungsanregungen des ungeordneten Fesktörpers beschreibt.

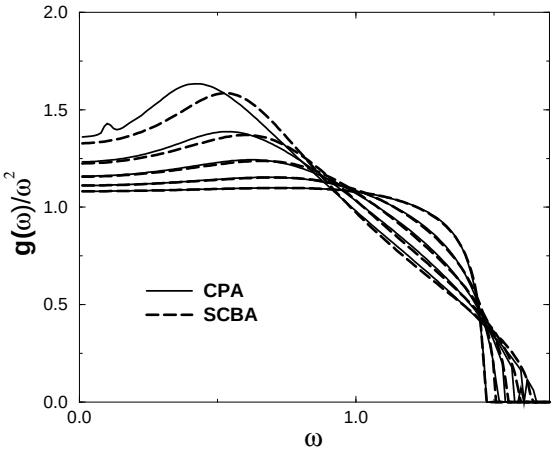

Abbildung 5.1:
Vergleich der SCBA mit der CPA für verschiedene Werte des Unordnungsparameters γ.

Setzt man die anharmonische Kopplung $g = 0$, so ist die MCT äquivalent zur selbstkonsistenten Born-Näherung (SCBA), die wiederum eine Vereinfachung der Coherent-Potential-

Approximation (CPA) zur Beschreibung des Schwingungsspektrums ungeordneter Festkörper darstellt. Insbesondere läßt sich die Überhöhung der Zustandsdichte im Vergleich zum Debyeschen ω^2-Gesetz („Boson-Peak“) in dieser Näherung als natürliche Konsequenz der Unordnung, charakterisiert durch den Parameter γ, beschreiben.

In Anwesenheit der anharmonischen Kopplung wird die Einteilchen-Molekularfeldtheorie mathematisch äquivalent zur Quanten-Version des sogenannten F-1-2-Modells von W. Götze [2]. Die numerische Lösung der Quanten-MCT-Gleichungen bereitete bisher Schwierigkeiten, deshalb liegen noch keine quantitativen Aussagen der Theorie bzgl. der anomalen Schwingungseigenschaften von ungeordneten Fesktörpern vor. Qualitativ lassen sich allerdings sehr wohl einige interessante Aussagen machen. Da die Spektralfunktionen der Quanten-MCT im Niederfrequenzlimes (genauer: für $\hbar\omega \ll k_B T$, T ist die Temperatur) mit denen der klassischen analogen Theorie übereinstimmen, gelten die asymptotischen Eigenschaften des F-1-2-Modells ebenfalls für die Quanten-Version. Wie Götze gezeigt hat [2] gibt es in diesem Modell in Abhängigkeit der Kontrollparameter λ_1 (bei uns proportional zu γ) und λ_2 (bei uns proportional zu $\gamma^2 gT$) Übergänge zu nichtergodischen Zuständen von unterschiedlichem Typ (s. Fig. 5.1)

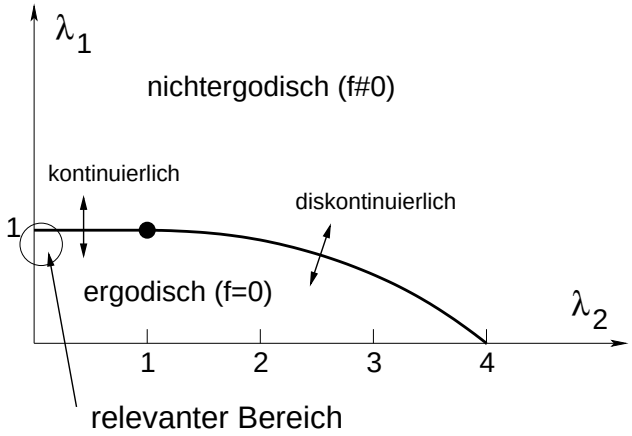

Abbildung 5.2:
Phasendiagramm des F-1-2-Modells von Götze [2]. Bei uns ist der Parameter λ_2 proportional zur anharmonischen Kopplung, multipliziert mit der Temperatur, der Parameter λ_1 ist proportional zum Unordnungsparameter γ.

Bei tiefen Temperaturen ist zu erwarten, dass der Parameter λ_2 sehr klein ist, so dass wir uns im Phasendiagramm (Abbildung 5.2) in der durch den Kreis bezeichneten Region befinden. Bei erhöhter Unordnung (Parameter λ_1) ergibt sich ein kontinuierlicher Übergang zu einer Phase mit einem nichtverschwindendem zusätzlichen Debye-Waller-Faktor (Nichtergodizitätsparameter). Das bedeutet, dass die erhöhte Unordnung zu einer Instabilität führt, so dass das Glas sich eine neue „Gleichgewichtsposition“ sucht. Der Boson-Peak und die anderen Tieftemperaturanomalien sind Vorankündigungen (Precursor) dieses Überganges.

[1] W. Schirmacher, M. P¨ohlmann, E. Maurer, phys. stat. sol. (b) **230**, 31 (2002)

[2] W. G¨otze, Z. Phys. B **56**, 13 (1984)

Bruchkontakt-Tunnelspektroskopie an dotierten Halbleitern

Olaf Bleibaum[1] [2], Barbara Sandow[3], Walter Schirmacher

[1] Phys. Dept. Univ. of Oregon, Eugene, OR, USA
[2] Fachbereich Physik, Univ. Magdeburg
[3] Fachbereich Physik, Freie Univ. Berlin

Tunnelspektroskopie ist eine der viel verwendeten Methoden, um die elektronische Zustandsdichte von Festkörpern auszumessen. Typischerweise wird der Strom zwischen zwei gut leitenden Materialen (meist Metallen) gemessen, die durch eine isolierende Schicht voneinander getrennt sind. Der resultierende Tunnelstrom $I(U)$ (bei angelegter Spannung U) ist eine Faltung der Zustandsdichten der Kontaktmaterialien. Ist die Zustandsdichte des einen Materials bekannt, kann die des anderen ausgemessen werden. Insbesondere zeigt sich, dass in vielen Fällen die differentielle Leitfähigkeit $\mathrm{d}I/\mathrm{d}U$ proportional zu $N(E = eU)$ ist, wobei $N(E)$ die Zustandsdichte des

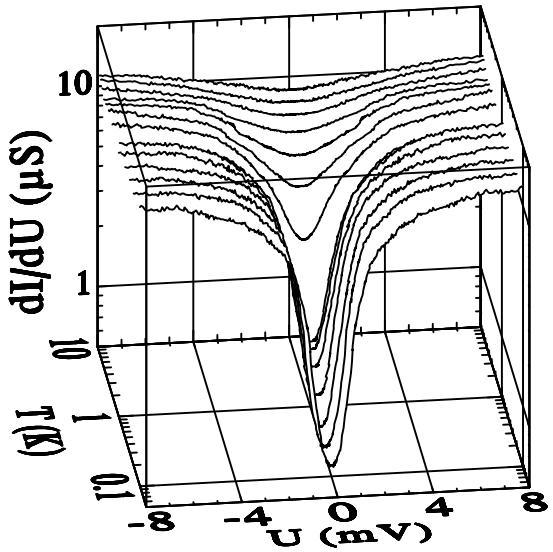

Abbildung 5.3: Differentielle Leitfähigkeit eines neutronentransmutationsdotierten Germanium-Bruchkontaktes in Abhängigkeit von der Spannung U und der Temperatur T

zu untersuchenden Materials ist. An der TH Darmstadt und der FU Berlin wurde eine spektroskopische Methode entwickelt, um die Zustandsdichte von dotierten Halbleitern auszumessen. Hier wird die Probe auf mechanisch kontrollierte Weise zerbrochen und der Tunnelstrom quer zum Bruchkontakt gemessen [1].

Dotierte Halbleiter bei tiefen Temperaturen sind deswegen besonders interessant, weil schon seit langer Zeit vorhergesagt wird, dass die Zustandsdichte (hier die Dichte der lokalisierten elektronischen Zustände) aufgrund der Coulomb-Wechselwirkung zwischen den Elektronen eine parabelförmige „Lücke“ von der Form $|E - E_F|^\gamma$ (mit $\gamma \approx 2$) in der Nähe des Ferminiveaus E_F aufweisen sollte („Coulomb-Gap“). Eine solche Anomalie wurde mit Hilfe der Bruchkontakt-Methode tatsächlich in dotiertem Germanium (Neutronentransmutationsmethode) bei tiefen Temperaturen gefunden (Fig. 1, [2]). Neuartig und unerwartet war, dass der Coulomb-Gap sich mit steigender Temperatur offenbar durch thermische Elektron-Loch-Anregungen auffüllt [2]. Die

„naive“ Auswertung und Interpretation mit Hilfe der für Metalle entwickelten theoretischen Ausdrücke wurde allerdings kritisiert [3] mit dem Hinweis darauf, dass der Transportmechanismus zwischen lokalisierten Zuständen („Hopping-Transport“) wesentlich komplizierter als der in Metallen ist und daher auch die Tunnelmessungen anders ausgewertet werden müssten (s. auch die Antwort [4]). Die Hauptfrage ist, ob der Spannungsabfall, der die Kennlinie produziert, nur am Bruchkontakt oder auch schon im Volumen der Kontakte stattfindet.

Wir haben daraufhin eine neue, auf den Fall des Hopping-Transports in dotierten Halbleitern zugeschnittene Theorie der Tunnelspektroskopie in Bruchkontakten entwickelt. Wichtigstes Ergebnis ist, dass man zwar im allgemeinen annehmen muss, dass die Tunnelübergänge zwischen den Kontakten unter Emission eines Phonons stattfinden. Das modifiziert den Ausdruck für den Tunnelstrom so, dass dem „Absorptionsvermögen“ des Phononenbades Rechnung getragen wird. Hat diese Spektralfunktion allerdings ein Maximum bei tiefen Frequenzen, ergibt sich die „quasielastische“ Formel, die auch für Metalle verwendet wird (e ist die Elemetarladung):

$$I(U) \propto \int_{E_F}^{E_F+eU} \mathrm{d}E N(E) N(E - eU). \tag{5.1}$$

und aus der sich die Daten in Fig. 5.3 als Zustandsdichte interpretieren lassen

[1] B. Sandow, K. Gloos, R. Rentzsch, A. N. Ionov, Physica **284**, 1852 (2000)

[2] B. Sandow, K. Gloos, R. Rentzsch, A. N. Ionov and W. Schirmacher, Phys. Rev. Lett. **86**, 1845 (2001)

[3] V. Kozub, Phys. Rev. Lett. **89**, 229701 (2002)

[4] B. Sandow, K. Gloos, R. Rentzsch, A. N. Ionov and W. Schirmacher, Phys. Rev. Lett. **89**, 229702 (2002)

6 Dynamik von Biomolekülen

Assoziation von Myoglobin unter Druck

R. Gebhardt, W. Doster

Aggregationsprozesse von Proteinen sind von wachsendem wissenschaftlichen und gesellschaftlichen Interesse, aufgrund ihrer Bedeutung bei einer Vielzahl von Krankheiten wie z.B. BSE (Bovine Spongiforme Encephalopathie) und der Alzheimer-Krankheit. Dabei nehmen Proteine eine unkorrekt gefaltete oder ungeordnete Struktur an und verklumpen schliesslich zu sogenannten Plaques. Um derartige Prozesse verstehen zu können, werden die kritischen Bedingungen erforscht, die eine Aggregation bei Proteinen auslösen. Diese werden durch Temperatur, Druck und chemisches Potential der Komponenten im Phasenraum bestimmt. Die Fähigkeit zur Assoziation macht Myoglobin zu einem geeigneten Modellsystem, welches wir mit Hilfe der dynamischen Lichtstreuung unter Druck untersuchen. Unter speziellen Salz- und pH-Bedingungen [1] konnte das Auftreten von fibrillären Myoglobinaggregaten beobachtet werden. Außerdem wurde die Bildung von Myoglobinaggregaten bei Normaldruck nach einer vorherigen Druckbehandlung beschrieben [2]. Wir konnten zeigen, dass Myoglobin bereits unter Druck assoziiert und Aggregate von einigen **?**m ausbildet [3]. Wir haben weiterführend die kritischen Bedingungen für die Assoziation von Myoglobin im p-T-Phasenraum und in Abhängigkeit von der Protonen- und Salzkonzentration untersucht. Dabei konnte gezeigt werden, dass die Keimbildung der Assoziation reversibel und bei geringen Drücken weit unterhalb der für die Proteindenaturierung benötigten Drücke erfolgt.

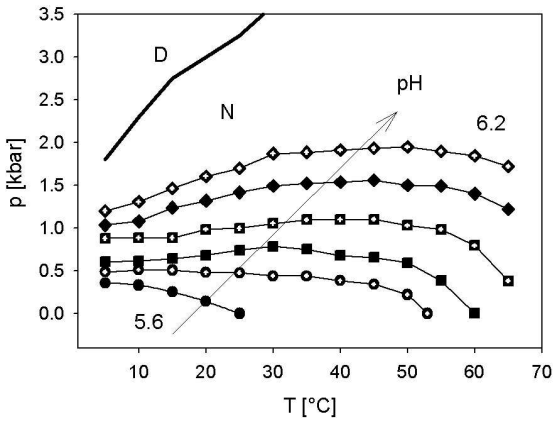

Abbildung 6.1: Phasendiagramm der Myoglobin-Assoziation N-nativ, D-denaturiert

Das Phasendiagramm zeigt ähnlich der Proteindenaturierung eine elliptische Form. Unterhalb eines pH-Wertes von 5.4 wird die Assoziation aufgrund einer durch saure Denaturierung bedingten Konformationsumwandlung unterbunden. Der kritische Druck für die Myoglobin-Assoziation nimmt mit steigendem pH-Wert zu und liegt bei einer Proteinkonzentration von 1 mg/ml, einem pH-Wert von 6.0 und 20 °C bei 1 kbar. Die Reversibilität der Assoziation wurde mit Hilfe von Druckzyklen getestet. In der Anfangsphase zerfallen die Assoziate nach Druckverminderung wieder. Mit ansteigender Assoziatgrösse wird aber die Reversibilität zunehmend eingeschränkt, was auf einen Konformationsübergang mit der Ausbildung von intramolekularen ß-sheet-Strukturen

zurückzuführen ist, wie FT-IR-Messungen zeigen. Unsere weiter Forschung wird sich mit der Klärung des zugrundeliegenden Reaktionsmechanismus und der Auswertung von Assoziationskinetiken befassen.

1 M. F¨andrich, M.A. Fletcher and C.M. Dobson (2002): *Amyloid Fibrils From Muscle Myoglobin.*, Nature 410, 165-166 (2001).

2 L. Smeller, P. Rubens, K. Heremans (1999): *Pressure Effect on the Temperature-Induced Unfolding and Tendency To Aggregate of Myoglobin*, Biochemistry 38, 3816-3820

3 R. Gebhardt et al. (2003): *Critical Association of Myoglobin*, High Pressure Research in Bioscience and Biotechnology, Ed. R. Winter, Springer Verlag (2003) in press

Casein-Mizellen unter Hochdruck

R. Gebhardt, W. Doster, B. Rademacher[1], U. Kulozik[1]

[1] Lehrstuhl f¨ur Lebensmittelverfahrenstechnik und Molkereitechnologie Weihenstephan, TU M¨unchen

Im Rahmen des Hochdruckprojektes wird in Zusammenarbeit mit dem Institut für Lebensmittelverfahrenstechnik und Molkereitechnologie der Einfluss von Hochdruck auf die Größe von Caseinmizellen untersucht, wobei die Herausforderung in der Messung der Lichtstreuung von trüben Proben liegt. Um das Problem der Vielfachstreuung zu minimieren, messen wir in 177° -Rückstreuung mit einem speziellen Rückstreudetektor nahe an der Probenzelloberfläche. Caseinmizellen bilden einen Hauptbestandteil der Milch und sind in der Lage große Mengen des ansonsten schlecht löslichen CaPO4 zu speichern. Die isolierten Proteinmizellen wurden mit Hilfe der dynamischen Lichtstreuung druck- und temperaturabhängig untersucht.

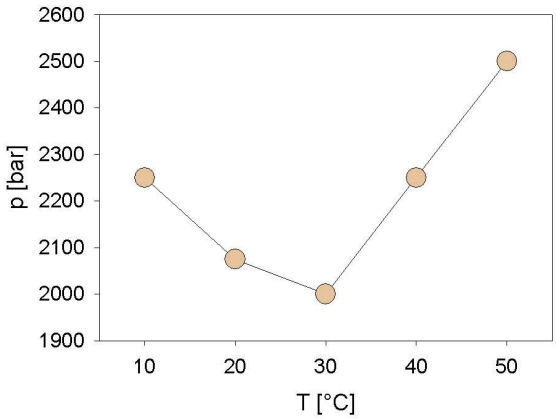

Abbildung 6.2:
Caseinmizelle unter Druck im p-T-Diagramm. Die Phasengrenze trennt den strukturell intakten vom strukturell zerfallenen Zustand der Proteinmizelle.

Im Druckbereich zwischen 2-3 kbar wurde ein Übergang festgestellt, bei dem die Casein-Mizelle strukturell zerfällt. Abbildung 6.2 zeigt die Abhängigkeit des Übergangsdrucks bei verschiedenen Temperaturen. In zukünftigen Messungen soll die Abhängigkeit dieser Stabilitätsgrenze von weiteren relevanten Parametern wie z.B. der Protonenkonzentration untersucht werden.

Protein Diffusion in Crowded Solutions

S. Longeville[1], and W. Doster

[1] Laboratoire Léon Brillouin, Saclay

The interior of living cells is a complex, crowded environment, composed of a large number of proteins at high concentration. The corresponding volume fractions range up to 0,4. Under these conditions protein-protein interactions play a central role. In vivo, transient clusters of enzymes are formed depending on physiological requirements. A particular aspect concerns the transport of small molecules like calcium or oxygen by protein diffusion. In red blood cells, hemoglobin molecules are densely packed.The exchange of oxygen in the lung is facilitated by macromolecular diffusion. This is also applies to the oxygen transport in muscle cells by myoglobin. The transport depends on a a delicate balance between two opposing factors: High protein concentrations, which will enhance the quantity of stored oxygen, and crowding, which will depress the speed of oxygen transport because of strong protein interactions. In fact an optimum concentration for the oxygen flux is observed. The goal of this project is to clarify the question, whether the mobility of different components in a living cell can be understood based on their intermolecular interactions. As a model system we study the diffusion of myoglobin and hemoglobin molecules versus concentration, but also diffusion of hemoglobin in blood cells. Interactions are derived based on the experimental intermolecular structure factors using low angle neutron scattering and MSA- analysis. The technique of neutron spin echo spectroscopy allows one to measure macromolecular diffusion in crowded environments and even in cells. During the last year we have studied the structure and dynamics of concentrated myoglobin solutions using the resonance-spin-echo spectrometer at the LLB in Saclay and IN15 in Grenoble. Extensive low angle neutron scattering experiments were performed to determine the intermolecular structure factor. Finally diffusion of hemoglobin inside erythrocytes was measured with the IN15 spin echo machine. We observe strong concentration dependent effects, the diffusion coefficient varies with q and hydrodynamic interactions have to be taken into account.

Elastic Resolution Spectroscopy of Weakly Scattering Samples

W. Doster, R. Gebhardt, R. Lechner [1] and J. Pieper [1]

[1] Hahn Meitner Institut Berlin

With this project we intend to establish a modified time-of-flight method, which allows to analyze the molecular dynamics of weakly scattering samples. This aspect is particularly relevant in the context of molecular biology, where more than a few milligrams of sample are rarely available. With conventional time-of-flight spectroscopy one needs typically several hundred milligrams of material. Due to the solid-like nature, most bio-molecules display an intense elastic line in the neutron scattering spectrum. However, the quasi-elastic wings of such spectra, which carry the relevant dynamic information, are typically by two orders in magnitude less intense than the narrow central line. To derive high quality spectral information thus involves large samples and long exposure times. We propose an alternative procedure based on the sum rule: Changes in the quasi-elastic spectrum will affect the elastic line such that the frequency integral is preserved. Since

the elastic line is generally much narrower than the quasi-elastic spectrum, changes in the latter will be amplified in the elastic range. Thus focusing on the strong elastic intensity allows one to operate with much less material, where the signal to background ratio is still tolerable. The time axis is introduced by changing the width of the instrumental resolution function. The elastic intensity displayed as a function of the reciprocal instrumental width provides a close approximation to the intermediate scattering function in the time domain. Such experiments can be performed with existing TOF-TOF spectrometers. The resolution is modified by varying the speed of the choppers between 1000 and 20 000 rpm and the incoming wavelength. The most recent ERS-experiment was performed using the V3 TOF-TOF machine at the HMI in Berlin in collaboration with R. Lechner and J.Pieper. With alanine-dipeptide and lactalbumin we could demonstrate the feasibility of the method using V3. Special sample holders are developed to reduce the background intensity in such experiments. The figure shows an analysis of 23 mg of myoglobin 6.3.

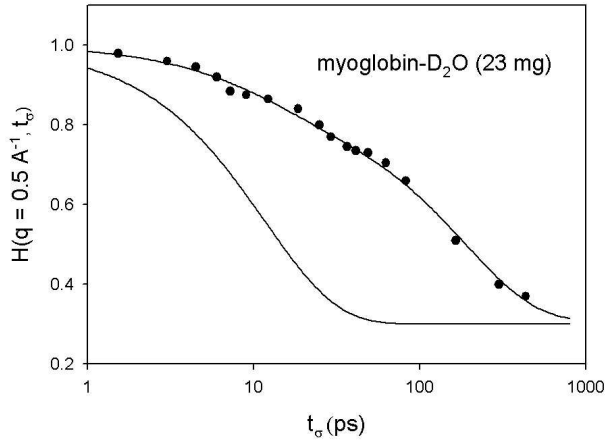

Abbildung 6.3: ERS-correlation function and 2-component analysis (10 and 150 ps)

FTIR-Spektoskopie an Proteinen und Bakterienmembranen

A. Schober, W. Doster, R. Gebhardt, H. Harlandt und A. Schulte

Fourier Transform Infrarot Spektroskopie (FTIR) erlaubt die Untersuchung von Schwingungsbanden, die auf Änderung in der Sekundär- und Tertiärstruktur von Proteinen empfindlich sind. Insbesondere eignen sich diese zur Untersuchung Temperatur und Druck induzierter Faltungsprozesse. Es wurde eine temperaturstabilisierte Flüssigkeitszelle entwickelt und Messungen zwischen 270 K und 360 K an Myoglobin und Lysozymlösungen durchgeführt. Die Absorptionspektren von Myoglobinlösungen im Temperaturbereich zwischen 340 K und 355 K zeigen Änderungen in der Linienform der Amidbanden und Auffalten des Proteins.
Im Rahmen einer Werkstudenten-Tätigkeit hat Herr Schober Messungen am FTIR-Spektrometer an Proteinen und Milchbakterien durchgeführt. Speziell wurden die Absorptionsspektren von an Myoglobin und Lysozym adsorbiertem Wasser als Funktion der Temperatur untersucht. Bei der thermischen Auffaltung zeigen sich drastische Änderungen in den Amidbanden und der Wasserabsorption. Ein wichtiger Test war die Temperaturabhängigkeit der C-H Streckschwingung bei Milchsäuerebakterien. In Zusammenarbeit mit Herrn Gänzle (Mikrobiologie in Weihenstephan)

wurde die Stabilisierung der Bakterienmembran durch Saccharose nachgewiesen. Die Membranen zeigen einen Phasenübergang bei etwa 20°C von einer festen zu einer flüssig-kristallinen Phase, die sich über eine Verschiebung der C-H Streckschwingung beobachten lässt. Durch die Saccharose wird die Übergangstemperatur leicht verschoben (untere Kurve in Abbildung 6.4).

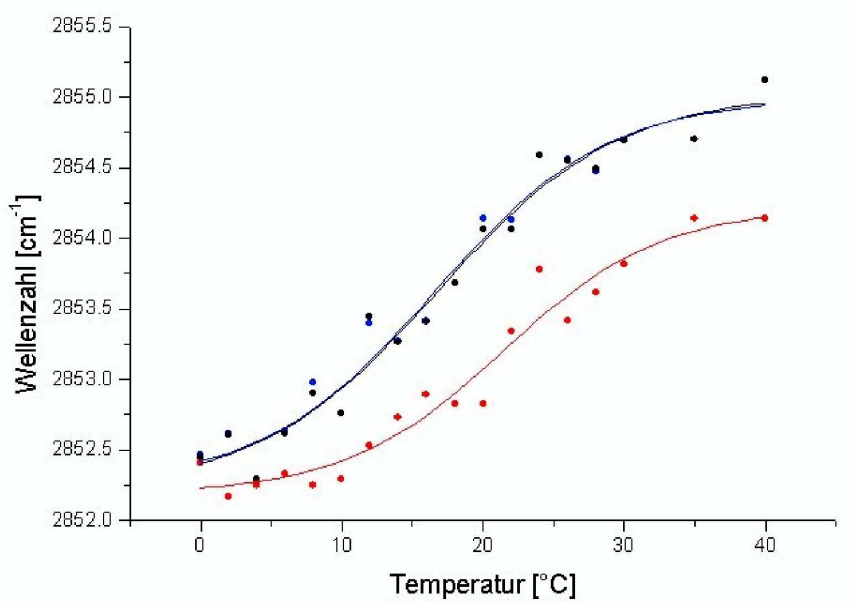

Abbildung 6.4:
C-H Streckschwingung der Membran von Milchsäuere Bakterien als Funktion der Temperatur mit und ohne Saccharose

7 Lehrveranstaltungen

Vorlesungen und Praktika

Sommersemester 2002

Priv. Doz. Dr. W. Doster, *Proseminar Physikalische Grundlagen der Biotechnologie*

Dr. A. Meyer, *Festkörperphysik mit Neutronen II*

Dr. P. Müller-Buschbaum, *Polymerphysik II*

Priv. Doz. Dr. W. Schirmacher, *Proseminar Dynamische Systeme und Chaos*

Prof. Dr. A. Schulte, *Experimentalphysik II für Vermessungsingenieure und Geologen*

Wintersemester 2002/2003

Priv. Doz. Dr. W. Doster, *Dynamik der Wärme*

Dr. A. Meyer, *Festkörperphysik mit Neutronen I*

Dr. habil. P. Müller-Buschbaum, *Polymerphysik I*

Prof. Dr. R. Röhlsberger, *Experimentalphysik I für Vermessungsingenieure und Geologen*

Priv. Doz. Dr. W. Schirmacher, *Computer Physik*

Priv. Doz. Dr. W. Schirmacher, *Mathematische Ergänzungen zur Experimentalphysik I*

Betreute Praktikumsversuche

Degree of dissociation and the freezing point depression (DIS)
Anfängerpraktikum

Dynamische Lichtstreuung an Latexkugeln
Fortgeschrittenenpraktikum

Thermische Analyse
Fortgeschrittenenpraktikum

Viskosität
Anfängerpraktikum

Fortbildungsveranstaltung f¨ur Gymnasiallehrer

EDGAR–LÜSCHER–PHYSIKSEMINAR 2002

Klima, Energieversorgung der Zukunft und Probleme der Kernenergie

Freitag, 12. April bis Sonntag, 14. April 2002
Gymnasium Zwiesel

Veranstalter: Der Ministerialbeauftragte für die Gymnasien in Niederbayern, G. Rauprich

Wissenschaftliche Leitung: Prof. Dr. K. Heinloth, Univ. Bonn und
Priv. Doz. Dr. W. Schirmacher, Technische Universität München

Organisation am Ort: Gymnasium Zwiesel (OStD H. Kratzer, OStR G. Haller)

PROGRAMM

Freitag, 12. 4. 2002	
16.15 – 16.30	PD Dr. W. Schirmacher, TU München *Begrüßung, Organisatorisches*
16.30 – 17.30	Prof. Dr. K. Heinloth, Univ. Bonn *Einführung*
17.30 – 18.00	*Pause*
16.30 – 17.30	Prof. Dr. K. Heinloth, Univ. Bonn *Klimaverträglichkeit von Arten der Energiegewinnung*
Samstag, 13. 4. 2002	
9.00 – 10.30	Prof. Dr. W. Seiler, Inst. f. Meteorologie, Garmisch *Simulation von Klimaänderungen*
11.00 – 12.30	Prof. Dr. W. Petry, TU München *Der Hochtemperatur-Kernreaktor: Eine Chance für die Zukunft*
15.00 – 16.30	Prof. Dr.-Ing. D. Hein, TU München *Emissionsfreie Energieversolgung mit biogenen und fossilen Brennstoffen*
17.00 – 18.30	Dr. M. Eikerling, TU München] *Brennstoffzellen*
Sonntag, 14. 4. 2002	
9.00 – 10.30	Prof. Dr.-Ing. H. J. Wagner, Ruhr-Univ. Bochum *Windenergie*
11.00 – 12.30	Dr. Ch. Nebel, TU München *Sonnenenergie*

8 Allgemeine Zusammenstellungen

Diplomarbeiten, Dissertationen, Habilitationschriften, Auszeichnungen

Diplomarbeiten

Edith, Maurer
Feldtheoretische Behandlung von Schwingungen in ungeordneten Festkörpern
Mai 2002

Florian Kargl
Struktur und Dynamik von Natrium-Silikat-Schmelzen untersucht mit inelastischer Neutronenstreuung
Juli 2002

Dissertationen

Ingo Köper
Influence of trehalose on the dynamics of the S-phyco-cyanin Protein; a quasielastic neutron scattering study
Juli 2002

Habilitationschriften

Peter Müller-Buschbaum
Nanostrukturierte Polymerfilme
Juni 2002

Andreas Meyer
Atomarer Transport in mehrkomponentigen, zähen Schmelzen
November 2002

Auszeichnungen

A. Meyer
Forschungsstipendium zur Untersuchung des *Einfluss von Wasser auf atomare Dynamik und Struktur von Silikatschmelzen und Gläsern* verliehen vom Bund der Freunde der Technischen Universität München e.V., Juni 2002

R. Röhlsberger
Innovationspreis Synchrotronstrahlung 2002, verliehen vom Verein der Freunde und Förderer des BESSY, Berlin, Dezember 2002

Drittmittelförderung

Deutsche Forschungsgemeinschaft

Im Rahmen des Schwerpunktprogrammes: “Phasenumwandlungen in mehrkomponentigen Schmelzen”
Untersuchung des Einflusses der atomaren Dynamik auf Materietransport, Segregation und Erstarrung mehrkomponentiger Schmelzen
Förderkennzeichen: Me 1958/2-1

Im Rahmen einer Forschergruppe: ”Einfluss von Hochdruck auf molekulare und zelluläre Systeme in Lebensmitteln”
Förderkennzeichen: FOR358/2-2, Teilprojekt A1

Im Rahmen des Normalverfahrens:
Dynamik von einfachen und zähen Flüssigkeiten untersucht mit dynamischer Lichtstreuung und inelastischer Neutronenstreuung
Förderkennzeichen: Me 1958/3-1

Im Rahmen des Normalverfahrens:
Wärmeleitfähigkeit von Gläsern
Förderkennzeichen Schi308/6-1

Bundesministerium f¨ur Bildung und Forschung

Weiterentwicklung der Infrastruktur der ESRF-Messplätze für Kernresonanzstreuung
Förderkennzeichen 05KS1WOC/2

Kollektive Dynamik von Proteinen und Proteinkomplexen
Förderkennzeichen 03DOE2M/1

Die Morphologie einer neuen Klasse von Verbundmaterialien: Dünne Copolymerfilme mit eingebauten magnetischen Nanopartikeln
Förderkennzeichen 03DUOTU1/4

Multiskalige Polymermischungsfilme
Förderkennzeichen 03MBE3M1

Abhängigkeit des Haftvermögens dünner Polymerfilme von der Oberflächenmorphologie
Förderkennzeichen 03CO333

Bau eines thermischen Dreiachsenspektrometers am FRM-II
Förderkennzeichen 03EC5SRM/1

Veröffentlichungen

K. Achterhold, C. Keppler, A. Ostermann, U. van Bürck, W. Sturhahn, E. E. Alp, F. G. Parak
Vibrational dynamics of myoglobin determined by the phonon-assisted Mössbauer effect.
Phys. Rev. E **65**, 051916 (2002).

T. Asthalter, H. Franz, U. van Bürck, K. Messel, E. Schreier, R. Dinnebier
Structure and dynamics of octamethyl-ethinyl-ferrocene: an organometallic rotator phase.
J. Phys. Chem. Solids (im Druck)

T. Asthalter, M. Bauer, U. van Bürck, I. Sergueev, H. Franz, A.I. Chumakov
Phonons in confinement and the Boson Peak using nuclear inelastic absorption.
(zur Veröffentlichung eingereicht)

O. Bleibaum, B. Sandow, W. Schirmacher
Break-Junction Tunneling Spectroscopy for Doped Semiconductors in the Hopping Regime
Phys. Rev. B, (eingereicht)

A. Brodin, M. Frank, S. Wiebel, G. Shen, J. Wuttke, H.Z. Cummins, *Brillouin Scattering Study of Propylene Carbonate: An Evaluation of Phenomenological and Mode Coupling Analysis*
Phys. Rev. E **65**, 051503 (2002)

U. van Bürck, W. Potzel, P. Schindelmann, G. V. Smirnov, S. L. Popov, E. Gerdau, Yu. V. Shvyd'ko, H. D. Rüter, O. Leupold
Inversion of target sequence in nuclear forward scattering of synchrotron radiation.
Hyperfine Interactions **141/142**, 151 (2002).

Z. Chowdhuri, R. M. Dimeo, P. M. Gehring, D. A. Neuman, A. Meyer, J. M. Rowe
The Backscattering Spectrometer at the NIST Center for Neutron Research
Applied Physics A. Material Science and Processing (im Druck)

W. Doster, M. Diehl, H. Schober, W. Petry, J. Wiedersich
Effect of pressure and pressure denaturation on fast molecular motions of solvated myoglobin.
Trends in High Pressure Bioscience and Biotechnology, Ed. R. Hayashi
Elsevier Science, 107-110 (2002).

W. Doster, R. Gebhardt, A. Soper
Pressure-induced unfolding of myoglobin: neutron diffraction and dynamic scattering experiments
High Pressure Bioscience and Biotechnology, Springer Verlag 2002 (im Druck).

W. Doster
TOF-Elastic Resolution Spectroscopy: Dynamic Analysis of Weakly Scattering Samples
Chemical Physics 2002, QENS Special Edition, (eingereicht)

H. Franz, T. Asthalter, M. Dommach, A. Ehnes, K. Messel, I. Sergueev
Investigations of solid state dynamics at the NRSSR beamline at PETRA II. An overview.
Hyperfine Interactions **141/142**, 131 (2002).

R. Gebhardt, W. Doster, J. Friedrich, W. Petry
Critical association of myoglobin under pressure
High Pressure Bioscience and Biotechnology, Springer Verlag 2002 (im Druck)

J. S. Gutmann, P. Müller-Buschbaum, M. Stamm
Film thickness dependence of structure formation in ultra-thin polymer blend films
Applied Phys A 74, S463 (2002)

I. Köper, M.-C. Bellissent-Funel, W. Petry
Hindered protein dynamics in the presence of a cryoprotecting agent
Applied Physics A. Material Science and Processing (im Druck)

C. Lorenz-Haas, P. Müller-Buschbaum, J. Kraus, D. G. Bucknall, M. Stamm
Nucleated dewetting of thin polymer films
Applied Phys A 74, S383 (2002)

A. Meyer, H. Schober, D. B. Dingwell
Structure, Structural Relaxation and Ion Diffusion in Sodium Disilicate Melts
Europhys. Lett. **59**, 708 (2002).

A. Meyer
Atomic Transport in Dense, Multicomponent Metallic Liquids
Phys. Rev. B **66**, 134205 (2002)

A. Meyer, H. Schober, D. B. Dingwell
Sodium Silicate Melts: Structure, Relaxation and Ion Diffusion
Scientific Highlights, Institut Laue–Langevin, 56 (2002)

A. Meyer, R. M. Dimeo, P. M. Gehring, D. A. Neuman
The Backscattering Spectrometer at the NIST Center for Neutron Research
Rev. Sci. Instr. (im Druck)

A. Meyer
Flüssig–Glas–Übergang in "Effekte der Physik und ihre Anwendungen", M. von Ardenne, G. Musiol, S. Reball (Hrg.), Harri Deutsch, Frankfurt am Main, 3. Auflage (im Druck)

A. Meyer, W. Petry, M. Koza, M.-P. Macht
Fast Diffusion in ZrTiNiCuBe Melts
(zur Veröffentlichung eingereicht)

P. Müller-Buschbaum, J. S. Gutmann, C. Lorenz-Haas, O. Wunnicke, M. Stamm, W. Petry
Dewetting of thin diblock copolymer films
Macromolecules 35, 2017 (2002)

P. Müller-Buschbaum, R. Cubitt, W. Petry
Phase separation of weakly incompatible polymer blends confined into isolated droplets
Applied Phys A 74, S342 (2002)

P. Müller-Buschbaum, W. Petry, O. Wunnicke, M. Stamm, R.Cubitt
Stabilisation of thin polymer films
ILL Annual Report: 72 (2002)

P. Müller-Buschbaum
Soft condensed matter investigated with synchrotron radiation: Status and perspectives
in "Application of Synchrotron Radiation in Chemistry", ISBN 3-924330-53-0 (2002).

W. Petry
FRM-II, ein einzigartiges Mikroskop für Naturwissenschaften, Technik und Medizin
TUM Mitteilungen **2** (2001/2002).

W. Petry
Neutronen bringen Licht ins Dunkel in "... und er würfelt doch! Von der Erforschung des ganz Grossen, des ganz Kleinen und der ganz vielen Dinge
Hrg.: H. Müller-Krumbhaar und H.-F. Wagner, Wiley-VcH, Weinheim, Seite 482 – 493 (2002).

S. Roth, A. Zirkel, J. Bossy, J. Neuhaus, J. Peters, H. Schober, W. Petry
Measurement and Simulation of the Inelastic Resolution Function of a Time-of-Flight Spectrometer
Applied Physics A. Material Science and Processing (im Druck)

B. Sandow, K. Gloos, R. Rentzsch, A. N. Ionov, W. Schirmacher
Sandow et al. reply
Phys. Rev. Lett. **89**, 229702 (2002).

P. Schindelmann, U. van Bürck, W. Potzel, G. V. Smirnov, S. L. Popov, E. Gerdau, Yu. V. Shvyd'ko, J. Jäschke, H. D. Rüter, A. I. Chumakov, R. Rüffer
Radiative decoupling and coupling of nuclear oscillators by stepwise Doppler-energy shifts.
Phys. Rev. B **65**, 023804 (2002).

W. Schirmacher, M. Pöhlmann, E. Maurer
Anharmonic Interactions and the Low-Temperature Thermal Anomalies in Glasses
Phys. Stat. Sol. (b) **230**, 31 (2002).

I. Sergueev, H. Franz, T. Asthalter, W. Petry, U. van Bürck, G. V. Smirnov
Structural relaxation in a viscous liquid studied by quasielastic nuclear forward scattering.
Phys. Rev. B **66**, 184210 (2002).

S. Wiebel, J. Wuttke
Structural relaxation and mode coupling in a non-glassforming liquid: depolarized light scattering in benzene
New J. Phys. **4**, 56 (2002).

M. Wolkenhauer, P. Müller-Buschbaum, O. Wunnicke, M. Stamm, J. Roovers, G. von Krosigk, R. Cubitt
Structure analysis of adsorbed starlike polymers with GISAS ans SFM
Applied Phys A 74, S433 (2002)

O. Wunnicke, C. Lorenz-Haas, P. Müller-Buschbaum, V. Leiner, M. Stamm
Retardation of the dewetting process due to the addition of functional copolymers at polymer-polymer interfaces
Applied Phys A 74, S445 (2002)

V. Zöllmer, A. Meyer, K. Rätzke, F. Faupel
Diffusion in a Metallic Melt at the Critical Temperature of Mode Coupling Theory
(zur Veröffentlichung eingereicht)

Auswärtige Vorträge von Institutsmitgliedern

U. van Bürck, 5^{th} Seeheim Workshop on Mössbauer Spectroscopy, Seeheim
SRPAC - a new method to study hyperfine interactions and dynamics in soft matter
22. 5. 2002

W. Doster, American Chemical Soc. Meeting in Boston 2002.
Applications of Neutron Scattering in Structural Biology and Biophysics
Probing the dynamical transition of proteins, surface-coupled and internal motions
18-22. 8. 2002

W. Doster, Satellite Meeting of ESS-European Conference of Science, Bonn, 2002
Perspective of inelastic neutron scattering on proteins
15. 5. 2002

W. Doster, Int. Union of Crystallography Meeting in Geneva, Switzerland
High pressure unfolding of proteins
12. 8. 2002

W. Doster, QENS 2002, Int. Conference of Quasielastic Neutron Scattering, Berlin
Molecular dynamcis and pressure-induced unfolding of proteins
4.-7. 9. 2002

W. Doster, Int. Conference on High Pressure Science and Biotechnology in Dortmund
Pressure-induced unfolding of myoglobin studied by dynamic neutron scattering
16.-19. 9. 2002

W. Doster, SFB 531, Licht-induzierte Dynamik von Proteinen und Peptiden, LMU München.
Time-resolved calorimetry by optical interferometry
6. 10. 2002

F. Kargl, Frühjahrstagung der Deutschen Physikalischen Gesellschaft in Regensburg
Strukturelle Änderungen und Ionentransport in Alkalisilikatschmelzen
12.3.2002

A. Meyer, Universität Kiel
Relaxation and Diffusion in Viscous Metallic Melts
17. 1. 2002

A. Meyer, Universität Mainz
Multicomponent Viscous Metallic Melts as Model Systems for the Test of Mode Coupling Theory
5. 2. 2002

A. Meyer, Laboratoire des Verres, Universitè Montpellier
Atomic Transport in Multicomponent Melts
21. 6. 2002

A. Meyer, CECAM Workshop on Atomic Structure and Transport in Glassy Networks, Lyon
Structure and Atomic Transport in Silicate Melts
24. 6. 2002

A. Meyer, Kolloquium zum DFG Schwerpunktprogramm: Bildung, Transport und Differenzierung von Silikatschmelzen, Hannover
Silicate Melts: Formation of Channels and Consequences for Atomic Transport
10. 10. 2002

A. Meyer, Arbeitstreffen zum DFG Schwerpunktprogramm: Phasenumwandlungen in mehrkomponentigen Schmelzen, Göttingen
Atomic Transport in Multicomponent Metallic Liquids
28. 11. 2002

P. Müller-Buschbaum, Status and perspectives of SAXS/WAXS, HASYLAB Hamburg
Grazing incidence small angle scattering
24. 1. 2002

P. Müller-Buschbaum, Seminar des SFB448 Mesoskopisch strukturierte Verbundsysteme, Berlin
Mesoskopisch-strukturierte Polymeroberflächen
29. 1. 2002

P. Müller-Buschbaum, BioSoft-Kolloquium des Hahn-Meitner Institutes, Berlin
Diffuse scattering - a tool for the investigation of thin polymer films
30. 1. 2002

P. Müller-Buschbaum, Fibers and polymers, Grenoble
Failure and fracture of polymer interfaces investigated with scanning micro-SAXS
12. 2. 2002

P. Müller-Buschbaum, Frühjahrstagung der Deutschen Physikalischen Gesellschaft im Rahmen des Sondersymposiums Struktur und Dynamik in dünnen Polymerfilmen, Regensburg
Nano-structured polymer surfaces
14. 3. 2002

P. Müller-Buschbaum, European Conference ESS, Bonn
Nanostructured polymer films
16. 5. 2002

P. Müller-Buschbaum, Synchrotron radiation in polymer science II, Sheffield
Dewetting of confined diblock copolymer films
4. 9. 2002

P. Müller-Buschbaum, 5 years of ADAM - neutron reflectometry at the ILL, Bochum
Stabilisation of thin polymer films on top of semiconductor surfaces
14. 9. 2002

P. Müller-Buschbaum, Application of Synchrotron Radiation in Chemistry, Hamburg
Soft condensed matter investigated with synchrotron radiation: status and perspectives
17. 9. 2002

P. Müller-Buschbaum, Condensed matter applications at PETRA III, Hamburg
Advanced scattering techniques for the investigation of thin polymer films
1. 10. 2002

P. Müller-Buschbaum, REFILL2002, Grenoble
Confined diblock copolymer films investigated with grazing incidence small angle scattering
25. 10. 2002

P. Müller-Buschbaum, Experiment and Theory in Polymer Science, Dresden
Dewetting of ultra-thin polymer films: A grazing incidence small angle scattering study
15. 11. 2002

P. Müller-Buschbaum, Projekttreffen Haftklebstoffe, Ludwigshafen
Tackiness of polymer surfaces
11. 12. 2002

W. Petry, Rotary Club, TUM, Garching
FRM-II, ein einzigartiges Mikroskop für Naturwissenschaften, Technik und Medizin
17. 01. 2002

W. Petry, DNS-ESS-Meeting, Institute of Science, Bangalore, Indien
Neutrons for Science, Engineering and Medicine, the New German Neutron Source FRM-II at the University of Technology, Munich
15. 03. 2002

W. Petry, Edgar-Lüscher-Physikseminar am Gymnasium Zwiesel, Thema: Klima, Energieversorgung der Zukunft und Probleme der Kernenergie
Der Hochtemperatur-Kernreaktor: Eine Chance für die Zukunft
13. 04. 2002

W. Petry, Diskussionsforum-Zukunft, Akademischer Seglerverein in München e.V.
Neutronen bringen Licht ins Dunkel - FRM-II, einzigartiges Mikroskop für Naturwissenschaften, Technik und Medizin
05. 05. 2002

W. Petry, Symposium Physik, Information und Informationssysteme - Ausgewählte Themen, Arnold Sommerfeld-Gesellschaft, Leipzig,
Die Neutronenquelle FRM-II, ein einzigartiges Mikroskop für Wissenschaft, Technik und Medizin
21. 06. 2002

W. Petry, Status Seminar of the MPG Initiative, Materials Science at the Neutron Source FRM-II, MPI Stuttgart
The Status of the Reactor in Garching
26. 06. 2002

W. Petry, DGK Arbeitskreistagung, Nichtkristalline und Partiellkristalline Strukturen, Jena
Atomarer Transport in mehrkomponentigen zähen Schmelzen
10. 09. 2002

W. Petry, Deutsches Museum, Vortragsserie: Physik und Technik, München
Licht im Dunkeln – Spektroskopie mit Neutronen
16. 10. 2002

W. Petry, MAI-Konferenz im Rathaus, Garching
Wirtschaft und Wissenschaft - getrennte Welten? Das Beispiel der Neutronenquelle FRM-II
08. 11. 2002

W. Petry, GSF Neuherberg (Prof. Paretzke)
Die Garchinger Neutronenquelle FRM-II und ihre geplante Nutzung
18. 11. 2002

W. Petry, Festvortrag anlässlich der Diplomandenehrung des VDI/VDE
FRM-II, ein einzigartiges Mikroskop für Naturwissenschaften, Technik und Medizin
28. 11. 2002

W. Petry, Symposium on the Neutron Backscattering in honour of Toni Heidemann, ILL, Grenoble, Frankreich
Neutrons always tell the truth, self diffusion in metals and the liquid-to-glass transition
29. 11. 2002

R. Röhlsberger, International Workshop on Magnetic Heterostructures, Bochum
Imaging the magnetic spin structure of exchange-coupled thin films
9. 10. 2002

R. Röhlsberger, International Workshop on X-Ray Spectroscopies of Magnetic Solids 2002, Dresden
Imaging the spin structure of magnetic thin films
8. 12. 2002

R. Röhlsberger, ESRF Seminar, Grenoble
Imaging the spin structure of exchange-coupled thin films
13. 12. 2002

W. Schirmacher, City-College, Univ. of New York
Theory of vibrational anomalies in disordered solids
8. 2. 2002

W. Schirmacher, Universität Augsburg
Hopping-Transport in ungeordneten Halbleitern
29. 5. 2002

W. Schirmacher, Universität Giessen
Theorie der Schwingungsanomalien in ungeordneten Festkörpern
25. 10. 2002

W. Schirmacher, Universität Marburg
Theorie der Schwingungsanomalien in ungeordneten Festkörpern
28. 10. 2002

I. Sergueev, VIII. Int. Conference on Mössbauer Spectroscopy and its Applications, St. Petersburg
SRPAC - a new method to study hyperfine interactions and dynamics in soft matter
11. 7. 2002

Eingeladene Vorträge an unserem Institut

Dr. Marilena Ricci, LENS, Universität Florenz
Dynamics of glass-forming liquuids by time resolved optical Kerr-effect
31. 01. 2002

Dr. Simona Loi, Universität Siegen
Two-dimensional structure of self-assembled alkyl substituted polyphenylene dendrimers on graphite
18. 04. 2002

Dr. Stephan Roth, ESRF, Grenoble
Material science in hard and soft condensed matter at ID 13
03. 05. 2002

Tarik Mehaddene, Universit´e de Strasbourg und Universit´e de Tizi-Ouzou (Algerien)
Diffuse and inelastic scattering on FePd alloys
06. 06. 2002

Prof. Hermann Z. Cummins, City College, New York
Polarized and depolarized light scattering in Salol: Effects at translation-rotation coupling
06. 06. 2002

Dr. Michael-Peter Macht, HMI, Berlin
Zwischen Schmelze und Festkörper-Forschung an metallischen Gläsern am HMI Berlin
14. 06. 2002

Dr. Niklas Engler, Technische Universität München (E17)
Proteinstrukturanalyse mit Neutronen: Struktur und Dynamik der Wasserstoffatome
19. 06. 2002

Dr. Herbert Schober, FZ Jülich
Simulation of Diffusion in Glasses and their Melts
11. 07. 2002

Prof. Dr. A.K. Sood, Department of Physics, Indian Institute of Science, Bangalore, Indien
Chaotic dynamics in nonlinear flow of wormlike micellar systems
12. 07. 2002

Prof. Dr. Sushanta Dattagupta, S.N. Bose National Centre for Basic Science, Salt Lake, Calcutta, Indien
Coherence versus decoherence in some problems of condensed matter physics
30. 07. 2002

Dr. Nadja Hermsdorf, Institut für Polymerforschung Dresden eV
Template für Nanodrähte und Nanoröhren - Herstellung und Charakterisierung
13. 09. 2002

Dr. Martin Letz, Schott Mainz
Optische Anisotropie und excitonische Anregungen im Calziumfluorid für Mikrolithographie bei 157 nm
28. 09. 2002

Dr. Liliana Birla, Universität Bukarest
Salt Effects on Albumin Structure
18. 10. 2002

Prof. Dr. Alexei Sokolov, Acron University, Michigan
Light Scattering Experiments on Liquids and Protein Solutions
28. 10. 2002

PD. Dr. Thomas Nawroth, Technische Universität München (E17)
Struktur-Dynamik von Membranen - Zeitauflösende Neutronenstreuung und Elektronenmikroskopie von Liposomen, Proteo-Liposomen und magnetischen Liposomen für die medizinische Anwendung
15. 11. 2002

Prof. Dr. Werner Keune, Universität Duisburg
Beobachtung des Boson-Peaks in amorphen FeTM Legierungsfilmen
22. 11. 2002

Dr. Munir Tarek, Equipe de Chimie et Biochimie Th´eoriques, CNRS Nancy
Glassy dynamics of proteins and their hydration water from Molecular Dynamics simulations
05. 12. 2002

Prof. Dr. Georg Krausch, Universität Bayreuth
Reorientation of Block Copolymer Microdomains in Electric Fields: An in-situ SAXS Study
06. 12. 2002

Mitarbeiter und Gäste

Leitung: Univ.-Prof. Dr. Winfried Petry

Prof. Dr. Alfons Schulte, Lehrstuhlvertretung von Herrn Prof. Petry bis August 2002
Prof. Dr. Ralf Röhlsberger, Lehrstuhlvertretung von Herrn Prof. Petry ab Oktober 2002

Wissenschaftliche Mitarbeiter

PD Dr. Wolfgang Doster
Dr. Valeria Lauter-Pasyuk (ILL)
Dr. Simona Loi
Dr. Andreas Meyer
Dr. habil. Peter Müller-Buschbaum
Dr. Jürgen Neuhaus (FRM II)
PD Dr. Walter Schirmacher
Dr. Ernst Schreier (bis Juni 2002)
Dr. Tobias Unruh (FRM-II)
Dr. Uwe van Bürck

Doktoranden

Ronald Gebhardt
Florian Kargl (ab September 2002)
Ingo Köper (bis August 2002)
Edith Maurer (ab Juli 2002)
Suresh Mavila Chathoth (ab März 2002)
Kirill Messel
Panteleimon Panagiotou
Markus Pöhlmann
Ilya Sergueev
Sabine Wiebel

Diplomanden

Patrick Dondl (ab Januar 2002)
Andreas Götzendorfer (ab August 2002)
Florian Kargl (bis Juli 2002)
Edith Maurer (bis Juni 2002)
Axel Müller (ab Dezember 2002)
Tobias Titz (ab Oktober 2002)
Anita Widmann (ab Februar 2002)

Werkstudenten

Stephan Camerer
Christian Carbagno
Alexander Diethert
Alexander Schober
Tobias Titz
Anita Widmann

Nichtwissenschaftliche Mitarbeiter

Joachim Dörbecker
Elke Fehsenfeld
Reinhold Funer
Josef Kaplonski
Helga Harlandt
Dieter Müller
Cornelia Simon
Max Wittich

Gäste

Dr. Peter Link (FRM-II)
Cornelia Lorenz-Haas
Jandal Ringe (FRM-II)